

NOTICE

When Government drawings, specifications, or other data are used for any purpose other than in connection with a definitely related Government procurement operation, the United States Government thereby incurs no responsibility nor any obligation whatsoever; and the fact that the government may have formulated, furnished, or in any way supplied the said drawings, specifications, or other data, is not to be regarded by implication or otherwise as in any manner licensing the holder or any other person or corporation, or conveying any rights or permission to manufacture, use, or sell any patented invention that may in any way be related thereto.

ACCESSION for	
NTIS	White Section <input checked="" type="checkbox"/>
D.C.	Buff Section <input type="checkbox"/>
UNANNOUNCED	<input type="checkbox"/>
JUSTIFICATION.....	
BY.....	
DISTRIBUTION/AVAILABILITY CODES	
Dist.	AVAIL. and/or SPECIAL
A	

Copies of this report should not be returned unless return is required by security considerations, contractual obligations, or notice on a specific document.

AIR FORCE/56780/21 June 1974 - 100

UNCLASSIFIED

AD-781066

DOCUMENT CONTROL DATA - R & D		
(Security classification of title, body of abstract and indexing annotation must be entered when the overall report is classified)		
1. ORIGINATING ACTIVITY (Corporate author) Air Force Aero Propulsion Laboratory (SFF) Wright-Patterson AFB, Ohio 45433		2a. REPORT SECURITY CLASSIFICATION UNCLASSIFIED
3. REPORT TITLE HIGH TEMPERATURE HYDROCARBON FUELS RESEARCH IN AN ADVANCED AIRCRAFT FUEL SYSTEM SIMULATOR ON FUEL AFFB-14-70		2b. GROUP
4. DESCRIPTIVE NOTES (Type of report and inclusive dates) Final Report, July 1970 to September 1972		
5. AUTHOR(S) (First name, middle initial, last name) Royce P. Bradley Richard Bankhead Warren E. Bucher, Captain, USAF		
6. REPORT DATE April 1974	7a. TOTAL NO. OF PAGES 140	7b. NO. OF REFS 9
8a. CONTRACT OR GRANT NO. A. PROJECT NO. 3048 c. Task No. 304805 d.		9a. ORIGINATOR'S REPORT NUMBER(S) AFAPL-TR-73-95
		9b. OTHER REPORT NO(S) (Any other numbers that may be assigned this report) None
10. DISTRIBUTION STATEMENT Approved for public release; distribution unlimited.		
11. SUPPLEMENTARY NOTES		12. SPONSORING MILITARY ACTIVITY Air Force Aero Propulsion Laboratory Wright-Patterson AFB, Ohio 45433
13. ABSTRACT Hydrocarbon fuels tend to form deposits in the thermal environment associated with high Mach number flight. These deposits can decrease heat exchanger efficiency and plug filter elements and nozzles. The Advanced Aircraft Fuel System Simulator provides thermal stability data on fuels which are used to determine aircraft fuel system design criteria, operational limits of fuels, and to aid in the development of small-scale thermal stability test devices. Fuel AFFB-14-70, the seventh fuel in a series, was tested under cyclic and steady-state conditions. No deposits formed in the wing tank at 200°F; however, significant deposits were evident at 300 and 375°F. A brown powder was detectable on the surfaces of the fuselage tank. There were no significant changes in performance of any of the components except for the manifold and nozzle. Very heavy deposits formed in the manifold in 59 simulated flights and the nozzle pressure drop increased 2.7%. Steady-state manifold test results and the results of tests on small-scale thermal stability test devices indicate that fuel AFFB-14-70 is of average quality in terms of thermal stability. Steady-state manifold tests were run to determine the effect of dissolved oxygen on thermal stability. Significant improvement resulted at oxygen concentrations below 30 parts-per-million (PPM) by weight. A Jet Fuel Thermal Oxidation Tester (JFTOT), which was run on-line with the Simulator, also showed thermal stability improvements below 30 PPM of dissolved oxygen.		

DD FORM 1473
1 NOV 65

UNCLASSIFIED

Security Classification

Reproduced by
NATIONAL TECHNICAL
INFORMATION SERVICE
U S Department of Commerce
Springfield VA 22151

UNCLASSIFIED

Security Classification

14. KEY WORDS	LINK A		LINK B		LINK C	
	ROLE	WT	ROLE	WT	ROLE	WT
Advanced Aircraft Fuel System Simulator						
Jet Fuel Deposits						
Thermal Stability of Jet Fuels						
Oxidative Stability of Jet Fuels						
Hydrocarbon Jet Fuels						
Jet Fuels						
Coker						
ASTM-CRC Fuel Coker						
JFTOT						
Jet Fuel Thermal Oxidation Tester						

UNCLASSIFIED

Security Classification

10

Form 1473 (Continued)

The results of tests using manifold tubes with widely different surface finishes are reported. The elapsed test time required to produce significant deposits was greatly increased by an improvement in the tube surface finish. However, once the surface was covered, the rate of deposit formation was unaffected by the tube surface finish.

AFAPL-TR-73-95

HIGH TEMPERATURE HYDROCARBON FUELS RESEARCH
IN AN ADVANCED AIRCRAFT FUEL SYSTEM SIMULATOR
ON FUEL AFFB-14-70

Royce Bradley
Richard Bankhead
Warren Bucher, Captain, USAF

Approved for public release; distribution unlimited.

///

FOREWORD

This report was prepared by the Fuels Branch (SFF), Fuels and Lubrication Division of the Air Force Aero Propulsion Laboratory, Wright-Patterson Air Force Base, Ohio under Project 3048, Task 304805, Messrs. Royce P. Bradley, Harry R. Bankhead, and Captain Warren E. Bucher project engineers.

The work described in this report was conducted as an in-house research project from July 1970 to September 1972 at the Air Force Aero Propulsion Laboratory.

The authors acknowledge the help of Mr. Anthony J. Vandenberg in the analysis of data used in this report.

This report was submitted by the authors on 30 May 1973.

This technical report has been reviewed and is approved.


ARTHUR V. CHURCHILL
Chief, Fuels Branch
Fuels and Lubrication Division

TABLE OF CONTENTS

SECTION	PAGE
I INTRODUCTION	1
II FUEL TESTED	3
III SIMULATOR TEST CYCLES	5
1. GENERAL DESCRIPTION	5
2. SUMMARY OF TEST PROCEDURES AND RESULTS	5
3. COMPONENT TEST PROCEDURES AND RESULTS	12
a. Wing Tank	13
b. Fuselage Tank	22
c. Altitude and Inerting	25
d. Vent Heating	25
e. Fuel Condensate	26
f. Airframe Fuel Filter and Lines	26
g. Airframe Heat Exchanger	26
h. Engine Pump Subsystem	28
i. Engine Fuel Filter and Lines	31
j. Engine Heat Exchanger	31
k. Manifold	38
l. Nozzle Subsystem	44
IV SIMULATOR STEADY-STATE MANIFOLD TESTS	50
1. STEADY STATE OPERATIONAL PROCEDURE AND RESULTS	50
a. System Revision	50
b. Operational Procedure	50
c. Results	52

TABLE OF CONTENTS (CONTD)

SECTION	PAGE
V EFFECT OF DISSOLVED OXYGEN ON DEPOSIT FORMATION	65
1. SYSTEM REVISION	65
2. OPERATIONAL PROCEDURE	65
3. MANIFOLD RESULTS	66
4. JFTOT RESULTS	83
VI EFFECT OF SURFACE FINISH ON DEPOSIT FORMATION	85
VII SMALL SCALE TESTS	88
1. ASTM-CRC FUEL COKER	88
2. JET FUEL THERMAL OXIDATION TESTER	88
VIII CONCLUSIONS	98
IX RECOMMENDATIONS	99
APPENDIX I MANIFOLD ANALYSIS	101
APPENDIX II MICROMETER MEASUREMENT OF MANIFOLD DEPOSIT THICKNESS	120
APPENDIX III TABULATED DATA (ASTM-CRC FUEL COKER AND JFTOT)	121
REFERENCES	128

ILLUSTRATIONS

FIGURE	PAGE
1. Advanced Aircraft Fuel System Simulator	6
2. Fuel Flow Rate Schedule	7
3. Tank Pressure Schedule	8
4. Wing Tank Dry Skin Temperature	9
5. Component Fuel Temperature	10
6. Time-Temperature History of Vapor in Wing Tank (300°F)	15
7. Time-Temperature History of Vapor in Wing Tank (375°F)	16
8. Time-Temperature History of Vapor in Wing Tank (225°F)	17
9. Artists Conception of the 300°F Wing Tank Deposits	20
10. Artists Conception of the 375°F Wing Tank Deposits	21
11. Time-Temperature History of Fuel and Vapor in Fuselage Tank	24
12. Pressure Drop Across Airframe Filter	27
13. Overall Heat Transfer Coefficient of Airframe Heat Exchanger	29
14. Pressure Drop Across Airframe Heat Exchanger	30
15. Pressure Drop Across Engine Filter	32
16. Engine Heat Exchanger Calibration Test Results	34
17. Overall Heat Transfer Coefficient of Engine Heat Exchanger	36
18. Pressure Drop Across Engine Heat Exchanger	37
19. Manifold Electrical Connection Locations	39

ILLUSTRATIONS (CONTD)

FIGURE	PAGE
20. Calculated Deposit Thermal Resistance of the Cyclic Test Series Manifold	41
21. Cyclic Test Series Manifold Calculated Deposit Thickness	43
22. Cyclic Test Series Manifold Measured Deposit Thickness	46
23. Pressure Drop Across Manifold	47
24. Pressure Drop Across Engine Nozzle	48
25. Steady-State-Flush Test Condition	51
26. Calculated DTRMIL for Test 10.801	53
27. Calculated DTRMIL for Test 10.802	55
28. Calculated DTRMIL for Test 10.803	57
29. Comparison of Calculated and Measured Deposit Thicknesses	60
30. Comparison of Steady-State Deposit Rates	61
31. Comparison of Steady-State-Flush Deposit Rates	62
32. Comparison Between Steady-State-Flush Data and Test Cycle Data	64
33. Calculated DTRMIL for Test 10.807	68
34. Calculated DTRMIL for Test 10.817	70
35. Calculated DTRMIL for Test 10.818	72
36. Calculated DTRMIL for Test 10.819	74
37. Calculated DTRMIL for Test 10.820	76
38. Calculated DTRMIL for Test 10.821	78
39. Calculated DTRMIL for Test 10.822	80
40. Effect of Oxygen in the Simulator	82

ILLUSTRATIONS (CONTD)

FIGURE	PAGE
41. Effect of Oxygen on JFTOT Breakpoint	84
42. Microphotograph Comparison of Manifold Tube Inner Surfaces, 553X Magnification	86
43. Effect of Manifold Tube Inner Surface	87
44. ASTM-CRC Fuel Coker Rating Results	89
45. ASTM-CRC Fuel Coker Pressure Drop Results	90
46. 2.5 Hour JFTOT Results Based on TDR Ratings	92
47. 5 Hour JFTOT Results Based on TDR Ratings	94
48. 2.5 Hour JFTOT Results Based on Visual Ratings	95
49. 5 Hour JFTOT Results Based on Visual Ratings	96
50. Manifold Instrumentation and Arrangement	102
51. Manifold Insulation Heat Loss vs. Outside Tube Wall Temperature	105
52. Curve Fit to Determine Film Convection Coefficient	117

TABLES

TABLE	PAGE
I Summary of Previous Testing	2
II AFFB-14-70 Fuel Analysis	4
III Summary Manifold Data - 10th Test Series	42
IV Comparison of Rate of Change in DTRML Between Two Manifolds Used During 10th Test Series	45
V Summary of Manifold Data 10.801	54
VI Summary of Manifold Data 10.802	56
VII Summary of Manifold Data 10.803	58
VIII Dissolved Oxygen Test Conditions	67
IX Summary of Manifold Data 10.807	69
X Summary of Manifold Data 10.817	71
XI Summary of Manifold Data 10.818	73
XII Summary of Manifold Data 10.819	75
XIII Summary of Manifold Data 10.820	77
XIV Summary of Manifold Data 10.821	79
XV Summary of Manifold Data 10.822	81
XVI ASTM-CRC Fuel Coker Test Results	122
XVII 2.5 Hour JFTOT Results - 25 Sep 70 to 6 Oct 70	123
XVIII 5 Hour JFTOT Results - 14 Sep 70 to 21 Jan 71	124
XIX 2.5 Hour JFTOT Results - 23 Nov 71 to 14 Feb 72	125
XX 5.0 Hour JFTOT Results - 17 Sep 71 to 3 Jan 71	126
XXI 2.5 Hour JFTOT Results - 12 Jun 72 to 14 Jun 72	127

SECTION I

INTRODUCTION

This effort was designed to investigate advanced hydrocarbon fuel performance with respect to thermal stability under simulated high Mach number flight conditions. A preceding program, which was contracted to North American Rockwell, Los Angeles Division, provided the Advanced Aircraft Fuel System Simulator used in this study. North American evaluated five fuels of differing thermal stabilities in the simulator (Reference 1). A sixth fuel was evaluated by the Air Force Aero Propulsion Laboratory (AFAPL) (Reference 2) as the first in a series of fuels to be evaluated in-house. The results of these programs are summarized in Table I.

The in-house effort is designed to expand upon the North American Rockwell results and to pursue new areas of investigations with the Simulator. Generalized performance data provided by this effort will aid in the development of representative small-scale tests, provide a basis of relating small-scale test results to operational performance, and provide information on the operational limitations of currently available fuels to aid in designing specifications of fuels for future supersonic aircraft. This report describes the results of the evaluation of fuel AFFB-14-70.

TABLE I
SUMMARY OF PREVIOUS TESTING

Fuel Designation	Fuel Type	Test Objective	ALCOR JFTOT Breakpoint °F*	General Results
AFFB-8-67	Jet A-1	Establish baseline of heavy deposition	570	Heavy deposition in wing tank and manifold (Ref 3)
AFFB-9-67	JP-5	Establish baseline of heavy deposition	525	Heavy deposition throughout all system components (Ref 4)
AFFB-10-67	Aged JP-7	Advanced Fuel Testing	615	Moderate deposits in wing tank and manifold (Ref 5)
AFFB-11-68	Neat JP-7	Advanced Fuel Testing	750	Moderate deposits in wing tank and manifold. Less deposits than AFFB-10-67 (Ref 6)
AFFB-12-68	Spec JP-7	Advanced Fuel Testing	725	Results similar to AFFB-11-68 (Ref 7)
AFFB-13-69	Jet A-1	Advanced Fuel Testing	660	Moderate to heavy deposits in wing tank and manifold (Ref 2)

*Lowest control temperature where a Code 3 is first obtained on the test heater tube.

SECTION II

FUEL TESTED

The test fuel is designated AFFB-14-70 and was purchased from Ashland Oil, Inc. It was refined from U. S. mid-continent crude oil and is a neat kerosene.

This fuel was chosen to serve as a baseline for future testing of Simulator fuels to evaluate thermal stability characteristics resulting from various refinery treatments (desulfurization, hydrogenating, etc.).

Laboratory analysis for this fuel are presented in Table II.

TABLE II
AFFB-14-70 FUEL ANALYSIS

	Ashland Oil Tests, Jul 70	Aerospace Fuels Lab, Jul 70
Gravity, °API	45.0	45.1
Distillation		
IBP	329	326
10%	360	364
20%	371	378
50%	400	409
90%	449	460
FBP	489	505
Rec	99	98
Res, %	1	1
Loss, %	0	1
% @ 400°F	50	
Flash Point, °F	122	120
Freezing Point, °F	-52.6	Below -51
Viscosity @ -30°F, CS	9.07	
Net Heat of Combustion, Btu/lb	18,638	
	Btu/gal 124,539	
Aniline Point, °F	152	149
Aniline Gravity Constant	6,855	6,720
Total Sulfur, wt. %	0.021	0.018
Mercaptan Sulfur, wt. %	0.0005	0.0
Aromatics, Vol. %	11.6	10.8
Olefins, Vol. %	0.6	1.1
Potential Gum, mg/100 ml	2.9	1.2
Smoke Point, mm	26	25

SECTION III

SIMULATOR TEST CYCLES

1. GENERAL DESCRIPTION

The Advanced Aircraft Fuel System Simulator, a drawing of which is shown in Figure 1, comprises a 500 gallon fuel system consisting of airframe and engine fuel subsystems. The airframe subsystem has two fuel tanks, a refueling system, a vent system, a simulated aerodynamic heating and cooling system, a fuel feed system, a filter, and a heat exchanger. The engine fuel system consists of an engine pump and bypass system, a flow control valve, filter, heat exchanger system, manifold, and nozzle system. Additional information can be found in Reference 8.

2. SUMMARY OF TEST PROCEDURES AND RESULTS

One test series consisting of a total of 93 environmental test cycles (simulated missions) was conducted on fuel AFFB-14-70 in the Simulator. The fuel flow rate, tank pressure, and dry tank skin temperature profiles for the test series are shown in Figures 2, 3, and 4, respectively. The fuel-out temperatures for the various components are shown in Figure 5. The fuel nozzle temperature nearly coincides with the manifold outlet temperature.

Prior to each test cycle, the fuselage tank and the wing tank were filled with fresh fuel to 95% capacity. Altitude simulation and inerting of the fuel tanks were automatically controlled through the tank vent system. Vacuum pumps were used in this system to reduce the internal pressure of each tank and a nitrogen supply was provided to inert the vapor space during simulated descent. The fuel in the fuselage tank was heated from approximately 70°F at the start of the test cycle to 220°F at the end of the test cycle by radiation heaters to simulate aerodynamic heating. Simultaneously, the upper and lower wing tank skins were heated as follows to simulate aerodynamic heating.

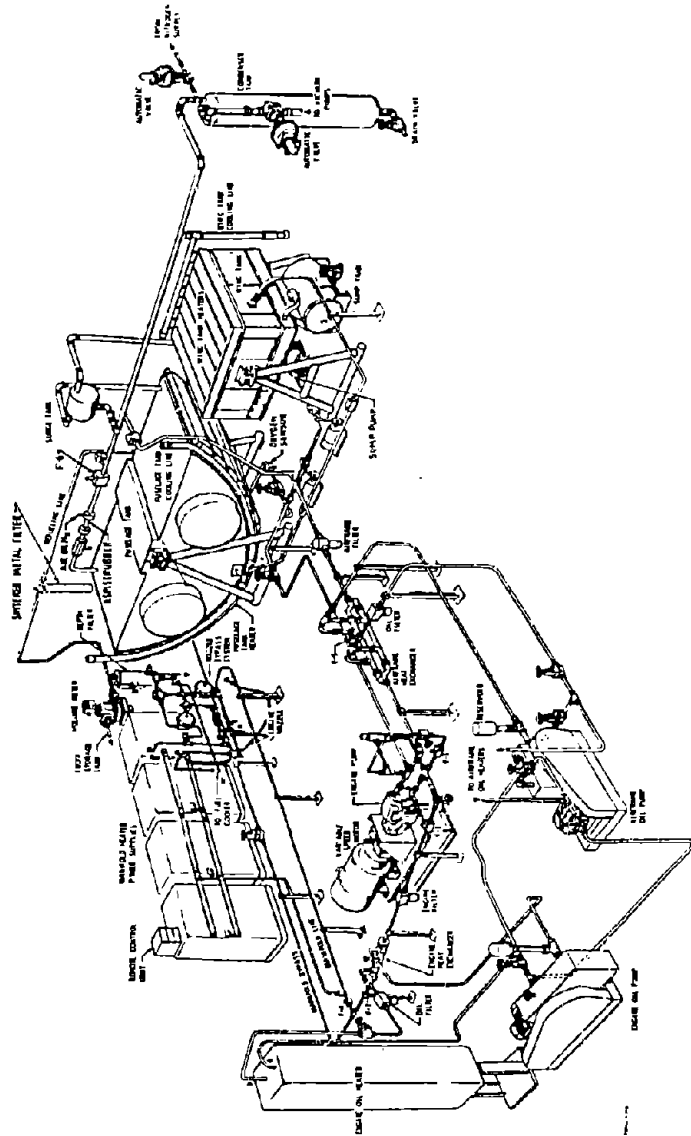


Figure 1. Advanced Aircraft Fuel System Simulator

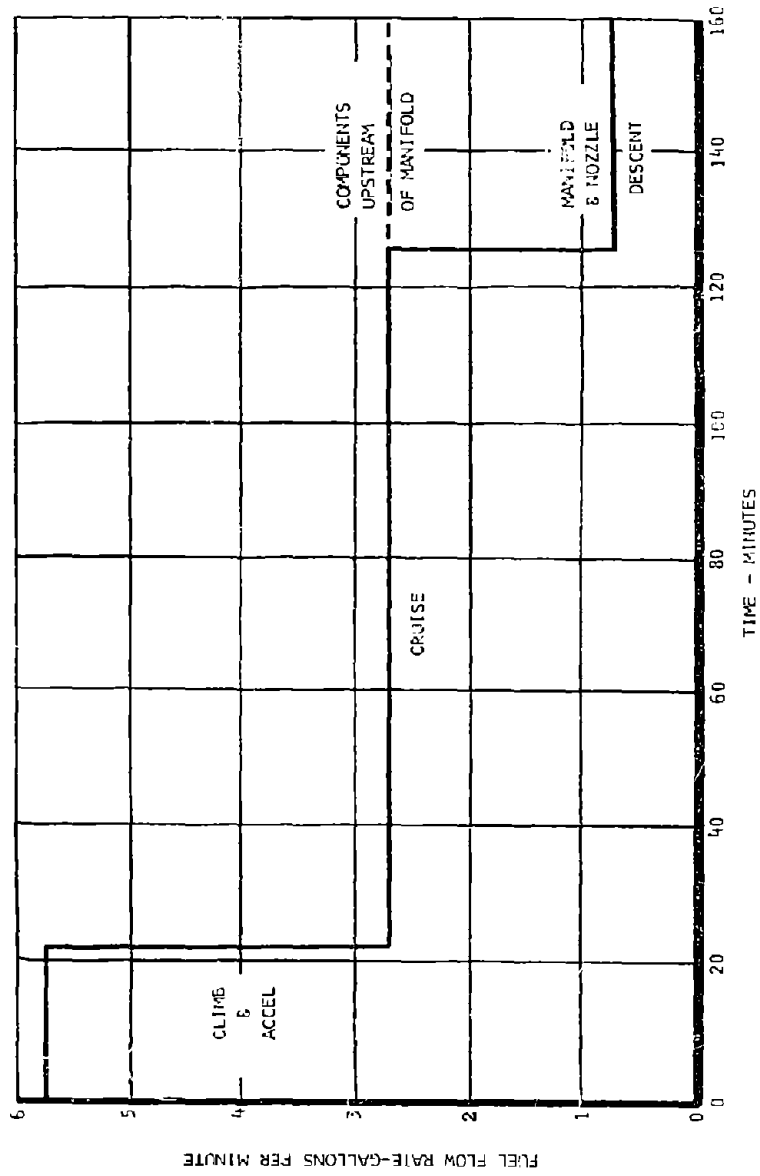


Figure 2. Fuel Flow Rate Schedule

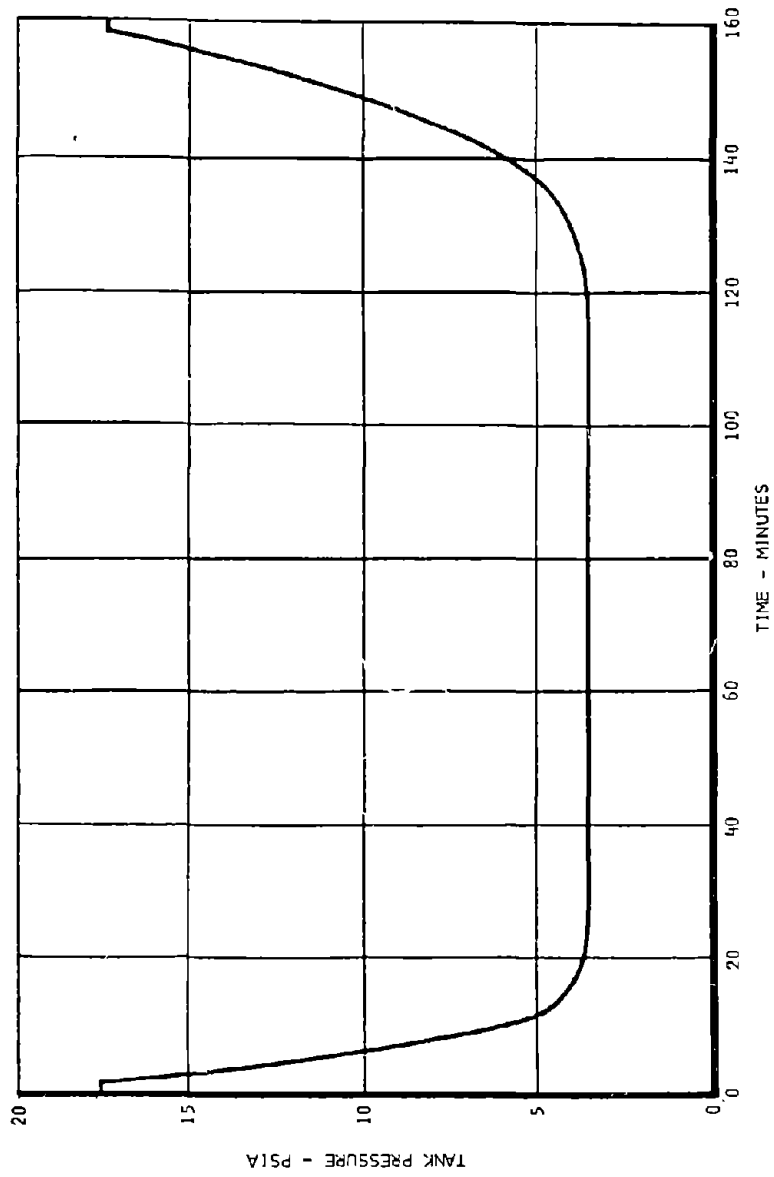


Figure 3. Tank Pressure Schedule

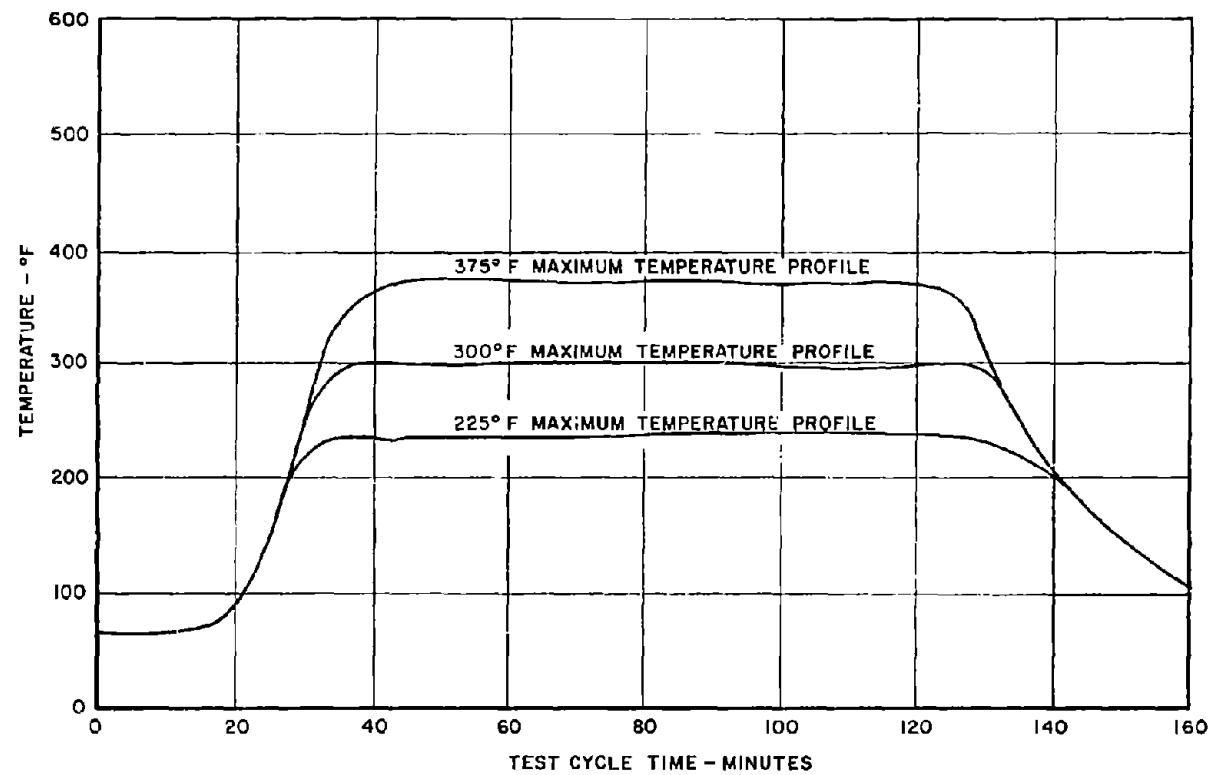


Figure 4. Wing Tank Dry Skin Temperature

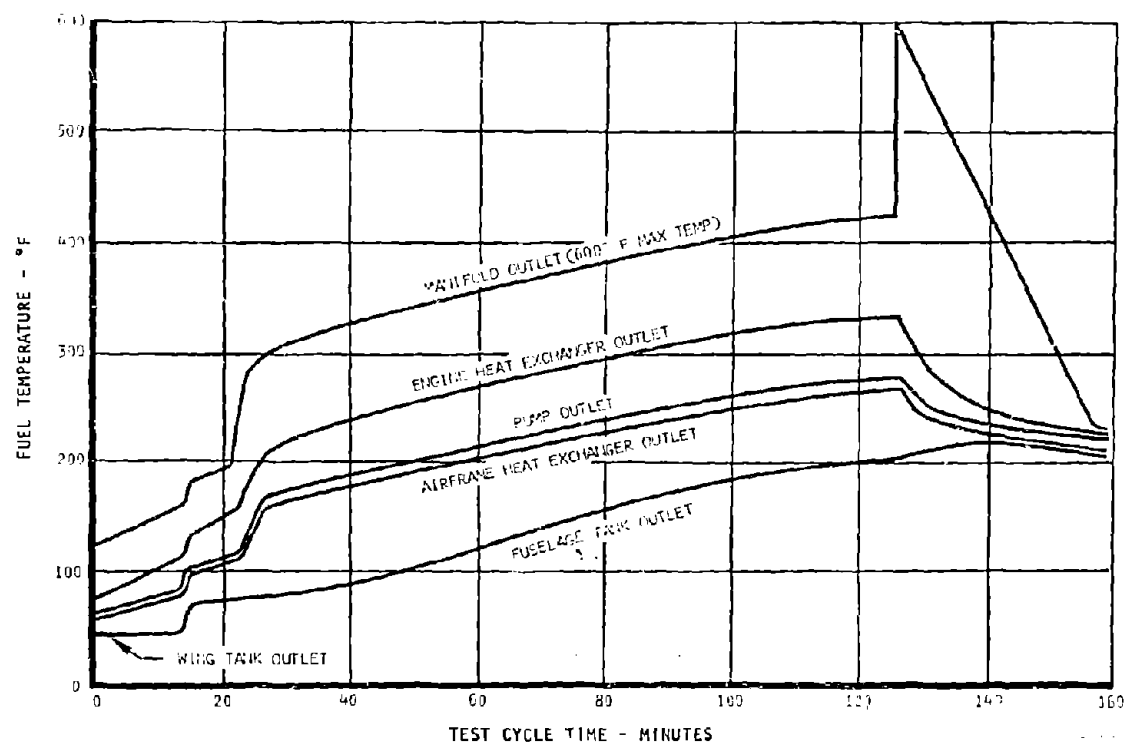


Figure 5. Component Fuel Temperature

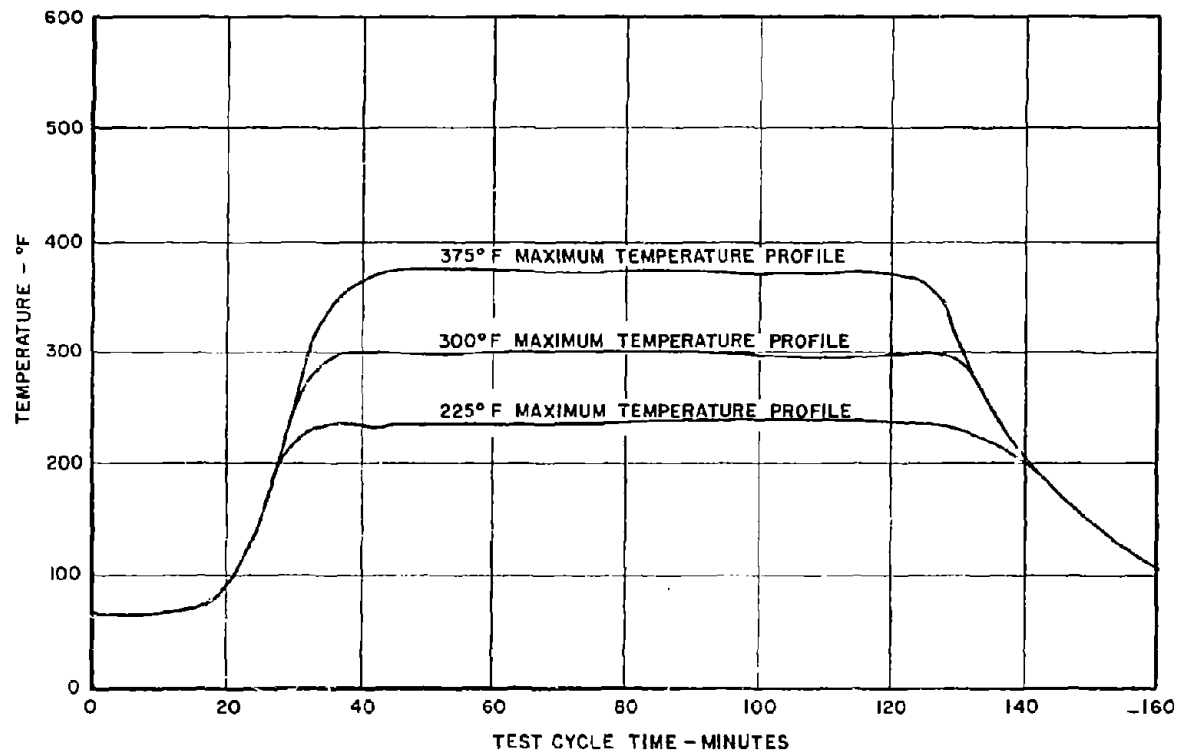


Figure 4. Wing Tank Dry Skin Temperature

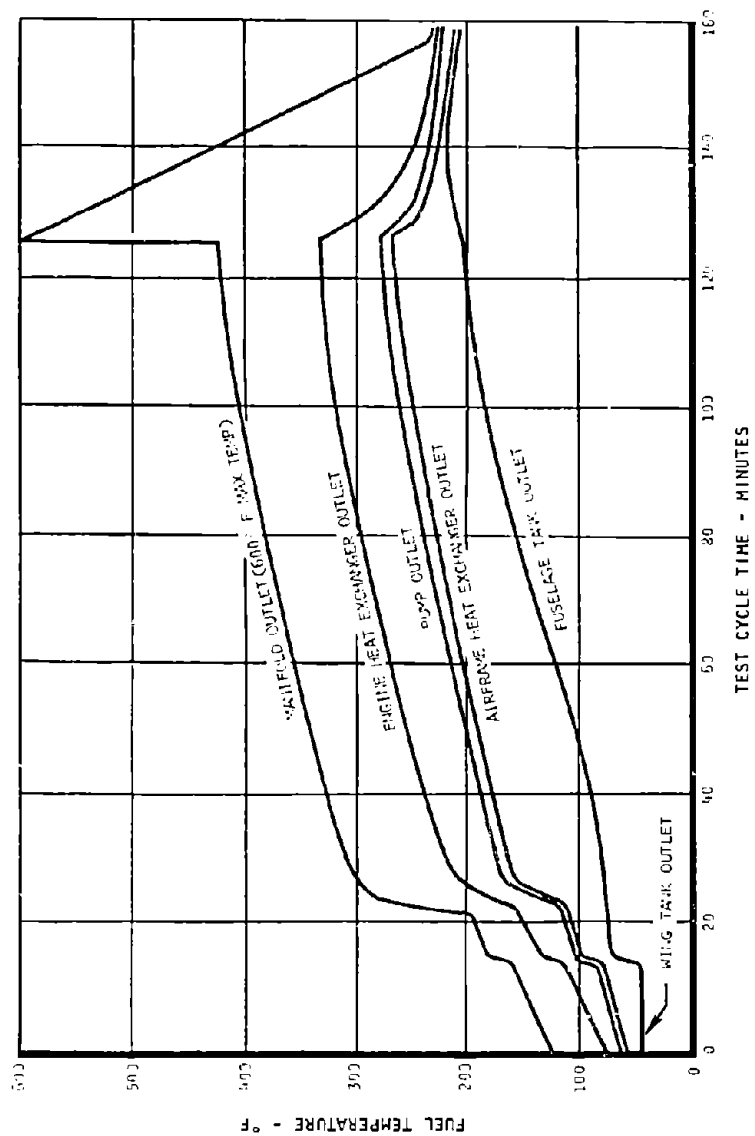


Figure 5. Component Fuel Temperature

<u>Test Cycles</u>	<u>Maximum Skin Temperature</u>
0 - 35	300°F
36 - 70	375°F
71 - 93	200°F

Vibration simulation was provided by utilizing a vibrator on each tank. The fuel was pumped from the tanks through a 75 micron airframe filter and an airframe heat exchanger.

The airframe heat exchanger system rejected heat to the fuel at a specified rate, resulting in an average increase in fuel temperature of 25° and 70°F for the acceleration and cruise conditions, respectively. The fuel entering the engine fuel system was pressurized and heated by the engine pump and bypass system. The average increase in temperature across the pump was 5°, 10°, and 10°F during acceleration, cruise, and descent conditions, respectively. The high pressure fuel flow was then regulated by a manual flow control valve and filtered by a 2-micron engine filter. The fuel was further heated by the engine heat exchanger system so that an additional increase in temperature of 25° and 60°F was obtained during the acceleration and cruise conditions, respectively. The fuel then passed through a heated manifold where average added temperature increases of 47° and 85°F were produced for the acceleration and cruise conditions.

At the beginning of descent conditions, the engine and airframe heat exchanger heating systems were de-energized. Three-quarters of the fuel passing through the engine exchanger during descent was returned to the fuselage tank. The remaining fuel passed through the heated manifold, where the fuel-out temperature rapidly increased to 600°F. The heat input to the manifold was then slowly decreased to simulate descent cooling of the manifold line. The fuel exiting the manifold line passed through the nozzle where temperature increases of 2° and 8°F were attained for the cruise and descent conditions, respectively. During and at the completion of the test series, the simulator was inspected and the data analyzed.

A summary of the results of the 93 test cycles is as follows. Inspection of the simulator showed that the fuselage tank internal surfaces were covered with a brown powder that could be detected only by wiping the surface with a white wiper. The puddle areas of the wing tank were discolored at maximum skin temperatures of 300°F and 375°F but were clean at 200°F. The deposit rated a maximum of 6 and 9 on the Coordinating Research Council (CRC) Lacquer Rating Scale at maximum skin temperatures of 300° and 375°F, respectively. No loose deposits were present. Puddle areas were noted by concentric rings of deposit.

The airframe filter showed no discoloration; however, an increase in pressure drop of 0.06 inches of water was measured which is considered insignificant. The inlet and outlet of the airframe heat exchanger were unchanged in color with no significant change in performance. There was no evidence of engine pump performance degradation during the testing.

The engine fuel lines and components contained no noticeable deposit. The engine filter (2 microns) was replaced three times during the 93 test cycles as the result of increases in pressure drop. The engine heat exchanger contained no noticeable deposits and no significant change in performance was evident.

The manifold contained medium-brown to dark-brown deposits. The calculated maximum deposit increase per test cycle was 0.0130 mil, using a deposit thermal conductivity of 0.07 BTU-ft/ft²-hr-°F. The engine nozzle was covered with a powdery deposit and the pressure drop across the nozzle increased 2.7%.

3. COMPONENT TEST PROCEDURES AND RESULTS

The following is a detailed discussion of the test cycle procedure and the results for each component. The results obtained are expressed in terms of component performance degradation, calculated deposit thickness, and color scale ratings. The use of a color scale for quantifying the fuel degradation in the simulator is far inferior to

measurements of performance degradation and deposit. However, the CRC Lacquer Rating Scale was used so comparisons can be made to previous fuel testing results. Unless otherwise stated, the brown rather than the gray scale was used. Additionally, selected components were rated using the Advanced Aircraft Simulator (AAS) scale.

a. Wing Tank

(1) System Revision

All previous testing was conducted using an internally mounted aircraft boost pump (Reference 8). It was necessary to cool the boost pump during the high temperature portion of each test cycle. This resulted in a cool surface that condensed fuel vapors which ran back to the bottom of the tank and again were vaporized. Heavy deposits resulted beneath the boost pump. The life of the boost pump was relatively short even with cooling and replacement was inconvenient and time consuming. The pump was replaced with an externally mounted pump providing longer life and easier replacement. An "Aurora" all stainless steel turbine pump, Model No. G4S-SS, was selected.

(2) Operational Procedure

Prior to each test cycle, the wing tank was filled with fresh fuel, ranging in temperature from 44° to 64°F, through a totalizing flowmeter to 95% of its capacity based on the fuel density at a temperature of 70°F. This quantity, 651.3 pounds, was used for each test cycle within a repeatability tolerance of less than 0.3 percent. After the tank was filled, the test cycle commenced by energizing the boost pump, establishing a fuel flow of approximately 5.8 gallons per minute out of the wing tank and automatically reducing the internal pressure of the wing tank in accordance with the required pressure schedule (Figure 3). The wing tank and probe heaters were energized at 14 and 16 minutes after start-up, respectively, in accordance with the heating schedule ascertained during the initial test cycles.

The first 35 test cycles were conducted at a maximum wing tank skin temperature of 300°F (See Figure 6). Visual inspection indicated that deposits were being formed in the puddle areas. The tank was cleaned and the maximum skin temperature raised to 375°F (See Figure 7) for the second 35 test cycles in order to provide information on the effect of temperature on deposit formation in the wing tank. A significant increase in the amount of deposit formed was observed when the tank was inspected at the end of the second 35 test cycles.

Since both of the test temperatures (i.e., 300° and 375°F) were well below the minimum temperature at which deposits start to form in the manifold, the maximum temperature was lowered to a level that would permit a rough determination of the breakpoint of the fuel in the wing tank. The tank was cleaned and testing commenced at a maximum skin temperature of 225°F (See Figure 8). The tank was again inspected following test cycle 93 (23 cycles at 225°F), and no deposits were visible in the tank. Testing was stopped since further testing would not provide any additional information in any of the system components.

As in past test series, probes were placed in the vapor space of the wing tank in order to determine the effect on deposit formation of various temperatures and materials. The number of probes was reduced to three from four since better data could be obtained by placing both stainless steel and titanium specimens on each probe instead of having three stainless steel probes and one titanium probe. The maximum temperature attained by each of the probes during the three temperature profiles used for the wing tank during the tenth test series was as follows:

Max. Skin Temperature of the Wing Tank	Maximum Probe Temperatures		
	Probe 1	Probe 2	Probe 3
300°F	300°F	255°F	240°F
375	375	335	320
225	225	180	180

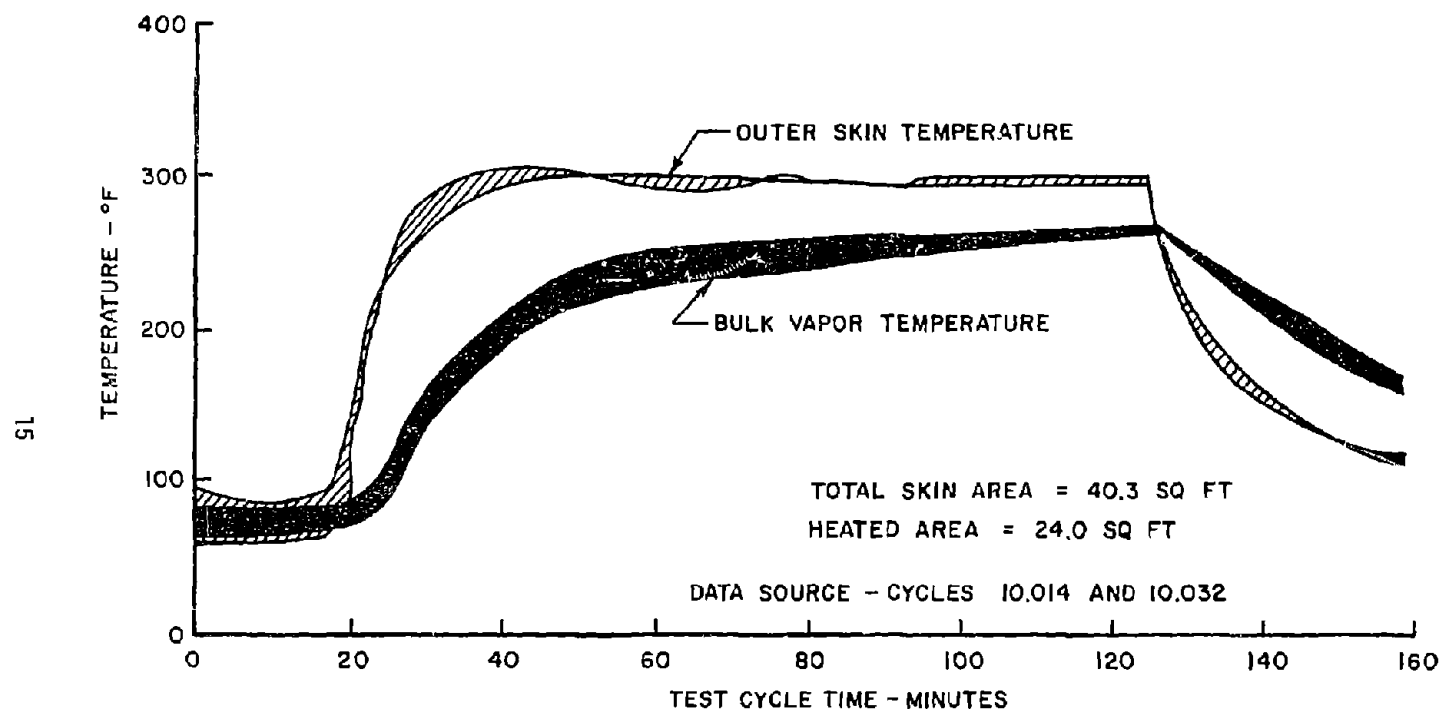


Figure 6. Time-Temperature History of Vapor in Wing Tank (300°F)

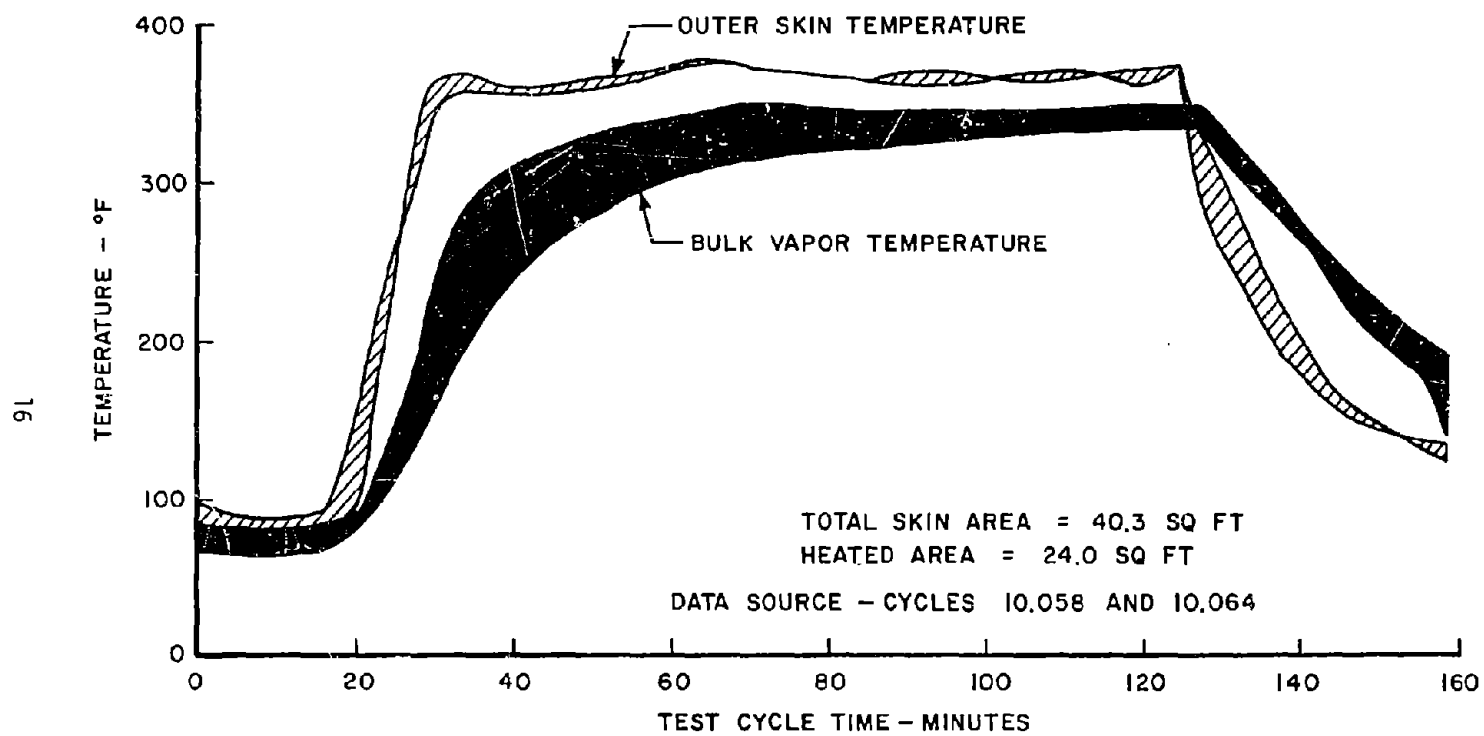


Figure 7. Time-Temperature History of Vapor in Wing Tank (375°F)

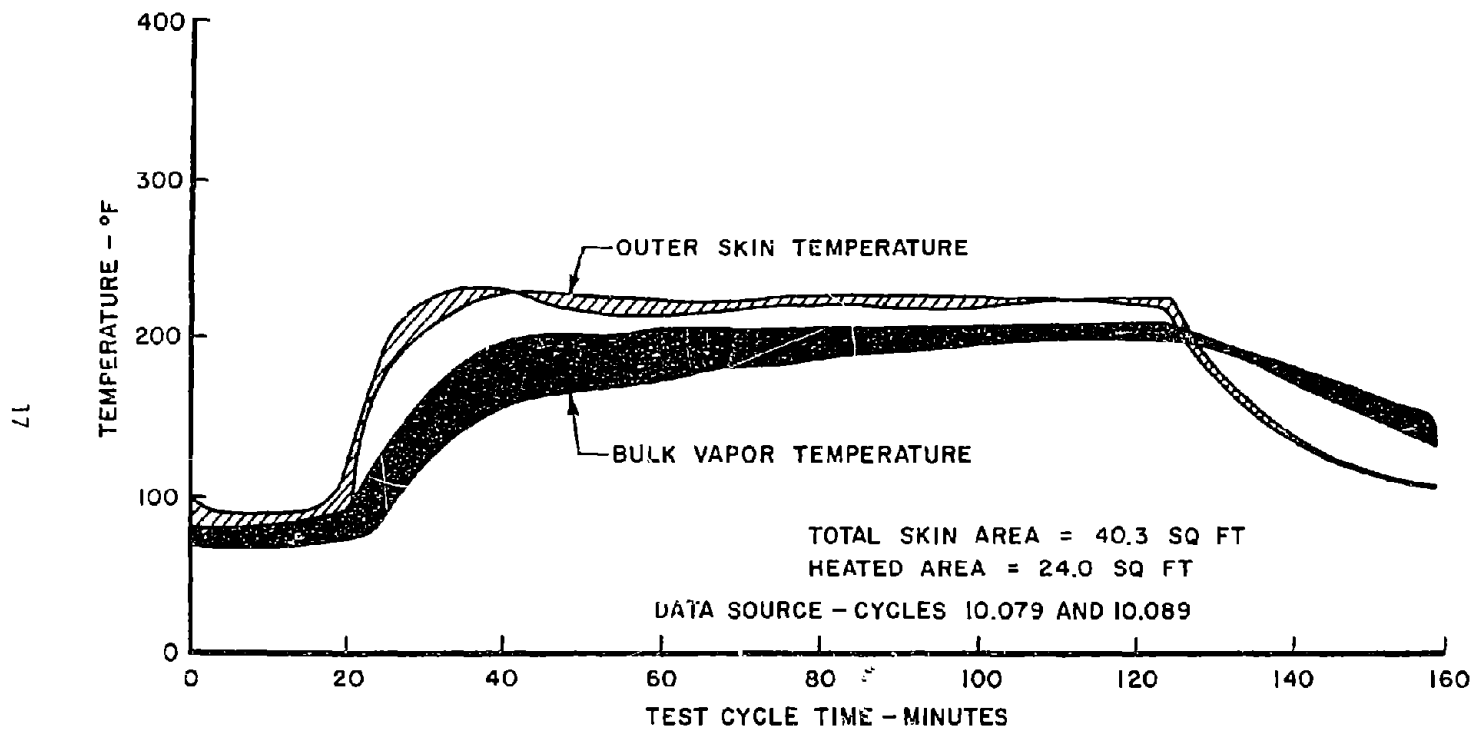


Figure 8. Time-Temperature History of Vapor in Wing Tank (225°F)

The temperature of probe 1 was controlled to produce the same temperature profile as the dry wing tank skin. The temperature of probe 2 was controlled to simulate the side of the wing tank, and probe 3 was unheated in order to duplicate the lowest temperature in the tank. In order to provide specimens that had been subjected to the dry skin and fuel puddle conditions of the bottom of the wing tank, two dishes and one disk were placed on the bottom of the tank.

The airframe fuel pressure diminished at 16 minutes after test start-up, indicating that the fuel depth in the wing tank was approximately 1 inch and the pump was cavitating. This condition was immediately followed by a decrease in fuel flow. The fuselage pump was then energized and the wing pump de-energized. The wing tank fuel dump valve was opened at 17 minutes. Most of the remaining fuel in the wing tank drained through the valve into a sump tank and the fuel dump valve was closed 28 minutes later. The wing tank attitude was calibrated to cause approximately 1450 milliliters of fuel to remain in tank after it was drained. During the cruise condition, which commenced 22 minutes after test start-up, the temperature of the dry heated portion of the wing tank skin was increased and stabilized at the desired maximum skin temperature.

Vibration and simulated aerodynamic cooling were commenced 126 minutes after test start-up. The vibrator was shut off at 136 minutes and cooling continued through the end of the test cycle.

(3) Results

The wing tank was opened after completion of testing at each of the three maximum skin temperatures to visually examine the deposits in the wing tank. The entire wing tank was rated by making a sketch of the tank showing the location, area, and rating of the

deposits using the CRC Lacquer Rating Scale. These visual examinations are summarized as follows:

<u>Test Cycle</u>	<u>Max. Skin Temp.</u>	<u>Sides</u>	<u>Vent Area</u>	<u>Tube Trusses</u>	<u>Bottom Dry Area</u>	<u>Bottom Puddle Areas</u>
35	300°F	Clean	Clean	Clean	Clean	4-5
70	375°F	Clean	Clean	Clean	2-4	3-9
93	225°F	Clean	Clean	Clean	Clean	Clean

Sketches were made of the wing tank after 35 and 70 test cycles and are shown in Figures 9 and 10, respectively. The tank was found to be clean following the first 35 test cycles (maximum temperature of 300°F) except for small stains in the puddle areas. The tank was cleaned and 35 additional test cycles conducted at a maximum skin temperature of 375°F. Inspection revealed that the entire bottom of the tank was covered with deposit; the heavier deposit being predominantly in the puddle areas. The remainder of the tank was clean. The tank was again cleaned and 23 test cycles conducted at a maximum skin temperature of 225°F. There was no evident discoloration of the tank following this testing.

The stainless steel and titanium probes were rated and replaced each time the tank was cleaned and after the test series. There was no significant difference in the discoloration of the titanium and stainless steel probes. The probes removed after the first 35 test cycles were dull when compared to an unused probe. The 300°F probes were slightly yellowed. The 240 and 255°F probes were very similar in appearance with little, if any, yellowing.

The probes removed after the second 35 test cycles were all slightly yellowed. The 320°F probe was only very slightly yellowed and the 375°F probe was the most discolored of all of the probes. The probes removed

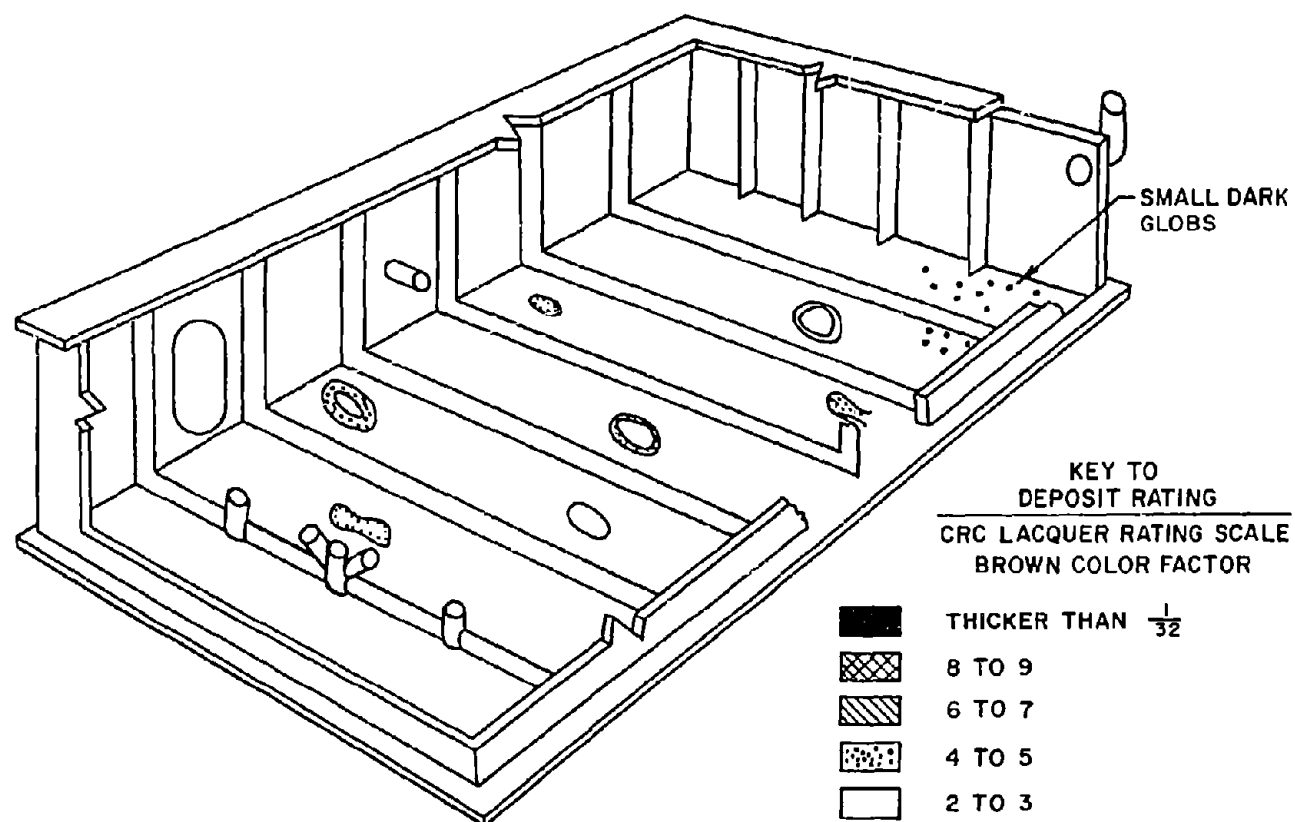


Figure 9. Artist's Conception of the 300°F Wing Tank Deposits

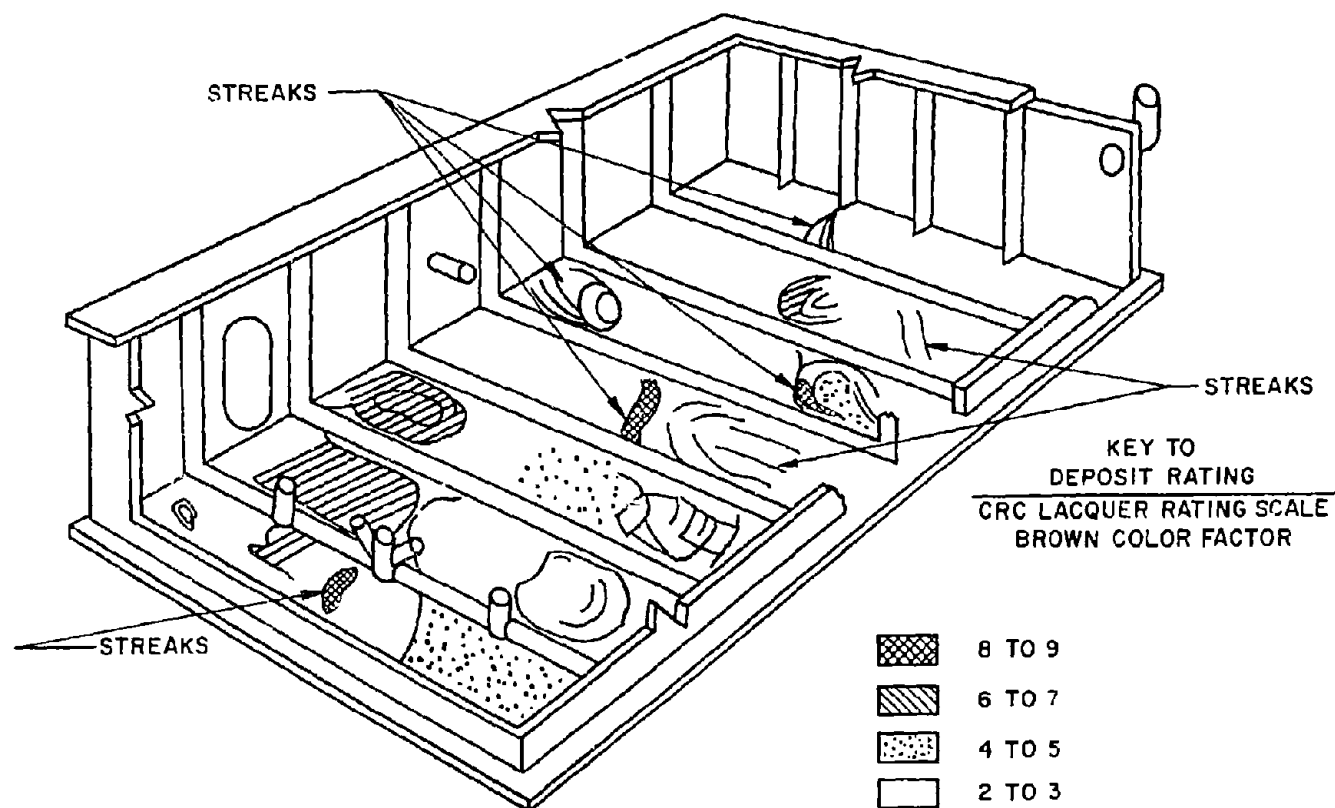


Figure 10. Artist's Conception of the 375°F Wing Tank Deposits

AFAPL-TR-73-95

after the 23 test cycles at a maximum temperature of 225°F were not discolored. The ranking of the probes in order of increasing discoloration is as follows:

180°F (225°F)	180°F (225°F)	225°F (225°F)	Least Discoloration
240°F (300°F)			
255°F (300°F)			
320°F (375°F)			
335°F (375°F)			
300°F (300°F)			
375°F (375°F)			Most Discoloration

NOTE: The numbers in parenthesis are the maximum wing tank skin temperatures.

The dishes and disk removed after the first 35 test cycles were slightly yellowed and rated less than 2 on the CRC Lacquer Rating Scale. There was no significant difference in the appearance of the dishes and disk. The dishes and disk removed after completion of the second 35 test cycles (375°F maximum skin temperature) were covered with brown and gray deposits rating from 3 to 6 on the CRC Lacquer Rating Scale. A small amount of multicolored deposit was evident on one of the dishes. Dishes and disk were not included in the testing at 225°F.

b. Fuselage Tank

(1) System Revision

All previous test series were conducted using an internally mounted aircraft boost pump. The pump was exposed to temperatures during each test cycle that were well above the rated temperature limits of the pump. This resulted in a significant reduction in the mean-time-to-failure. Therefore, the pump was replaced with an external boost pump as discussed previously for the wing tank.

(2) Operational Procedure

Prior to each test cycle the fuselage tank was filled to 95% of the capacity. The average weight of fresh fuel used to fill the tank was 2114 pounds. The average weight ratio of residual fuel to fresh fuel was 0.19. A time-temperature history of the fuel and vapor in the fuselage tank is shown in Figure 11. Following refueling, the tank was pressurized with nitrogen to 17.4 PSIA and the test cycle commenced. The internal pressure of the tank was automatically reduced in accordance with the pressure schedule. At 14 minutes after start-up, the fuselage tank heaters were energized in accordance with the heating schedule ascertained during the initial test cycles. This heating schedule was established to produce the required fuselage fuel outlet temperature. At 15.5 minutes (average) after start-up when the wing tank fuel diminished, the fuel source was switched to the fuselage tank. As the fuel level dropped below each section of heated fuselage tank skin, the temperature of that section approached 500°F. The schedule provided for heating the tank until 100 minutes after start-up. At 100 minutes, the heaters adjacent to the wetted areas were de-energized to minimize the fuselage fuel outlet temperature during descent in order to approximate the overall design profile requirements.

The unwetted fuselage tank skin remained at a temperature of 500°F until tank cooling commenced at 126 minutes after test start-up. The tank cooling continued until the tank and residual fuel were sufficiently cooled so that the resultant fuel temperature after refueling was below 90°F.

Vibration of the tanks normally commenced at 126 minutes and lasted for 10 minutes; however, it was discovered during the testing that the external boost pump does not produce sufficient agitation in the fuselage tank to bring about release of the dissolved gases in the fuel as it is heated and the pressure in the tank reduced. As a result, commencing with cycle 60 the vibrator was run for the entire simulated mission.

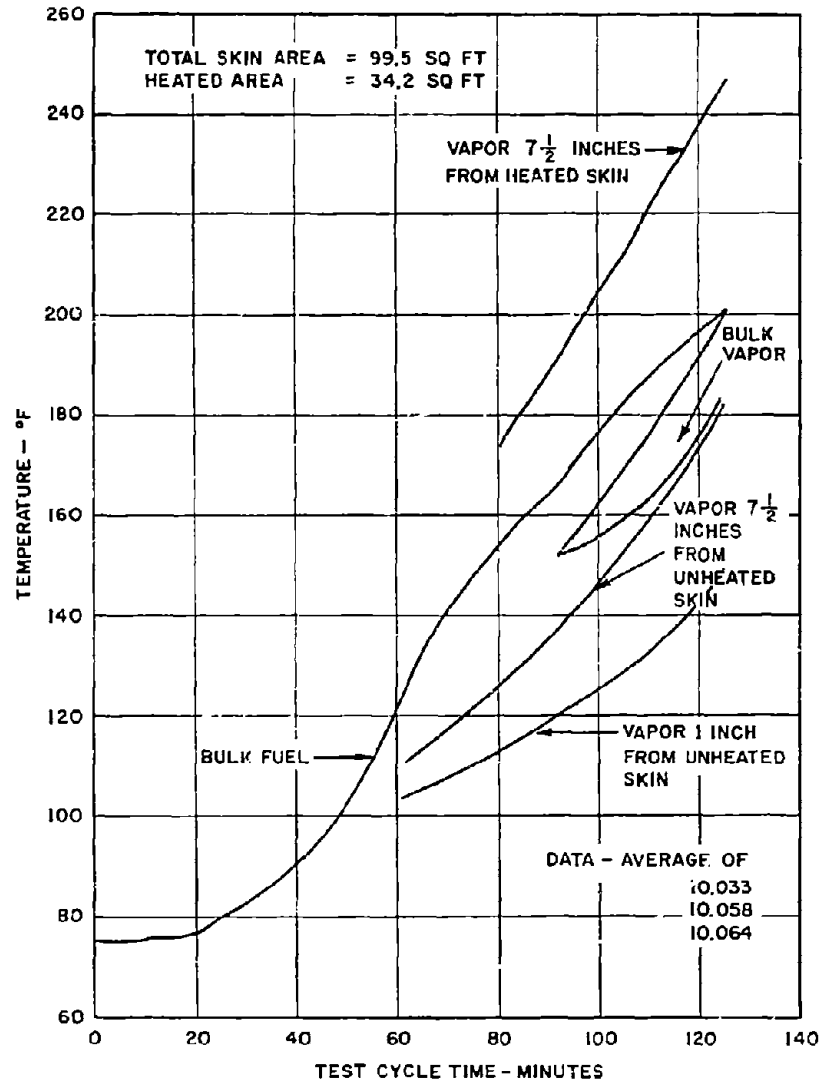


Figure 11. Time-Temperature History of Fuel and Vapor in Fuselage Tank

(3) Results

The fuselage tank was inspected after 35, 70, and 93 cycles. There was no deposit or discoloration present in the tank at these times.

c. Altitude and Inerting

(1) Operational Procedure and Results

Prior to test cycle start-up, the automatic altitude control solenoid valve and the vacuum pumps were energized and the fuselage and wing tanks pressurized to 17.4 PSIA with gaseous nitrogen. At test cycle start-up, the altitude programmer was energized and automatically controlled the tank pressure as shown in Figure 3 to within 0.5 PSI. The maximum rate of pressure reduction during simulated climb was 1.6 PSI per minute. At 16 minutes after test start, the pressure of the tanks reached 3.5 PSIA, and this pressure was maintained during cruise. At 126 minutes after test cycle start-up (beginning of descent), the pressure of the tanks was automatically increased by the addition of gaseous nitrogen to 17.4 PSIA at a maximum rate of 1.0 PSI per minute.

d. Vent Heating

(1) Operational Procedure and Results

At 16 minutes after test cycle start-up, the resistance heater tapes on the fuselage and wing tank vent lines were energized to simulate aerodynamic heating. A variable voltage control and temperature controller were used for each vent line to produce the same metal temperature at 47 minutes after testing start-up as the maximum unwetted skin temperature in the tank to which the vent line was connected. This temperature was maintained throughout the cruise portion of the test cycle. At the beginning of descent, the heater tapes were de-energized. The temperature of the fuselage and wing tank vent lines decreased at a linear rate to less than 300°F at 159 minutes. The vent lines were inspected for deposit following the test. Both vent lines were clean.

e. Fuel Condensate

(1) Operational Procedure and Results

Upon completion of each test cycle, the condensate resulting from tank fuel boil-off was drained from the vacuum system condenser tank and measured. The average amount of condensate for each of the three maximum wing tank temperature conditions; i.e. 300°, 375°, and 225°F, was 78, 197, and 0 milliliters, respectively.

f. Airframe Fuel Filter and Lines

(1) Operational Procedure and Results

Approximately 39,000 gallons of fuel ranging in temperature from 44° to 215°F passed through the airframe lines and were filtered through the 75 micron filter system during the test series. The pressure drop across the filters, measured during the climb (maximum fuel flow) condition of the test cycles, is shown in Figure 12. A small amount of debris consisting mainly of lint was found in the filter folds; however, the filter element and the filter bowl were not discolored. There was no accumulation of debris in the airframe filter system that could be related to the deposits formed in the wing tank. The lines in the airframe system were deposit free.

g. Airframe Heat Exchanger

(1) Operational Procedure

A naphthenic mineral oil was circulated through the shell side of the heat exchanger at a flow rate of 3 GPM. This oil was heated by an electrical heater, having a variable heat control, to simulate the heat rejected to the fuel by the various airframe subsystems. The heat input to the oil was set at a level established during the initial test cycles. The heater was energized at test cycle start-up and de-energized 126 minutes later. The heat input to the fuel during this period was an average of 600 BTU per minute. The average fuel temperature rise across

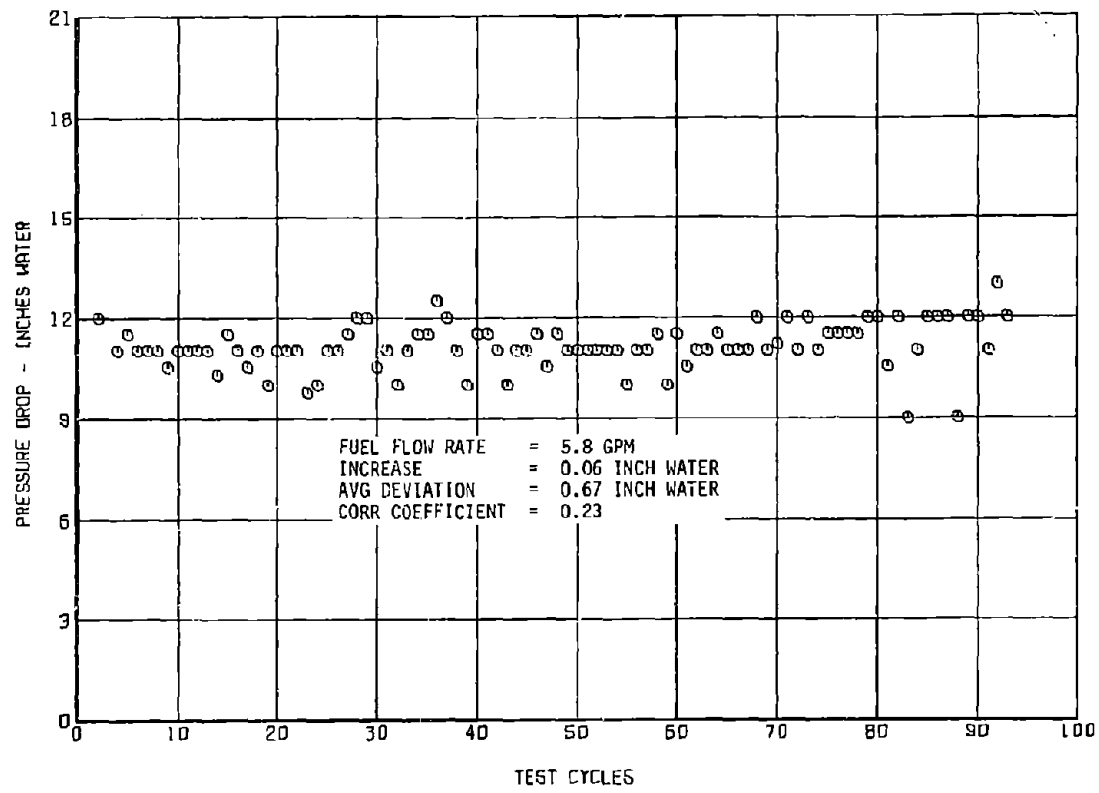


Figure 12. Pressure Drop Across Airframe Filter

the airframe heat exchanger during cruise conditions was 70°F, and a maximum fuel-out temperature of 270°F was reached during the test cycle.

(2) Results

The overall heat transfer coefficient and pressure drop of the airframe heat exchanger were determined for every other test cycle and are shown in Figures 13 and 14, respectively. The heat transfer coefficients are corrected to an average fuel temperature of 210°F in the heat exchanger. Analysis of the overall heat transfer data using the sum of the least squares method indicates that the heat transfer coefficient decreased -0.31% during the 93 test cycles with a correlation coefficient of 0.13 (Figure 13). Analysis of the pressure drop data showed the pressure drop increase was -0.24 PSI for the 93 test cycles with a correlation coefficient of -0.34 (Figure 14). These changes are not considered significant. Inspection of the heat exchanger upon completion of 93 test cycles revealed no change in the color of the surfaces exposed to either the fuel or the oil.

h. Engine Pump Subsystem

(1) Operational Procedure and Results

The pump speed and two hand controlled throttling valves (main flow and bypass) were regulated during each test cycle to produce the specified temperature increase across the pump subsystem and the required fuel flow rate. The throughput flow rate was 5.8, 2.7, and 2.7 GPM during climb, cruise, and descent, respectively. The pump bypass flow rate was 0, 3.6, and 3.3 GPM during climb, cruise, and descent, respectively. The temperature of the fuel measured immediately downstream of the pump reached a maximum of 280°F during the test cycle. The inlet and outlet were clean when they were inspected on completion of the test series.

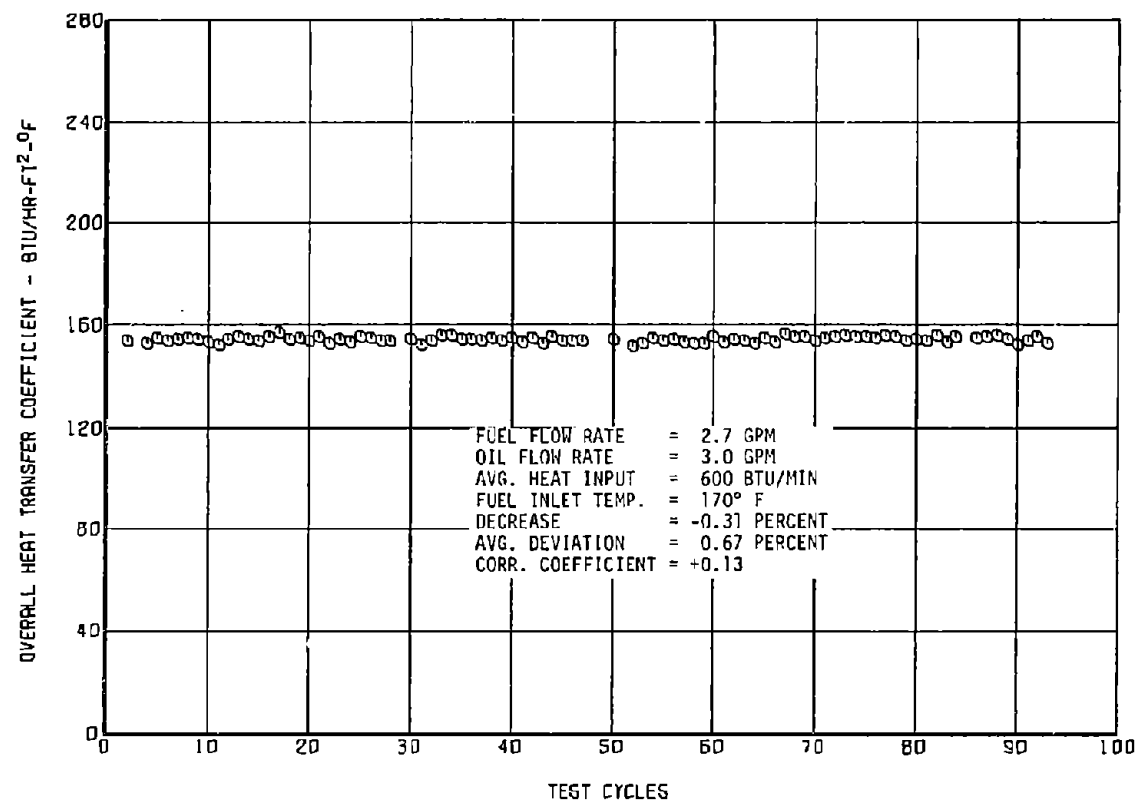


Figure 13. Overall Heat Transfer Coefficient of Airframe Heat Exchanger

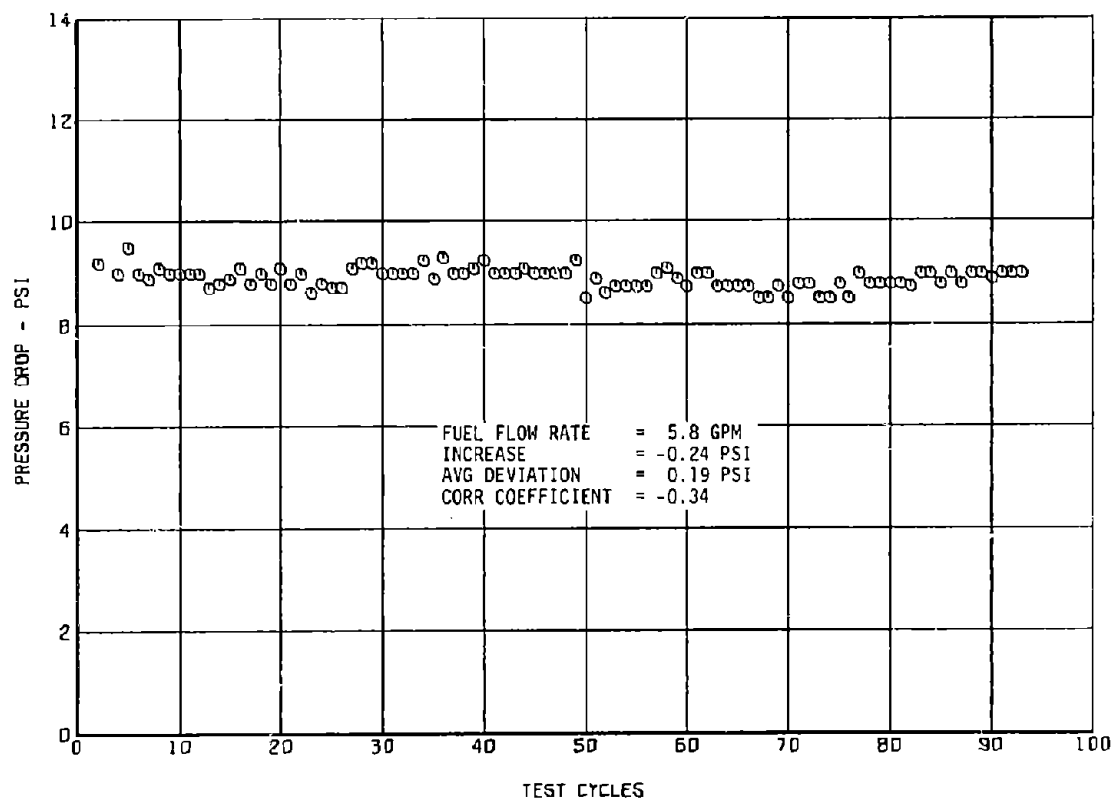


Figure 14. Pressure Drop Across Airframe Heat Exchanger

i. Engine Fuel Filter and Lines

(1) Operational Procedure and Results

Approximately 39,000 gallons of fuel ranging in temperature from 65° to 280°F were passed through the filter assembly and lines during the test series. The filter assembly contained a 2-micron nominal filter element. The element was replaced three times during the 93 test cycles due to plugging by fuel deposit generated in the heated tanks and the airframe heat exchanger. The pressure across the engine filter was measured during descent conditions and is shown in Figure 15. Replacement of the filter element was required each time the pressure drop exceeded 50 inches of water during descent. The engine fuel lines were deposit free when inspected following the test series.

j. Engine Heat Exchanger

(1) Calibration Test Procedure

The purpose of calibrating the engine heat exchanger was to:

- a. Determine more accurately the heat transfer efficiency loss by using higher heating capacity and flow rates.
- b. Determine if a calibration shift occurred.
- c. Determine if a physical change in the engine heat exchanger occurred.

The fuel was preheated in the fuselage tank to 190°F and was recirculated through the exchanger. The oil was heated to 468°F while recirculating through the shell side of the exchanger. The fuel flow rate was then adjusted to 12 GPM through the engine heat exchanger. After the fuel outlet temperature had stabilized, the test was repeated with fuel flow rates of 9, 6, and 3 GPM through the engine heat exchanger. The oil flow rate was 6 GPM for all tests.

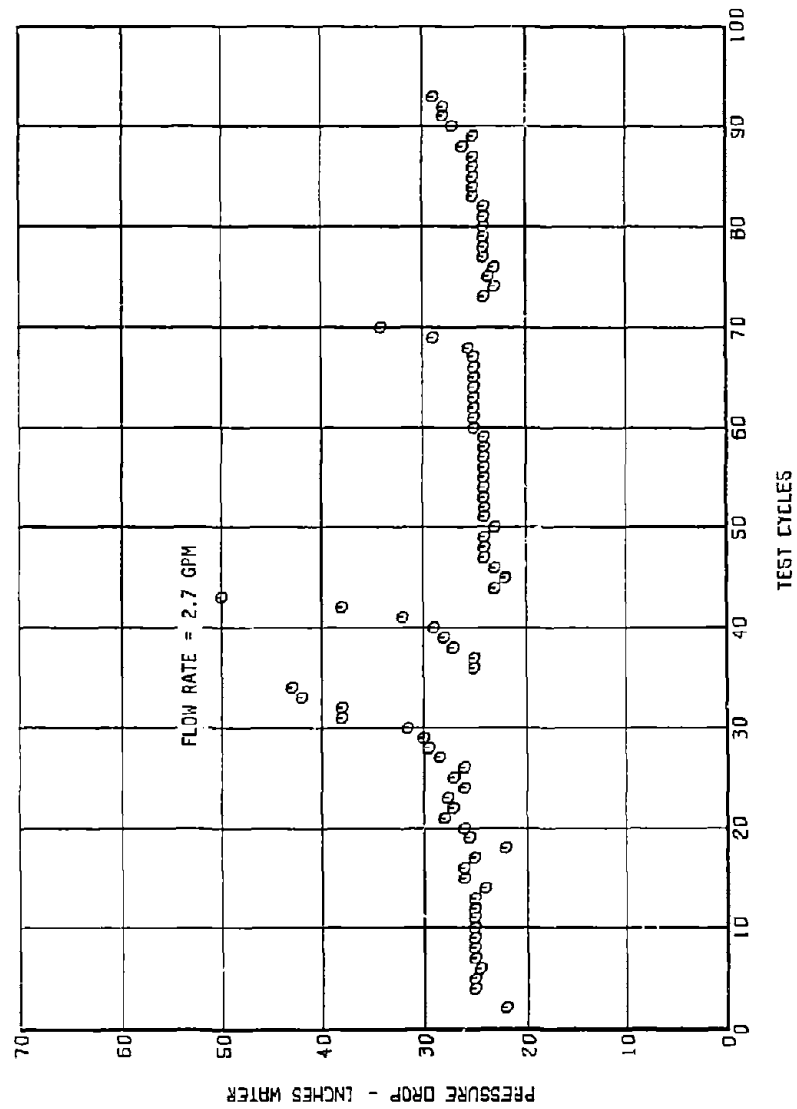


Figure 15. Pressure Drop Across Engine Filter

The heat input to the fuel was 1708 Btu per minute for the 12, 9, and 6 GPM tests and 1394 Btu per minute for the 3 GPM tests. The overall heat transfer coefficients were computed from measurements of fuel flow rate and fuel and oil temperatures. The engine heat exchanger overall heat transfer coefficients were corrected, using an empirically derived equation, to an average fuel temperature in the heat exchanger of 210°F, and an oil flow rate of 6 GPM.

The calibration was then repeated using another heat exchanger (standard) that was not used during the test series. Following the test series, both the engine and standard heat exchangers were again calibrated. The pretest and post-test series calibrations of the standard heat exchanger were conducted to determine whether any changes had occurred that would affect the comparison of the pretest and post-test series engine heat exchanger calibration test results.

(2) Calibration Results

The calculated heat transfer coefficients for the engine and standard heat exchangers, obtained during the calibration test, are shown in Figure 16. The heat transfer coefficients measured for the standard heat exchanger before and after the tenth test series decreased by 0.8, 0.9, 1.6, and 1.9 percent for the calibration flow rates of 12, 9, 6, and 3 GPM, respectively. This decrease indicates that a slight change occurred in the equipment used to measure engine heat exchanger heat transfer. The results from the engine heat exchanger calibration were corrected taking into account these equipment changes. After these corrections, the engine heat exchanger indicated a change in heat transfer coefficients from the pretest to post-test calibrations of 0.6, -0.1, -0.3, and -0.6 percent at the calibration flow rates of 12, 9, 6, and 3 GPM. These indicated changes are not considered significant.

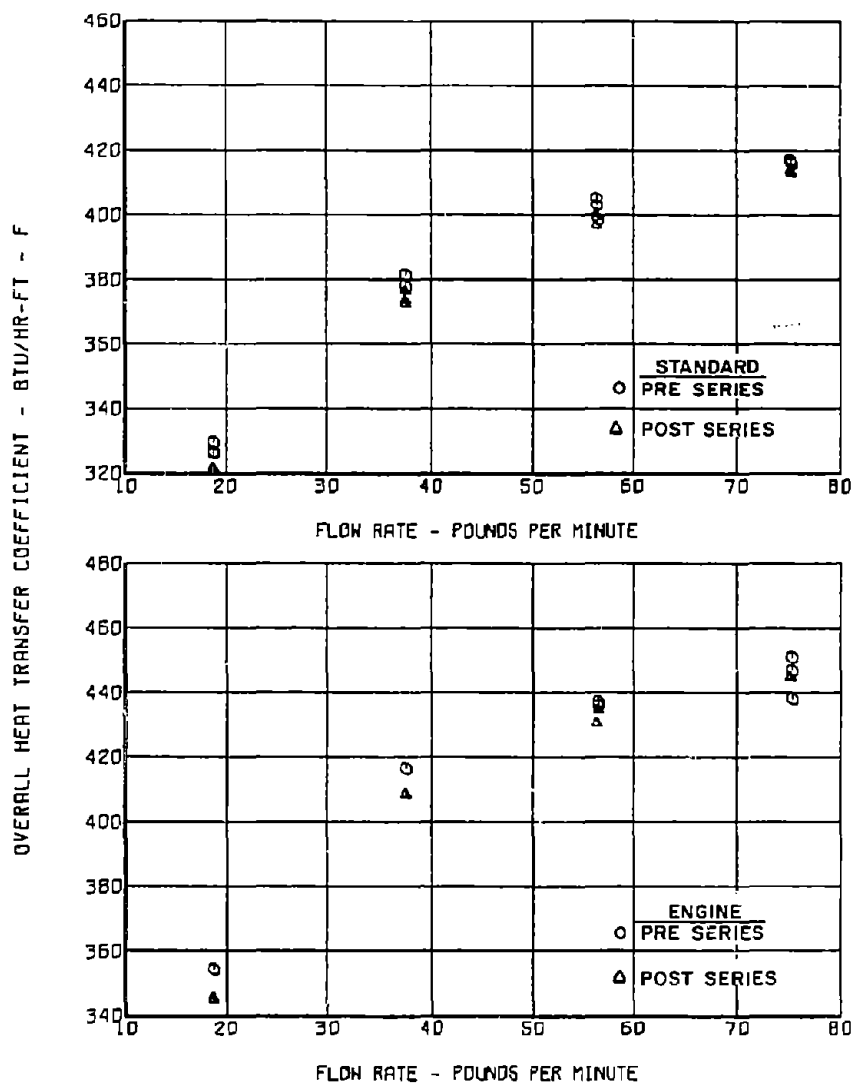


Figure 16. Engine Heat Exchanger Calibration Test Results

(3) Test Cycle Operational Procedure

A naphthenic mineral oil was circulated through the shell side of the engine heat exchanger at a flow rate of 3 GPM. This oil was heated by an electrical heater, having a variable heat control, to simulate the heat rejected to the fuel by the various engine subsystems. The heat input to the oil was set at a level established during the initial test cycles to produce the desired heat input to the fuel. The heater was energized at test cycle start-up and de-energized 126 minutes later. The heat input to the fuel during this period was an average of 537 BTU per minute. The average fuel temperature rise across the engine heat exchanger during cruise conditions was 60°F and a maximum fuel-out temperature of 340°F was reached during the test cycle.

(4) Test Cycle Results

The engine heat exchanger overall heat transfer coefficients measured during the 93 test cycles are shown in Figure 17. All values are corrected to an average fuel temperature of 210°F in the heat exchanger and an oil flow rate of 3 GPM. A linear curve fit of the data revealed a 1.26 percent decrease in the heat transfer coefficient. This indicated change is in general agreement with the instrumentation shift measured during the calibration tests. Thus, it is considered that no significant change in heat transfer occurred during the test series. This is confirmed by the visual inspection of the heat exchanger that was conducted following the testing. The heat exchanger was observed to be in a "like new" condition.

The pressure drop of the engine heat exchanger was measured and is shown in Figure 18. A least-squares, straight-line curve fit of the data showed that the pressure drop across the engine heat exchanger decreased 0.37 percent which is considered insignificant.

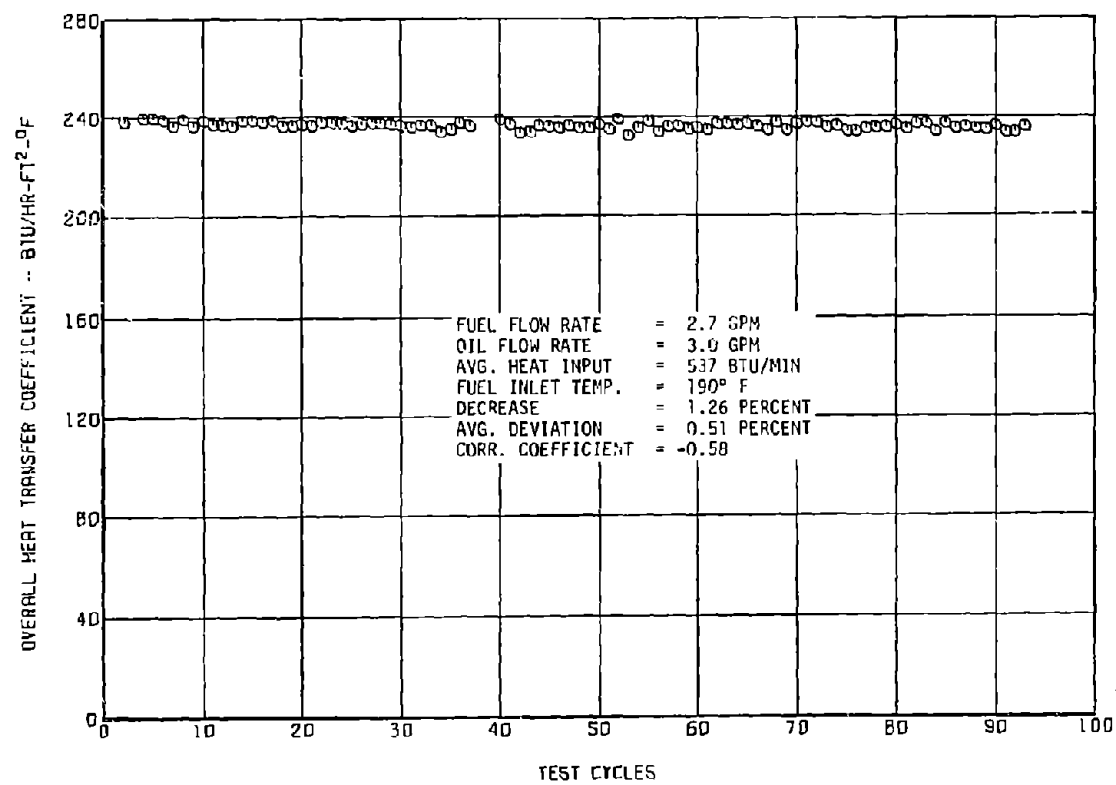


Figure 17. Overall Heat Transfer Coefficient of Engine Heat Exchanger

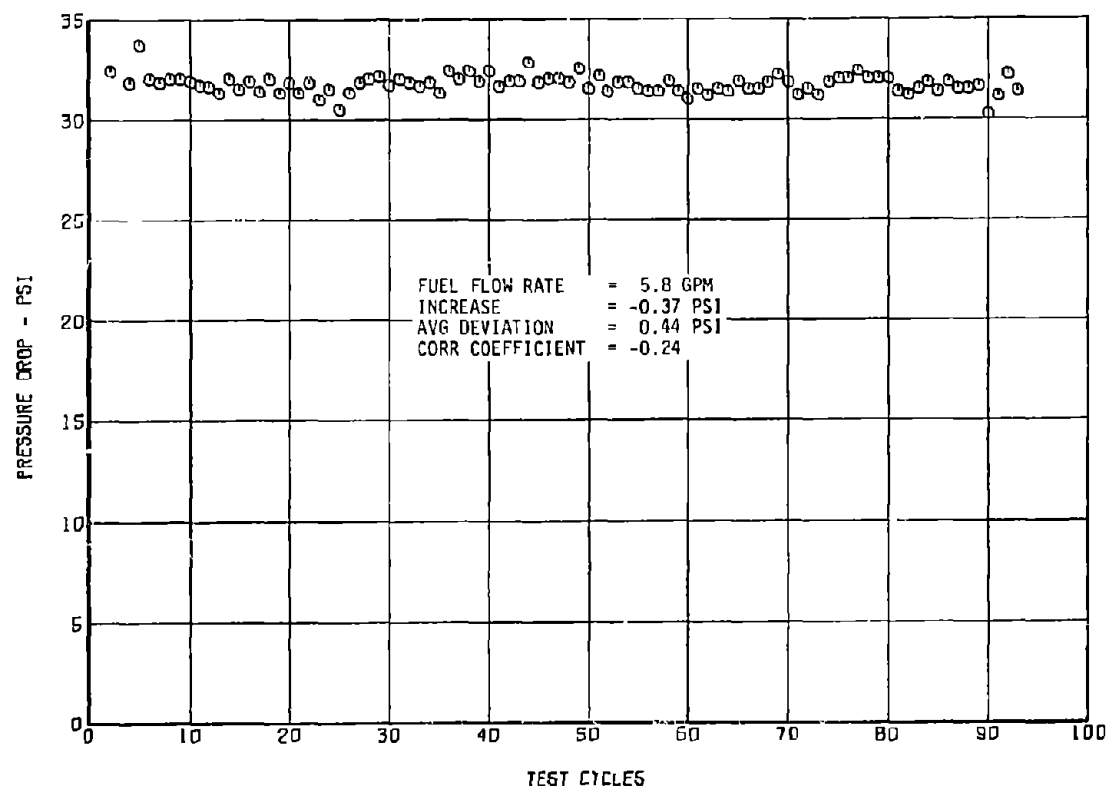


Figure 18. Pressure Drop Across Engine Heat Exchanger

k. Manifold

(1) System Revision

The manifolds subjected to testing in prior test series have all had electrical tabs welded to the center and ends of the manifold as shown in Figure 19 (a). A decision was made to omit both center tabs and the bottom tabs at each end of the manifolds as shown in Figure 19 (a). This change necessitated the addition of an isolation fitting upstream of the manifold to prevent electrification of the entire Simulator. The heat loss caused by the center tab was eliminated by this modification and the accuracy with which the deposit thermal resistance can be calculated was improved.

(2) Operational Procedure

The tubing used to simulate the manifold section was 321 stainless steel (.3125 inch OD by 0.028 inch wall by 120 inches long). Electrical connector tabs were welded to the ends of the manifold tube to permit terminal resistance heating. The heating power supply (four-10 KW DC welders connected in parallel) was energized at test start-up and produced the fuel temperatures shown in Figure 5. The same heat input (840 BTU/MIN) was used for both climb and cruise conditions. During descent, when the fuel flow rate was decreased from 2.7 GPM to 0.68 GPM, the fuel outlet temperature increased to 600°F. Maximum temperature was obtained within 1 minute and then was slowly decreased in accordance with the profile requirements by decreasing the power supply output.

The manifold was instrumented with ten 0.040-inch OD stainless steel sheathed thermocouples tack-welded to the outer wall. The thermocouples were equally spaced along the manifold. The temperatures obtained from these thermocouples were used to calculate the deposit thermal resistance (DTRMIL) by the method described in Appendix I. The acronym DTRMIL is used since the standard units for deposit thermal resistance, viz., $\text{FT}/(\text{BTU-FT/SQ FT-HR-}^{\circ}\text{F})$, have been multiplied by 1200 MIL/FT

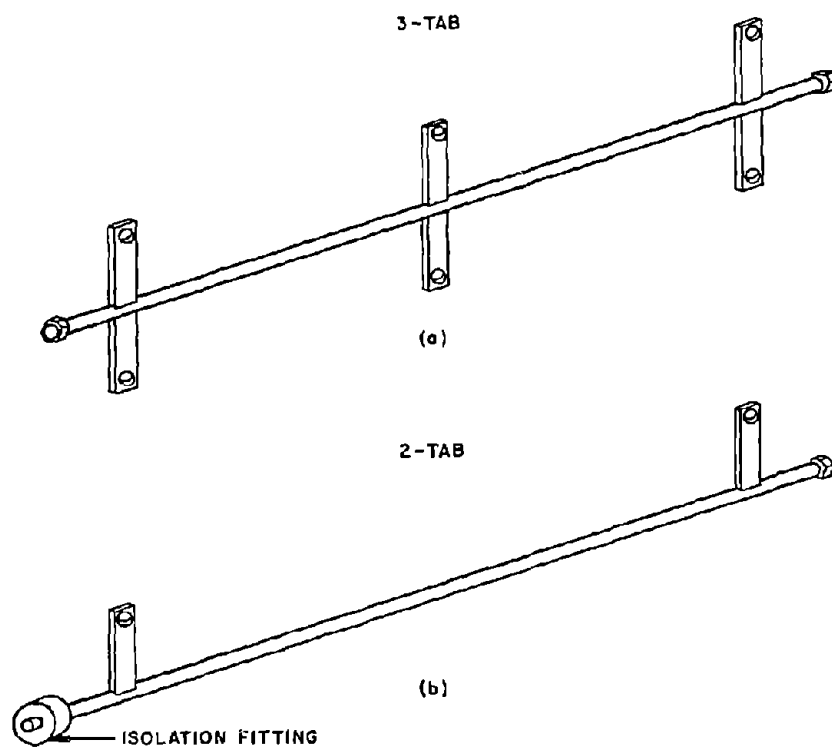


Figure 19. Manifold Electrical Connection Locations

throughout this report. The method described in Appendix I provides a significant improvement in the accuracy of calculation of DTRMIL, particularly at low deposit levels.

(3) Results

Two manifolds were subjected to testing, the first one being replaced following test cycle 59. Manifold performance data are composed of the following three groups:

- (a) DTRMIL calculated from test cycle data.
- (b) Micrometer measurements of deposit thickness.
- (c) Pressure drops recorded during testing.

The values of DTRMIL calculated for each of the 10 thermocouple locations for the first manifold are shown in Figure 20. A single first order curve fit was used for each thermocouple location to obtain the deposition rate over the linear range of deposit formation (test cycles 20 through 59). These values, along with the correlation coefficients and the total changes in DTRMIL, are shown in Table III.

The total change in DTRMIL was used to calculate the deposit thickness at each thermocouple for deposit thermal conductivities of 0.05, 0.07, and 0.09 BTU-ft/ft²-hr-°F. These values are plotted in Figure 21. The method used to calculate the deposit thickness is presented in Appendix I. In the calculations, it is necessary to use different values for the thermal conductivity of the deposit at different locations in the manifold. Photomicrographs of deposits showing the wide range of deposit porosity are shown on page 64 of Reference 6. It is apparent that the various forms of the deposit will have different average values of thermal conductivity.

Testing was stopped on the second manifold after having completed 34 test cycles when it became evident that the results were not

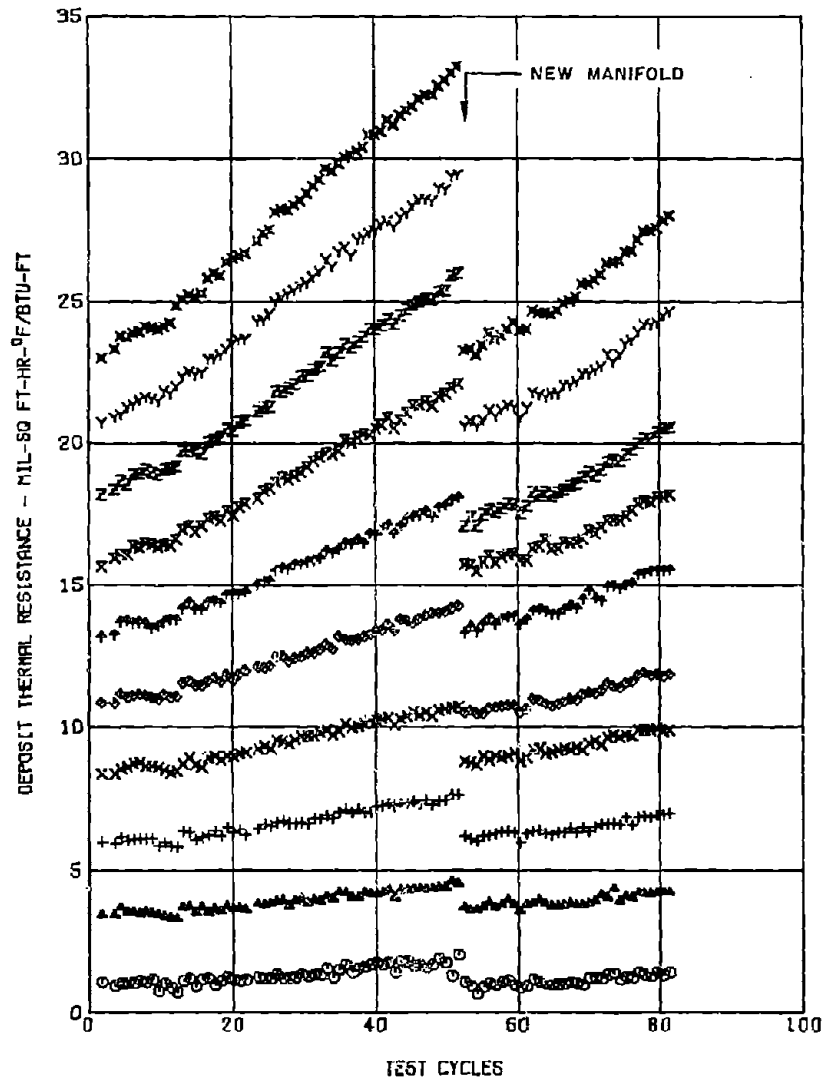


Figure 20. Calculated Deposit Thermal Resistance of the Cyclic Test Series Manifold

TABLE III
SUMMARY MANIFOLD DATA - 10TH TEST SERIES

THERMOCOUPLE NUMBER	DISTANCE FROM INLET ELECTRICAL TAB (INCHES)	CALCULATED MAX FILM TEMP ° F	RATE OF CHANGE IN DTRMIL		CORRELATION COEFFICIENT	TOTAL CHANGE IN DTRMIL (59 CYCLES)
			RANGE (Cycles)	RATE (DTRMIL CYCLE)		
1	5.75	355.0	20-59	0.0189	0.850	0.838
2	17.25	365.5	20-59	0.0229	0.960	1.017
3	28.75	372.0	20-59	0.0345	0.979	1.673
4	40.25	377.0	20-59	0.0467	0.987	2.397
5	51.75	389.0	20-59	0.0672	0.993	3.388
6	63.25	392.5	20-59	0.0921	0.996	4.741
7	74.75	402.1	20-59	0.1213	0.996	6.509
8	86.25	414.1	20-59	0.1466	0.997	7.897
9	97.75	418.1	20-59	0.1636	0.995	9.051
10	109.25	425.1	20-59	0.1862	0.998	10.361

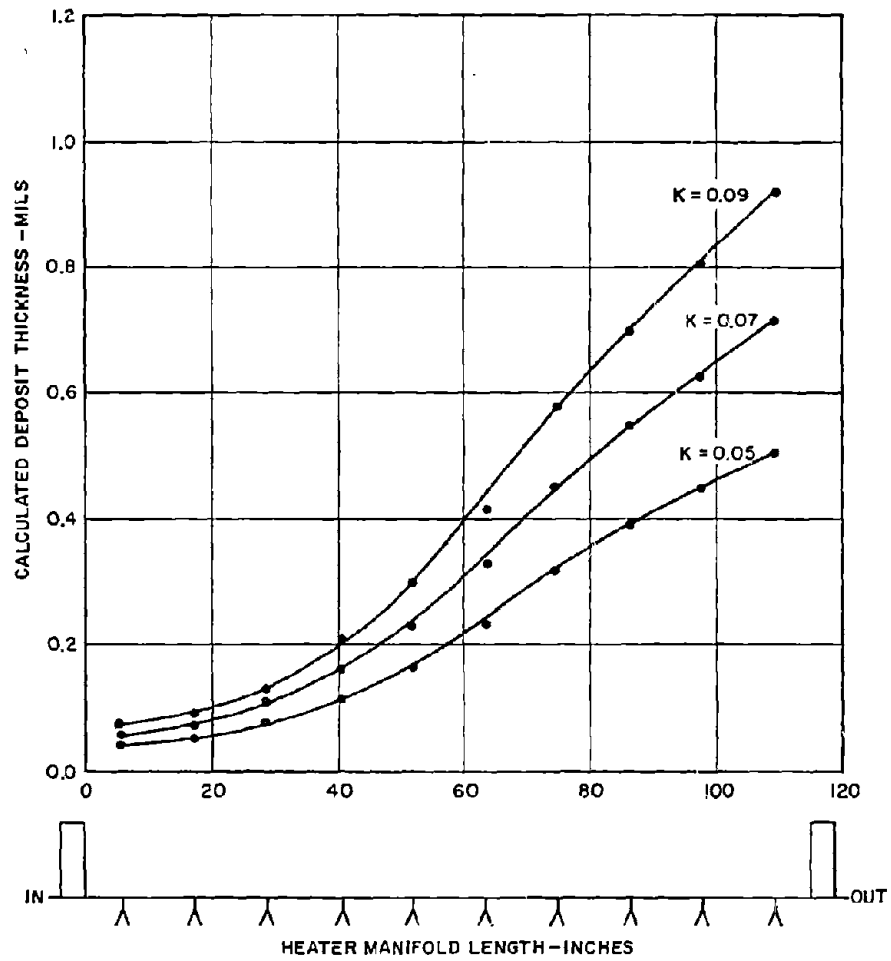


Figure 21. Cyclic Test Series Manifold Calculated Deposit Thickness

significantly different than the results obtained for the first manifold. A comparison of the results from the two manifolds are shown in Table IV.

Micrometer measurements of deposit thickness were obtained using the procedure presented in Appendix II. The results of these measurements are shown in Figure 22 along with the calculated deposit thicknesses. Deposit thickness measurements obtained using a micrometer are often less than the actual deposit thickness. For example, a small percentage of the deposit is lost due to the vibration produced in dissecting the tubes. Also, it has been observed that the 0.185 inch diameter cylinder used in the measuring process compresses the fine powdery surface of the deposit to some degree.

The pressure drop of the manifold was measured during the cyclic test series and is shown in Figure 23. Analysis of the data by the sum-of-least-squares method showed an increase in pressure drop of 8.7 PSI.

1. Nozzle Subsystem

(1) Operational Procedure

The nozzle heaters were energized at test startup and the output controlled to produce a temperature rise of 2°F during the cruise condition and 8°F during the descent condition. The same heat input was used for the acceleration condition. The nozzle heater was de-energized at 159 minutes after test start-up. The temperature of the fuel into the nozzle reached a maximum of 600°F during the test cycle.

(2) Results

The nozzle element was replaced following test cycle 59 when the manifold was replaced. The results of the measurement of pressure drop are shown in Figure 24. The pressure drop increase during the

TABLE IV
COMPARISON OF RATE OF CHANGE IN DTRMIL
BETWEEN TWO MANIFOLDS USED DURING 10TH TEST SERIES

<u>THERMOCOUPLE NUMBER</u>	<u>RANGE (CYCLES)</u>	<u>RATE DTMIL/CYCLE</u>	<u>CORRELATION COEFFICIENT</u>
1	15-34	0.0111	0.660
1	74-93	0.0235	0.879
2	15-34	0.0180	0.778
2	74-93	0.0286	0.854
3	15-34	0.0275	0.841
3	74-93	0.0397	0.959
4	15-34	0.0503	0.950
4	74-93	0.0470	0.959
5	15-34	0.0581	0.952
5	74-93	0.0639	0.970
6	15-34	0.0886	0.973
6	74-93	0.0886	0.975
7	15-34	0.1137	0.986
7	74-93	0.1098	0.990
8	15-34	0.1461	0.989
8	74-93	0.1303	0.995
9	15-34	0.1780	0.993
9	74-93	0.1586	0.991
10	15-34	0.1959	0.992
10	74-93	0.1846	0.997

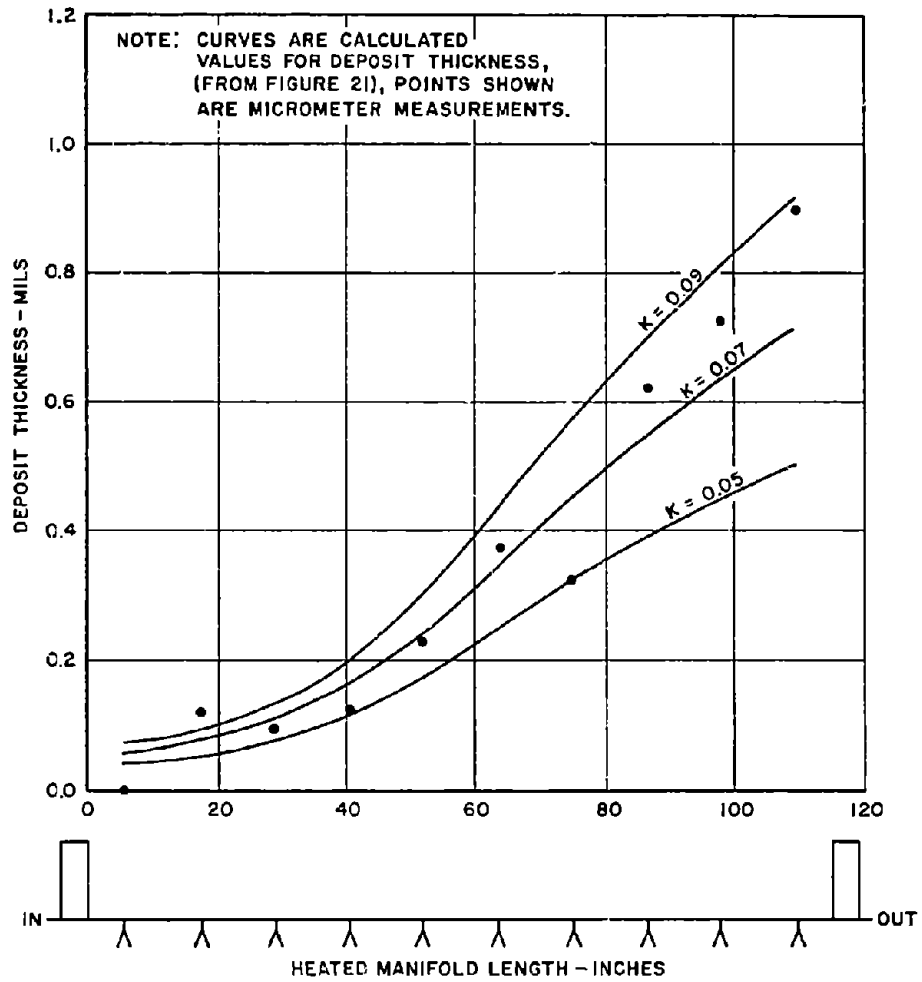


Figure 22. Cyclic Test Series Manifold Measured Deposit Thickness

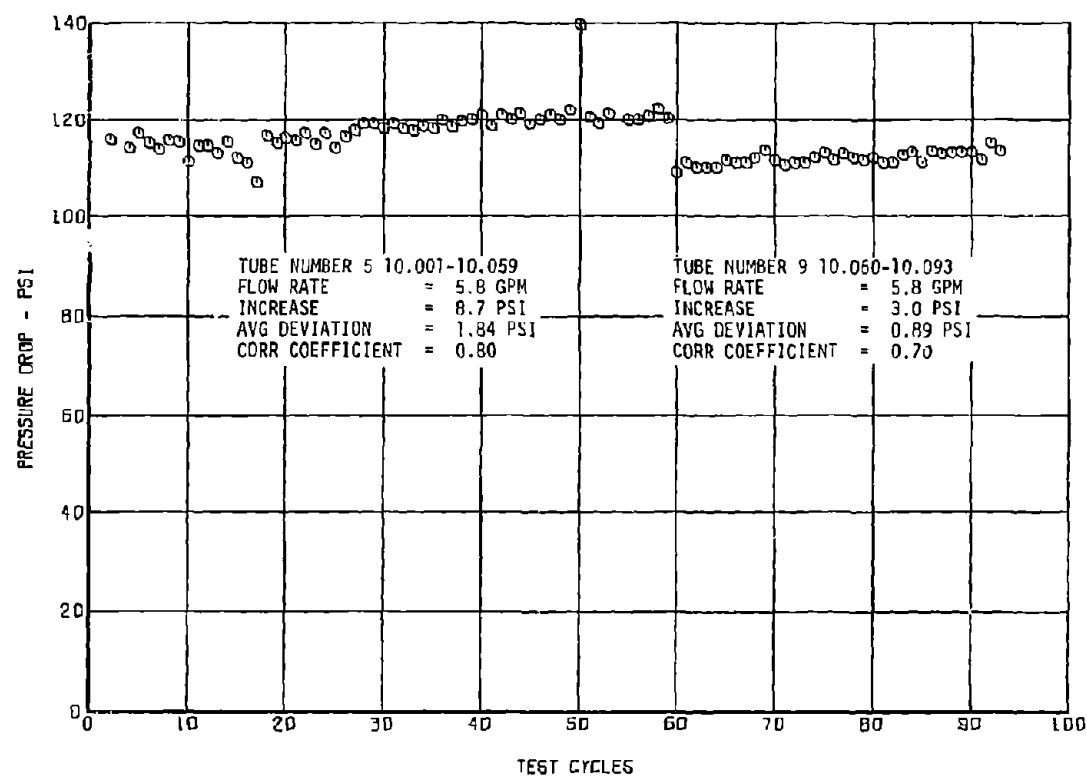


Figure 23. Pressure Drop Across Manifold

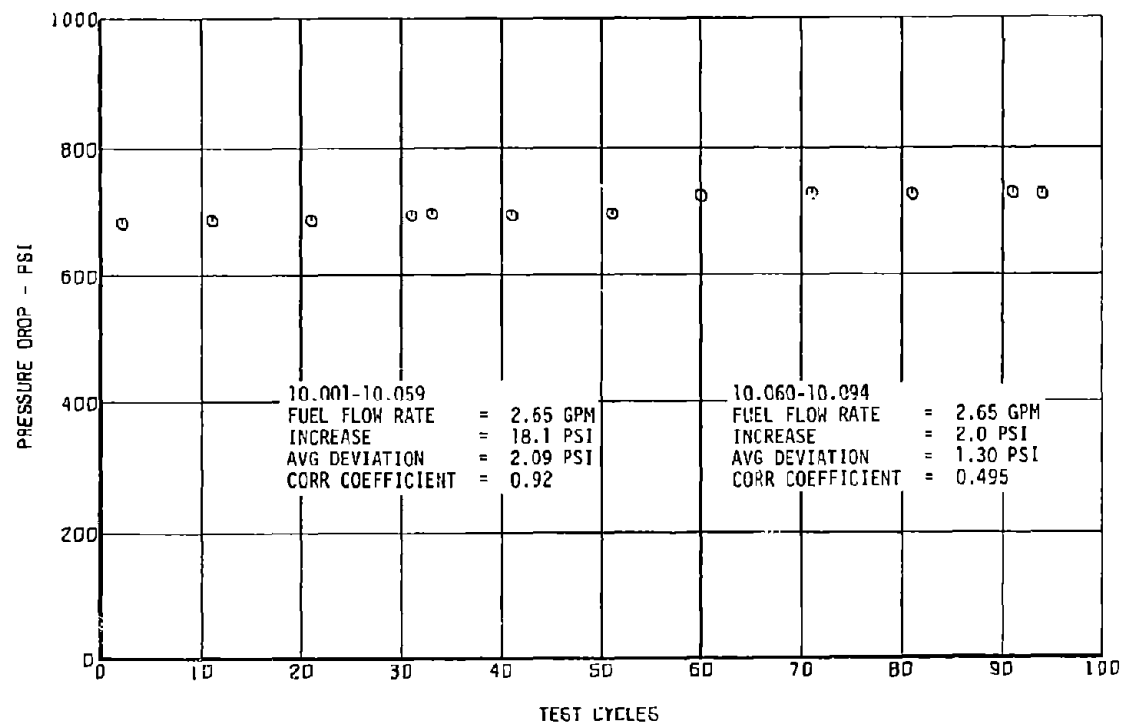


Figure 24. Pressure Drop Across Engine Nozzle

AFAPL-TR-73-95

test series for each of the two nozzles was 18.1 and 2.0 PSI for the first and second nozzles, respectively. The nozzle screens were covered with a brown, powdery deposit rating 9 and 8 on the CRC Lacquer Rating Scale for the first and second nozzle screens, respectively.

SECTION IV

SIMULATOR STEADY-STATE MANIFOLD TESTS

Steady-state manifold tests were conducted to determine the rate of deposit formation under constant temperature conditions. Steady-state test results are compared to the data obtained during cyclic tests and used to provide a basis of correlation to the small-scale tests which are operated in a steady-state manner. Only the manifold was tested under steady-state conditions since it was the only system component yielding sufficient quantitative deposit formation data during the cyclic tests. Since the rate of deposit formation is affected by the flow rate, see References 4 and 5, the steady-state tests included periods of simulated acceleration flow rate.

1. STEADY-STATE OPERATIONAL PROCEDURE AND RESULTS

a. System Revision

As previously indicated for the cyclic manifolds, a decision was made to omit the center tabs and the bottom tabs at each end of the manifolds as shown in Figure 19. This revision reduced the heat lost and improved the accuracy of the data analysis.

b. Operational Procedure

Three separate tests were conducted. The first test, identified as 10.801, ran for 60 hours with fuel inlet and outlet temperatures of 200°F and 460°F, respectively. The entire test was run at steady-state conditions with a flow rate of 0.68 GPM except for one 22 minute period of flush flow rate (5.8 GPM) at 53 hours.

The second test, identified as 10.802, ran for a total of 70 steady-state hours. The entire test was run under steady-state-flush conditions consisting of 22 minutes of flush flow rate after each hour of steady-state conditions as shown in Figure 25. The third test, identified as 10.803, was conducted under steady-state conditions (no flushing) using one of the three-tab type manifolds to provide a comparison between the two types of manifolds.

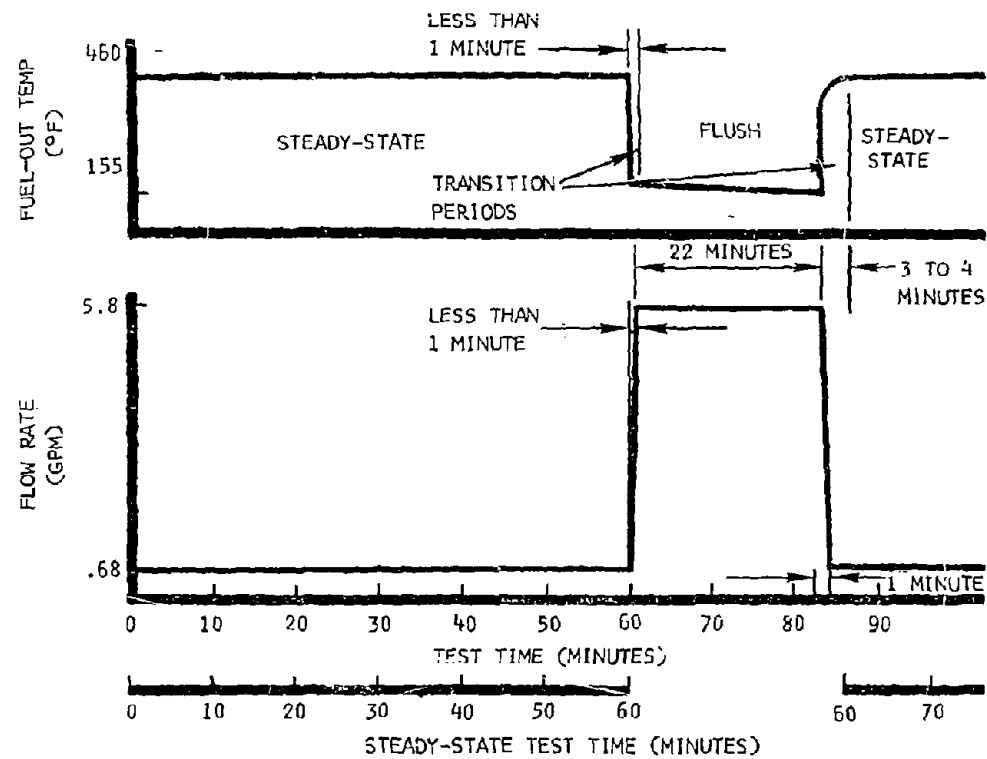


Figure 25. Steady-State-Flush Test Conditions

The tank pressure was 3.5 PSIA during all of the steady-state testing. This reduction in pressure was accompanied by a reduction in the dissolved oxygen in the fuel. The oxygen concentration in the system was measured during one of the steady-state tests as the fuel flowed through the system. The results indicate that the oxygen concentration of the incoming fuel was 68 PPM by weight. The reduced tank pressure lowered the dissolved oxygen of the fuel exiting the tank and entering the manifold to 20 PPM. Oxygen consumption in the hot manifold further reduced the oxygen concentration to 10 PPM.

c. Results

(1) Deposit Thermal Resistance

The temperature, electrical power, and flow rate data from each test were used to calculate the deposit thermal resistance (DTRMIL) in the manifold. The calculation method is presented in Appendix I. Plots of DTRMIL for each of the ten thermocouples for each of the three manifolds are shown in Figures 26, 27, and 28. The curves for each of the ten thermocouples on each manifold were offset from zero to improve readability. A statistical analysis was conducted to determine the rate of change in DTRMIL, the correlation coefficient, and the total change in DTRMIL. The results of the analysis performed on the data from each manifold are summarized in Tables V, VI, and VII.

The effect of the flushing action at 53 hours for manifold 10.801 is evident in Figure 26 for thermocouples 8, 9, and 10. Another indication of the effect of flushing can be obtained by comparing the results obtained on manifold 10.801 versus the results obtained on manifold 10.802. The comparison reveals that the rate of change of DTRMIL for the steady-state-flush test (10.802) is only 25% of the rate obtained without flushing (10.801).

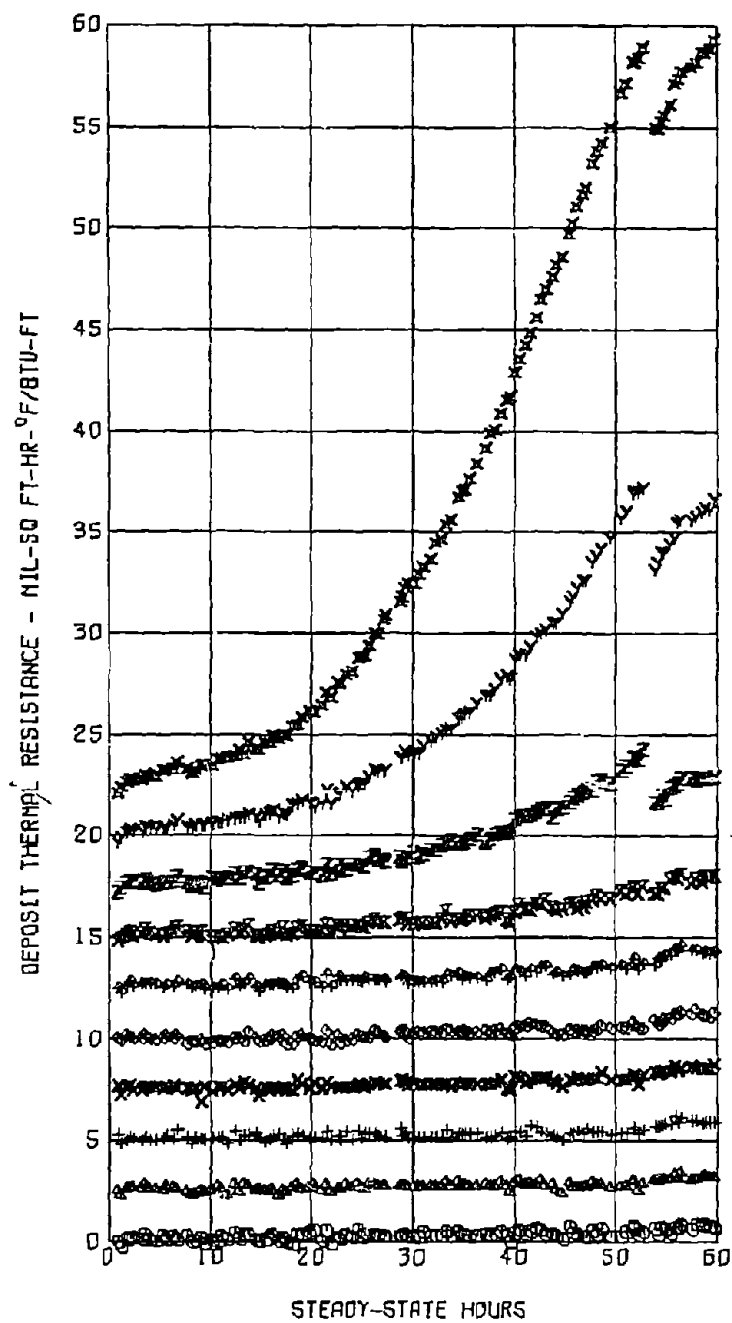


Figure 26. Calculated DTRMIL for Test 10.801

TABLE V
SUMMARY OF MANIFOLD DATA 10.801

THERMOCOUPLE NUMBER	DISTANCE FROM INLET ELECTRICAL TAB (INCHES)	CALCULATED MAX. FILM TEMP. °F	RATE OF CHANGE IN DTRMIL RANGE (HRS) RATE		CORRELATION COEFFICIENT	TOTAL CHANGE IN DTRMIL
1	5.75	411.7	40.1-52.6	.0028	.0699	.356
1*			53.9-59.7	.0470	.627	.273
2	17.25	429.2	40.1-52.6	-.0044	-.1120	.197
2*			53.9-59.7	.0143	.247	.083
3	28.75	447.1	40.1-52.6	.0039	.0982	.348
3*			53.9-59.7	.0202	.2886	.117
4	40.25	465.4	40.1-52.6	.0062	.171	.460
4*			53.9-59.7	.0397	.664	.231
5	51.75	484.2	40.1-52.6	.00628	.144	.495
5*			53.9-59.7	.0648	.636	.377
6	63.25	503.3	40.1-52.6	.0299	.594	.989
6*			53.9-59.7	.0586	.539	.341
7	74.75	523.0	40.1-52.6	.0790	.852	2.095
7*			53.9-59.7	.1094	.718	.636
8	86.25	542.9	40.1-52.6	.2529	.976	6.052
8*			53.9-59.7	.2035	.888	1.184
9	97.75	563.3	40.1-52.6	.6914	.994	16.472
9*			53.9-59.7	.5094	.956	2.963
10	109.25	584.1	40.1-52.6	1.259	.999	35.87
10*			53.9-59.7	.734	.972	4.274

* AFTER FLUSH AND STEADY STATE RESUMED

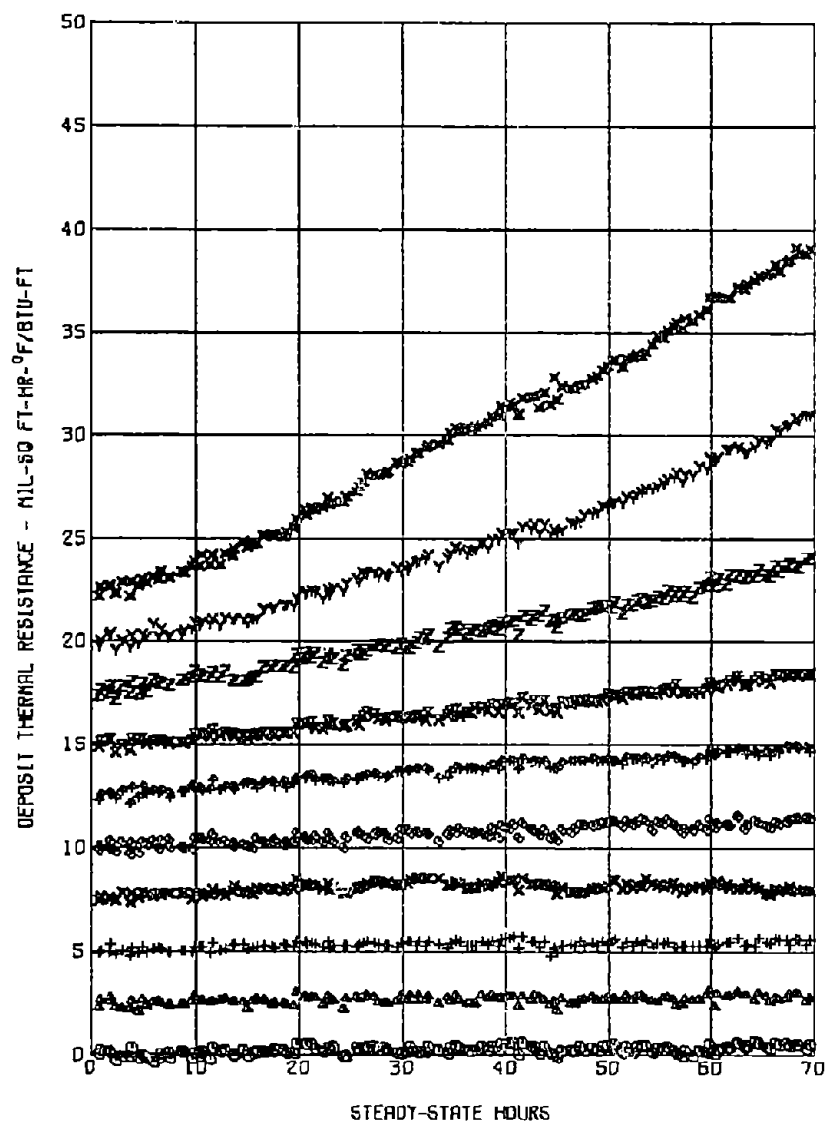


Figure 27. Calculated DTRMIL for Test 10.802

TABLE VI
SUMMARY OF MANIFOLD DATA 10.802

Thermocouple Number	Distance from Inlet Electrical Tab (Inches)	Calculated Max Film Temp °F	Rate of Change in DTRMIL		Correlation Coefficient	Total Change in DTRMIL
			Range (Hrs)	Rate		
1	5.75	409.3	0 - 69.7	.0059	.573	.389
2	17.25	424.3	0 - 69.7	.0045	.476	.311
3	28.75	442.4	0 - 69.7	.0052	.591	.360
4	40.25	453.4	0 - 69.7	.0050	.427	.348
5	51.75	479.4	0 - 69.7	.0185	.897	1.292
6	63.25	500.4	0 - 69.7	.0316	.976	1.637
7	74.75	524.4	45 - 69.7	.0588	.957	3.33
8	86.25	538.4	45 - 69.7	.1119	.981	6.253
9	97.75	563.5	45 - 69.7	.2161	.995	10.633
10	109.25	586.5	45 - 69.7	.289	.996	16.327

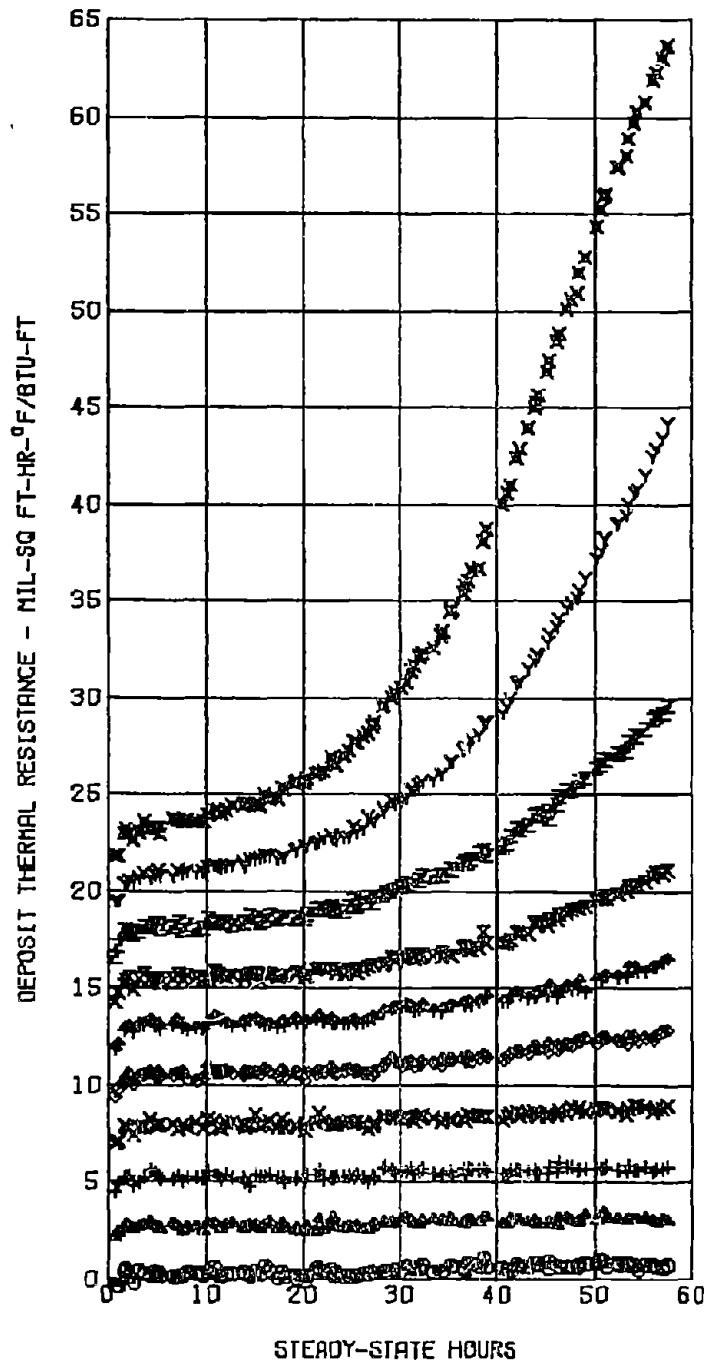


Figure 28. Calculated DTRMIL for Test 10.803

TABLE VII
SUMMARY OF MANIFOLD DATA 10.803

THERMOCOUPLE NUMBER	DISTANCE FROM INLET ELECTRICAL TAB (INCHES)	CALCULATED MAX. FILM TEMP. °F	RATE OF CHANGE IN DTRMIL		CORRELATION COEFFICIENT	TOTAL CHANGE IN DTRMIL
			RANGE (HRS)	RATE		
1	5.75	428.2	45.1 - 57.5	-.0024	-.085	1.14
2	17.25	445.0	"	.0057	.161	.90
3	28.75	462.2	"	.0012	.041	1.36
4	40.25	481.7	"	.0223	.532	1.93
5	51.75	496.2	"	.0562	.802	3.56
6	63.25	503.6	"	.1343	.942	4.71
7	74.75	523.7	"	.2126	.994	6.81
8	86.25	540.7	"	.4302	.995	12.96
9	97.75	559.7	"	.8803	.998	24.71
10	109.25	582.7	"	1.3564	.998	41.80

(2) Visual Inspection

The manifold tubes from the three steady-state tests were bisected for visual inspection. The deposit appears to gradually increase along the tube from the inlet to the outlet. That is, no sudden breakpoint is evident in any of the three manifolds. Deposit color changed from light blue-gray at the inlet to dark brown at the outlet. The deposit on manifold 10.802 appears to be darker than the deposit on either of the other two manifolds. This is probably due to the length of the test but may be due to the longer time required to lay down the same amount of deposit. That is, the deposit on the steady-state-flush manifold was subjected to more time at high temperature.

(3) Micrometer Measurements of Deposit Thickness

Deposit thicknesses were measured using a micrometer for comparison to the calculated values. The technique used is described in Appendix II. These measurements and the calculated deposit thicknesses at deposit thermal conductivities of 0.05, 0.07, and 0.09 BTU-ft/ft²-hr-°F are shown in Figure 29. The graph indicates that the thermal conductivity increases from approximately 0.05 at the inlet to 0.08 at the outlet.

(4) Comparison to Past Fuels

The deposit formation rates from tests 10.801 and 10.802 were compared to the deposit formation rates from past tests of other fuels. The results are shown in Figures 30 and 31. For both types of tests, i.e., steady-state and steady-state-flush, the data indicates that the thermal stability of AFFB-14-70 is approximately midway between the thermal stabilities of fuels AFFB-9-67 and AFFB-10-67.

(5) Correlation of Steady-State-Flush and Test Cycle Data

Data from steady-state-flush test 10.802 was correlated to test cycle data. This was done by predicting the deposit formation rate per test cycle based on the steady-state-flush data and comparing these results with those measured from cyclic tests. Prediction is made on the basis

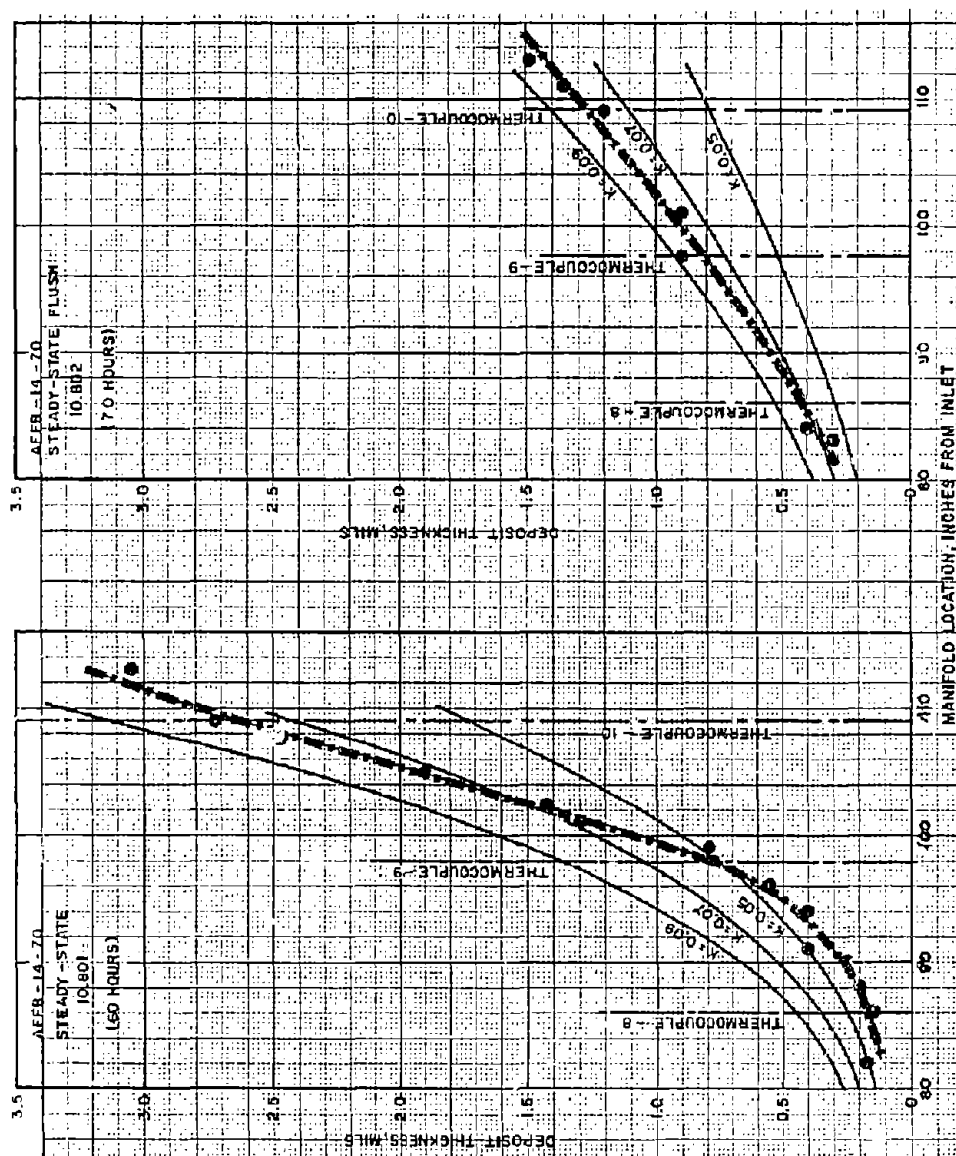


Figure 29. Comparison of Calculated and Measured Deposit Thicknesses

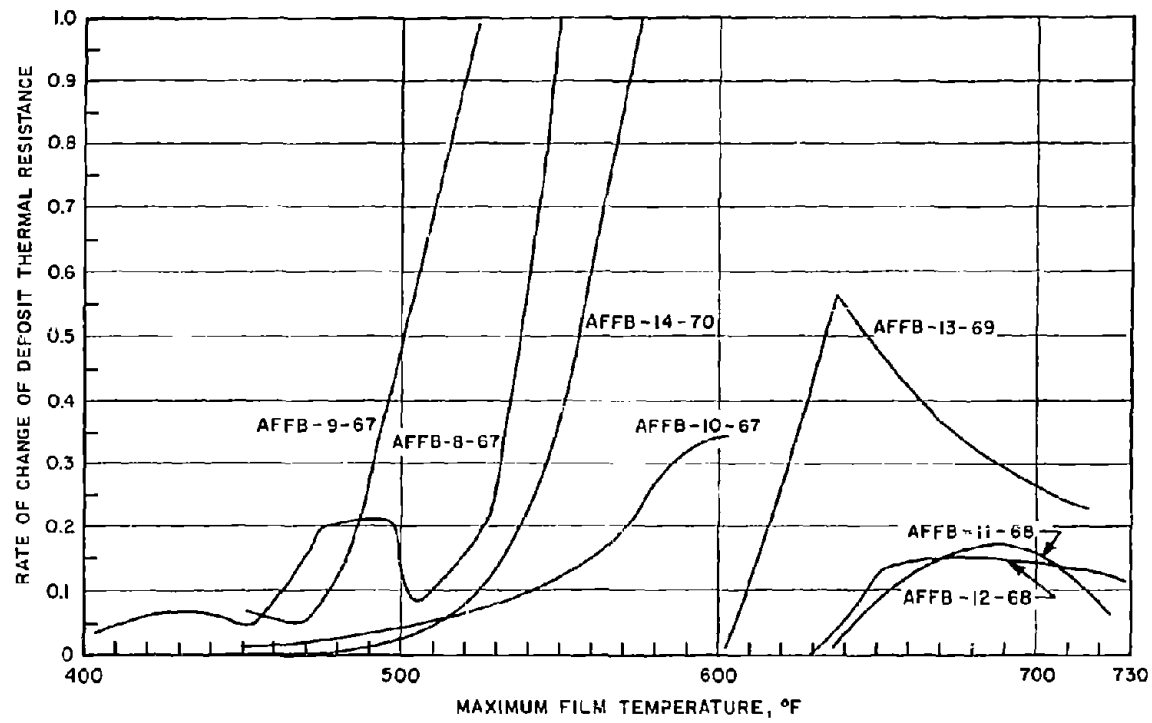


Figure 30. Comparison of Steady-State Deposit Rates

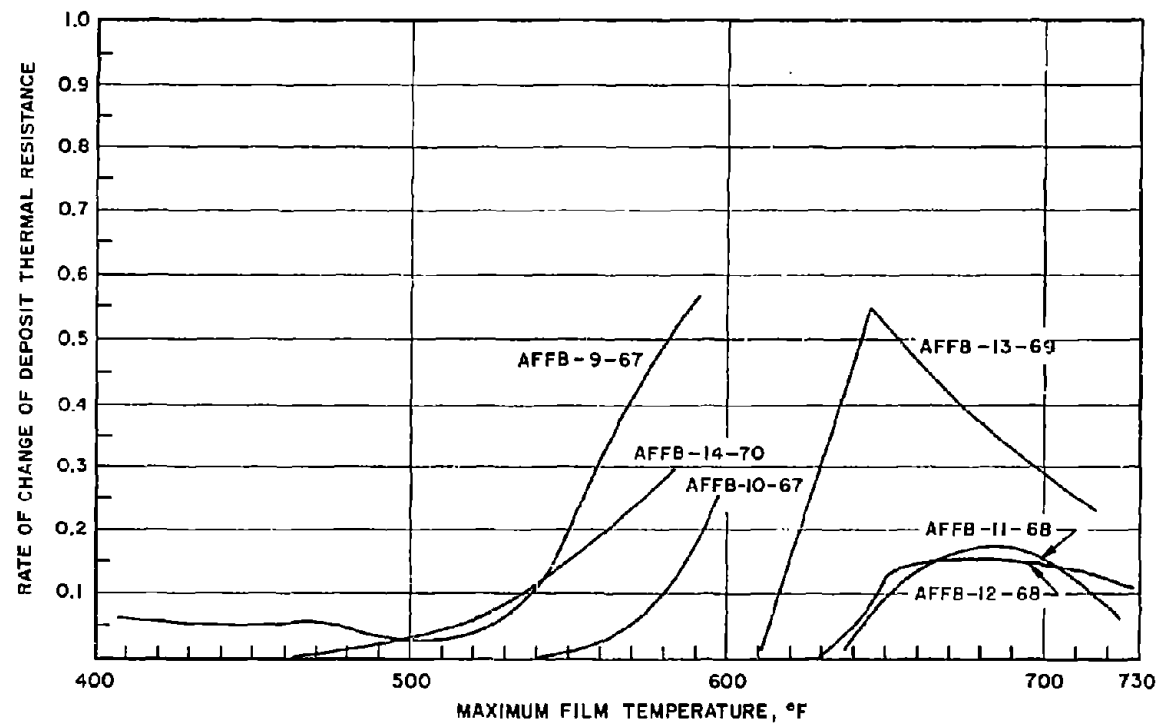


Figure 31. Comparison of Steady-State-Flush Deposit Rates

of a spectrum of fuel temperatures from the maximum film temperature to the average stream temperature. The initial outer wall temperature profile (temperature versus test cycle time) was used to calculate the maximum film temperature profile for each thermocouple. Using this profile along with the steady-state-flush curve of rate of change of deposit thermal resistance versus maximum film temperature (Figure 31), deposit rate versus test cycle time can be plotted. The area under this curve is the predicted deposit thermal resistance per test cycle for each thermocouple position.

The predicted test cycle deposit rates based on average stream temperature were found by the same method except that a plot of the rate of change of deposit thermal resistance versus average stream temperature was used and the average stream temperature profile was found by a linear interpolation of manifold inlet and outlet temperatures.

Figure 32 shows the predicted deposit thermal resistance per test cycle and the measured values. The measured rates compare more closely to rates based on the average stream temperature than to rates based on the maximum film temperature.

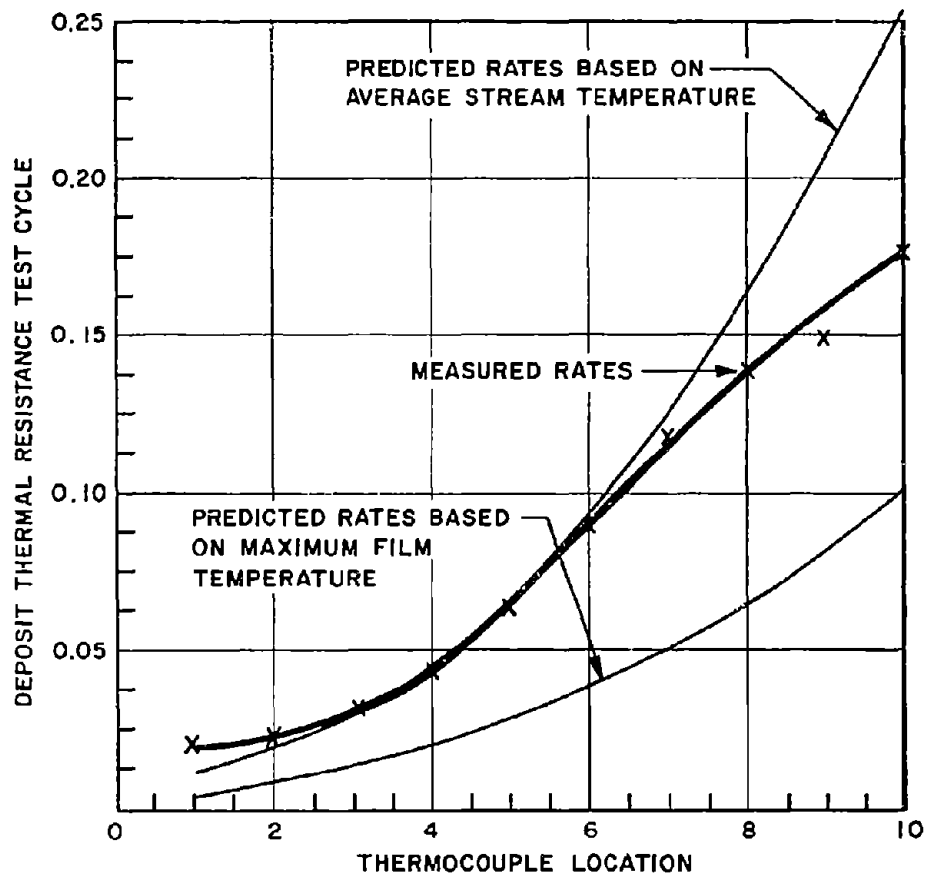


Figure 32. Comparison Between Steady-State-Flush Data and Test Cycle Data

SECTION V

EFFECT OF DISSOLVED OXYGEN ON DEPOSIT FORMATION

As aircraft capabilities continue to increase, a greater heat load is placed on the fuel since it is used as a coolant for airframe and engine components. Some jet aircraft produce temperatures that approach or possibly exceed the thermal stability limits of the fuel. Low cost, simple methods of increasing fuel thermal stability of current fuels are more desirable than developing new thermally stable fuels. Fuel deposit formation is a chemical reaction that can involve dissolved oxygen; therefore, one method of improving thermal stability is to remove oxygen from the fuel. The testing discussed in this section was done to show the effect of dissolved oxygen concentration on the thermal stability of fuel AFFB-14-70.

1. SYSTEM REVISION

A Parker-Hannifin nitrogen inerting system was installed on the Simulator as a dissolved oxygen reduction system. The system permits nitrogen or air to be injected into the fuel during refueling or while the fuel is being recirculated. The system includes two Beckman oxygen analyzers with probes in the ullage space and in a recirculation line to determine the oxygen level. The system is capable of producing dissolved oxygen levels from less than 1 PPM to air saturated.

2. OPERATIONAL PROCEDURE

Steady-state tests were conducted on fuel AFFB-14-70 at several levels of dissolved oxygen to determine the effect on thermal stability. The manifold fuel inlet and outlet temperatures were 200°F and 460°F respectively. The oxygen concentration was reduced to the desired level by injection of gaseous nitrogen into the fuel and by a simultaneous reduction of the tank pressure to a level slightly above the equilibrium pressure for the desired oxygen concentration. The fuel was continuously recirculated past an oxygen probe during a test and the output from the

analyzer was recorded throughout the entire test. The fuselage tank ullage space oxygen level was recorded in a similar manner. Control of oxygen concentration was accomplished by adding nitrogen or air as required.

Each test was run until the rate of change of DTRMIL at thermocouple ten (highest temperature location) became constant. A Jet Fuel Thermal Oxidation Tester (JFTOT) was operated simultaneously with the Simulator. The JFTOT was installed on-line to receive fuel directly from the manifold inlet. Both the manifold and the JFTOT operated at 400 PSIG. Both 2.5 hour and 5 hour JFTOT tests were run.

3. MANIFOLD RESULTS

Seven steady-state tests were conducted at oxygen concentrations ranging from 8 to 75 parts per million by weight. The test time and oxygen concentration for each test are listed in Table VIII.

A plot of deposit thermal resistance (DTRMIL) versus steady-state time for each test is shown in Figures 33 through 39. Tables IX through XV are the manifold data summaries for each test. The rate of change of DTRMIL at thermocouple ten for each test is plotted versus oxygen concentration in Figure 40. The curve shows that the deposit formation rate decreases as the oxygen in the fuel decreases. Very little change in deposit formation rate occurs until the oxygen concentration drops below 30 PPM. Most of the improvement in thermal stability occurs at oxygen concentration levels below 20 PPM. The rate of change of DTRMIL at 8 PPM is about one-third the rate at 75 PPM.

Air saturated and deoxygenated (0.1 PPM) tests have been conducted on fuel AFFB-14-70 by Esso Research and Engineering Company (Reference 9). The data generated over a temperature range of 300 to 600°F indicates that reducing the dissolved oxygen to 0.1 PPM results in an 87% reduction in the rate of deposit formation at 600°F. Tests were not conducted by Esso at intermediate dissolved oxygen levels.

TABLE VIII
DISSOLVED OXYGEN TEST CONDITIONS

TEST DESIGNATION	TEST TIME, HRS.	OXYGEN CONCENTRATION, PPM
10.807	37.2	16
10.817	46.8	75
10.818	37.9	75
10.819	105.8	8
10.820	40.3	55
10.821	59.9	12
10.822	63.1	22

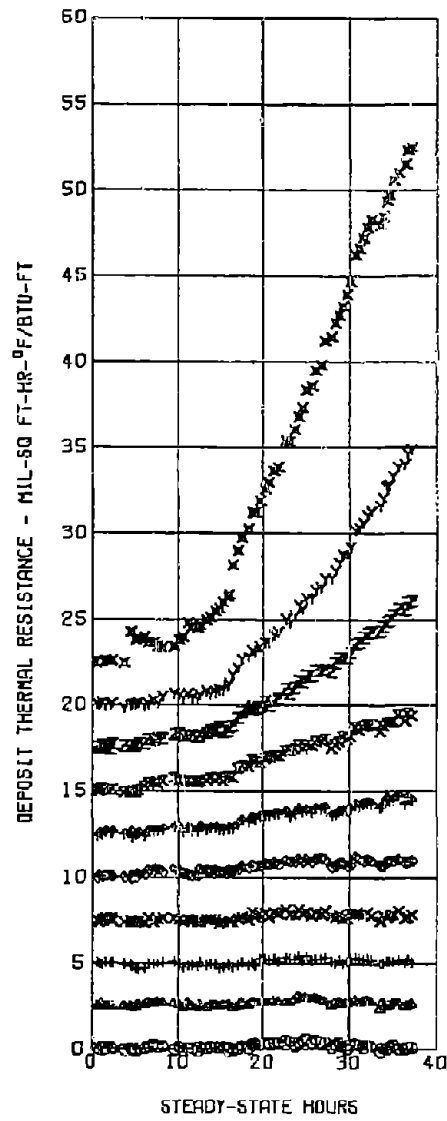


Figure 33. Calculated DTRMIL for Test 10.807

TABLE IX
SUMMARY OF MANIFOLD DATA 10.807 16 PPM

THERMOCOUPLE NUMBER	DISTANCE FROM INLET ELECTRICAL TAB (INCHES)	CALCULATED MAX FILM TEMP °F	RATE OF CHANGE IN DTRMIL RANGE RATE		CORRELATION COEFFICIENT	TOTAL CHANGE IN DTRMIL for 37.2 HRS
1	5.75	411.7	20.2-37.2	-.0253	-.705	.042
2	17.25	429.2	20.2-37.2	-.0162	-.519	.097
3	28.75	447.1	20.2-37.2	-.0115	-.503	.137
4	40.25	465.4	20.2-37.2	-.0117	-.386	.253
5	51.75	484.2	20.2-37.2	.0054	.183	.943
6	63.25	503.3	20.2-37.2	.0558	.880	2.031
7	74.75	523.0	20.2-37.2	.1468	.971	4.306
8	86.25	542.9	30.1-37.2	.3947	.989	8.471
9	97.75	563.3	30.1-37.2	.7645	.994	14.762
10	109.25	584.1	20.2-37.2	1.2205	.997	29.804

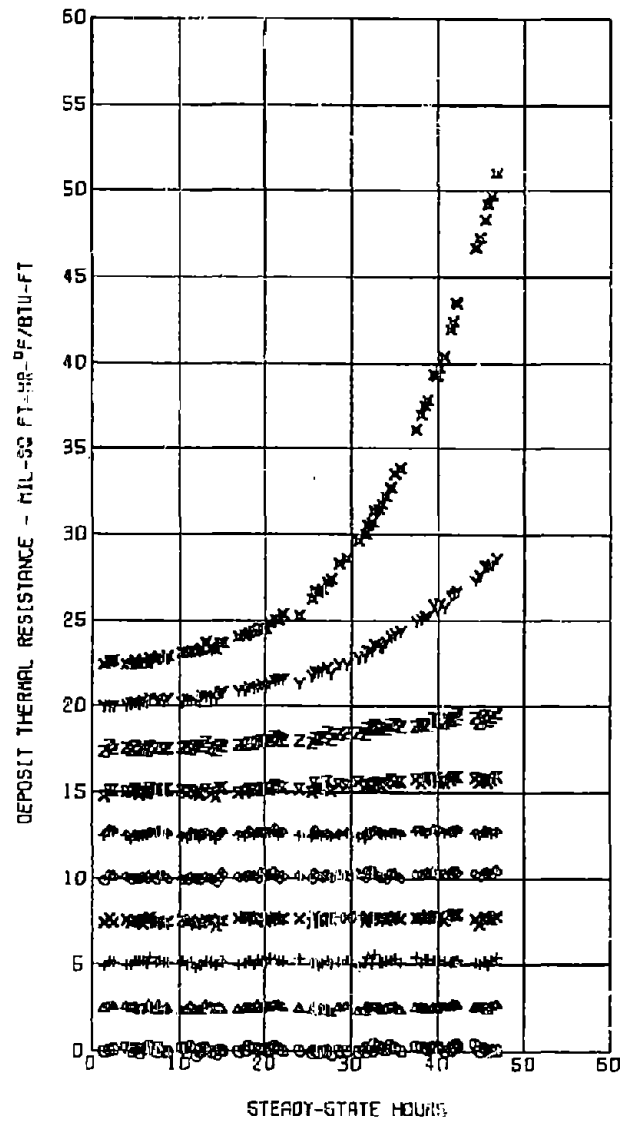


Figure 34. Calculated DTRMIL for Test 10.817

TABLE X
SUMMARY OF MANIFOLD DATA 10. 817 75 PPM

THERMOCOUPLE NUMBER	DISTANCE FROM INLET ELECTRICAL TAB (INCHES)	CALCULATED MAX FILM TEMP °F	RATE OF CHANGE IN DTRMIL		CORRELATION COEFFICIENT	TOTAL CHANGE IN DTRMIL FOR 46.8 HRS
			RANGE (HRS)	RATE		
1	5.75	411.7	1.4-46.8	.0044	.421	.205
2	17.25	429.2	"	.0016	.177	.074
3	28.75	447.1	"	.0039	.356	.182
4	40.25	465.4	"	.0066	.627	.307
5	51.75	484.2	"	.0078	.680	.367
6	63.25	503.3	"	.0051	.481	.237
7	74.75	523.0	25.4-46.8	.0292	.797	.862
8	86.25	542.9	25.4-46.8	.0675	.936	2.152
9	97.75	563.3	32.4-46.8	.3620	.995	8.392
10	109.25	584.1	37.5-46.8	1.6054	.998	27.955

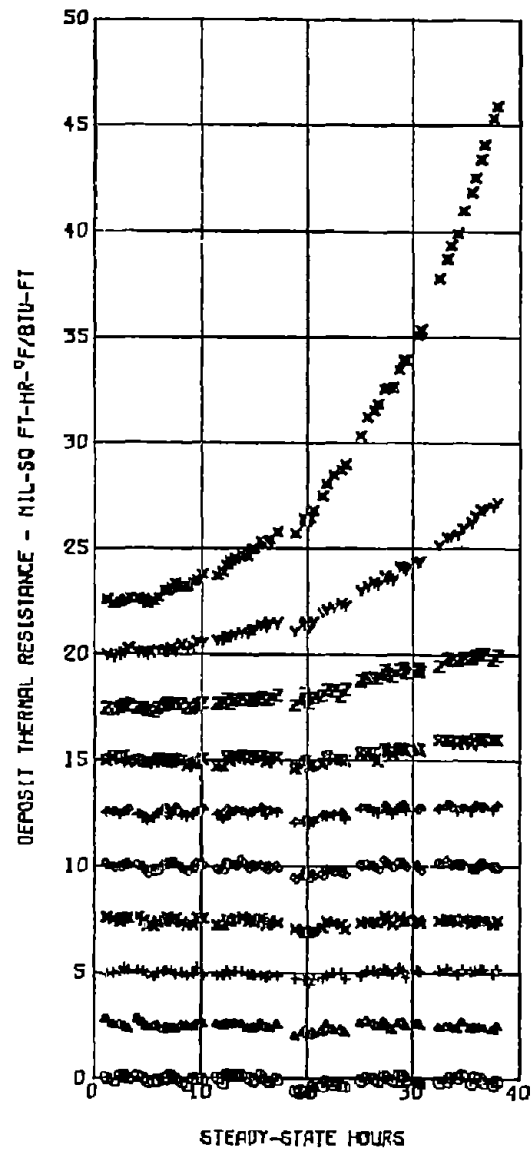


Figure 35. Calculated DTRMIL for Test 10.818

TABLE XI
SUMMARY OF MANIFOLD DATA 10.818 75 PPM

THERMOCOUPLE NUMBER	DISTANCE FROM INLET ELECTRICAL TAB (INCHES)	CALCULATED MAX FILM TEMP °F	RATE OF CHANGE IN DTRMIL		CORRELATION COEFFICIENT	TOTAL CHANGE IN DTRMIL FOR 37.9 HRS
			RANGE (HR)	RATE		
1	5.75	411.7	1.1-37.9	-.0026	-.139	-.098
2	17.25	429.2	"	-.0016	-.112	-.061
3	28.75	447.1	"	.0028	.195	.105
4	40.25	465.4	"	-.0005	-.029	-.0176
5	51.75	484.2	"	.0016	.094	.061
6	63.25	503.3	"	.0090	.454	.340
7	74.75	523.0	26.4-37.9	.0687	.889	1.154
8	86.25	542.9	26.4-37.9	.0971	.945	2.719
9	97.75	563.3	32.6-37.9	.3849	.985	6.946
10	109.25	584.1	32.6-37.9	1.543	.998	23.230

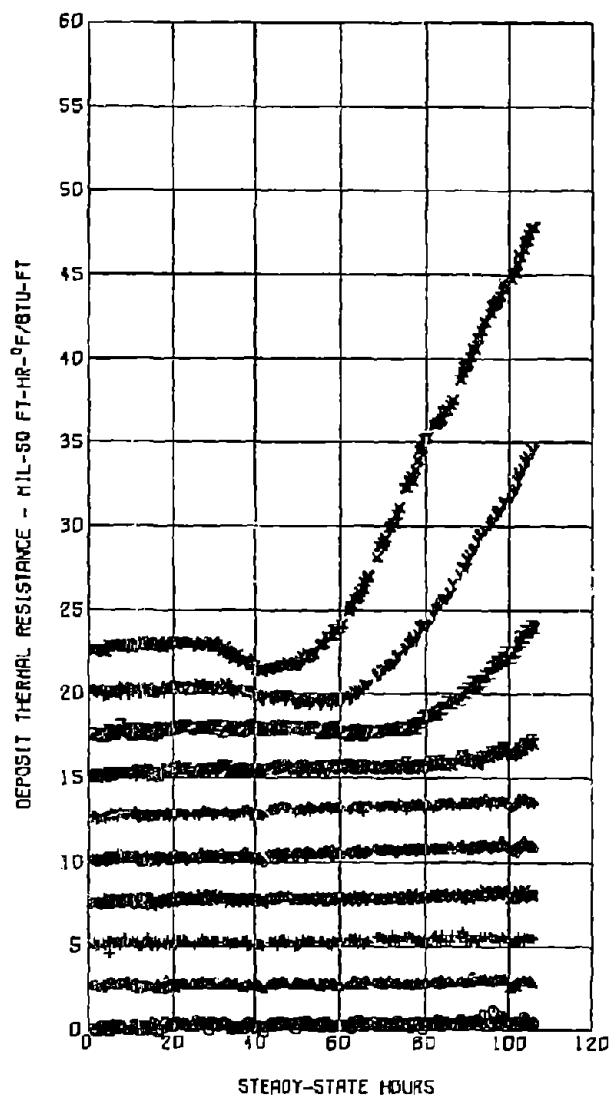


Figure 36. Calculated DTRMIL for Test 10.819

TABLE XII
SUMMARY OF MANIFOLD DATA 10.819 B PPM

THERMOCOUPLE NUMBER	DISTANCE FROM INLET ELECTRICAL TAB (INCHES)	CALCULATED MAX FILM TEMP °F	RATE OF CHANGE IN DIRMIL		CORRELATION COEFFICIENT	TOTAL CHANGE IN DIRMIL FOR 105.8 HRS
			RANGE (HRS)	RATE		
1	5.75	411.7	1.25-105.8	.0042	.693	.448
2	17.25	429.2	"	.0027	.580	.281
3	28.75	447.1	"	.0040	.671	.427
4	40.25	465.4	"	.00467	.797	.494
5	51.75	484.2	"	.0097	.928	.924
6	63.25	503.3	"	.0097	.936	1.240
7	74.75	523.0	75.3-105.8	.0457	.924	1.835
8	86.25	542.9	"	.2020	.991	6.094
9	97.75	563.3	"	.3910	.998	14.208
10	109.25	584.1	65.3-105.8	.5270	.999	25.398

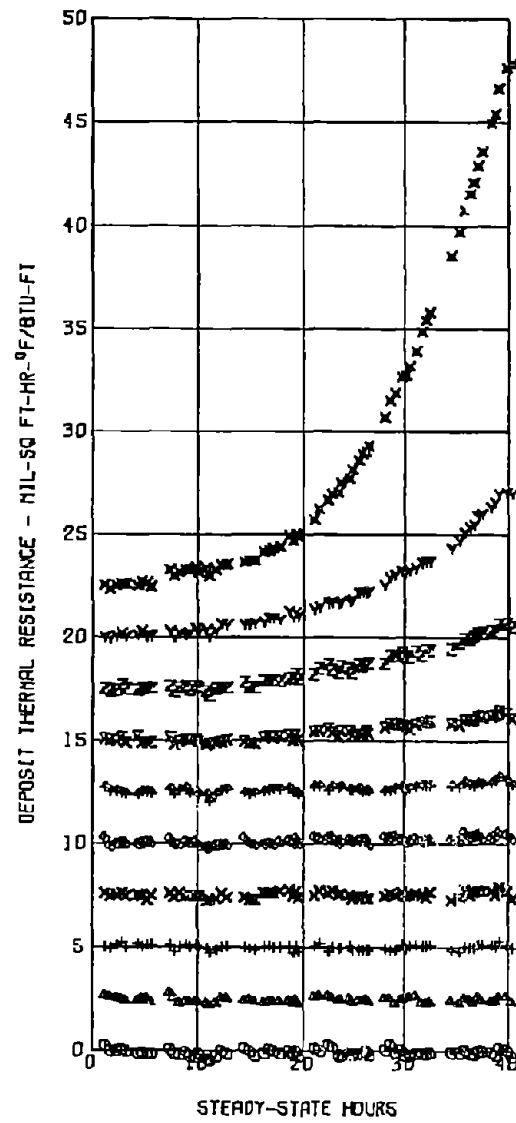


Figure 37. Calculated DTRMIL for Test 10.820

TABLE XIII
SUMMARY OF MANIFOLD DATA 10.820 55 PPM

THERMOCOUPLE NUMBER	DISTANCE FROM INLET ELECTRICAL TAB (INCHES)	CALCULATED MAX FILM TEMP °F	RATE OF CHANGE IN DTRMIL		CORRELATION COEFFICIENT	TOTAL CHANGE IN DTRMIL FOR 40.3 HRS
			RANGE (HRS)	RATE		
1	5.75	411.7	1.25-40.3	.0005	.038	.019
2	17.25	429.2	"	-.0001	-.013	-.006
3	28.75	447.1	"	.0001	.007	.003
4	40.25	465.4	"	.0036	.290	.146
5	51.75	484.2	"	.0111	.724	.446
6	63.25	503.3	32.5-40.3	.0352	.563	.288
7	74.75	523.0	"	.0661	.763	1.299
8	86.25	542.9	"	.1741	.958	3.184
9	97.75	563.3	"	.4750	.990	7.277
10	109.25	584.1	"	1.6300	.998	25.905

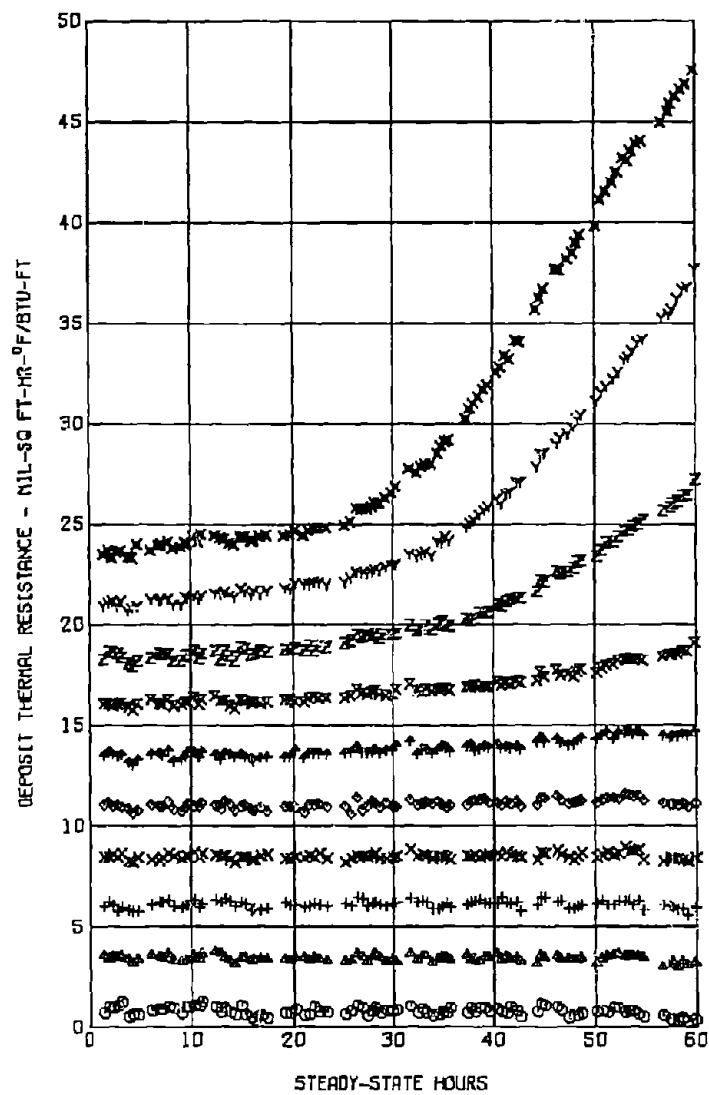


Figure 38. Calculated DTRMIL for Test 10.821

TABLE XIV
SUMMARY OF MANIFOLD DATA 10.821 12 PPM

THERMOCOUPLE NUMBER	DISTANCE FROM INLET ELECTRICAL TAB (INCHES)	CALCULATED MAX FILM TEMP °F	RATE OF CHANGE IN DTRMIL		CORRELATION COEFFICIENT	TOTAL CHANGE IN DTRMIL FOR 59.9 HRS
			RANGE (HRS)	RATE		
1	5.75	411.7	1.3-59.9	-.0044	-.352	-.265
2	17.25	429.2	1.3-59.9	-.0022	-.249	-.132
3	28.75	447.1	1.3-59.9	.0005	.048	.029
4	40.25	465.4	1.3-59.9	.0018	.218	.106
5	51.75	484.2	1.3-59.9	.0070	.601	.420
6	63.25	503.3	20.2-59.9	.0280	.895	1.124
7	74.75	523.0	40.4-59.9	.0923	.971	2.778
8	86.25	542.9	45.0-59.9	.3207	.995	8.437
9	97.75	563.3	45.0-59.9	.6110	.998	16.428
10	109.25	584.1	40.4-59.9	.7759	.997	24.442

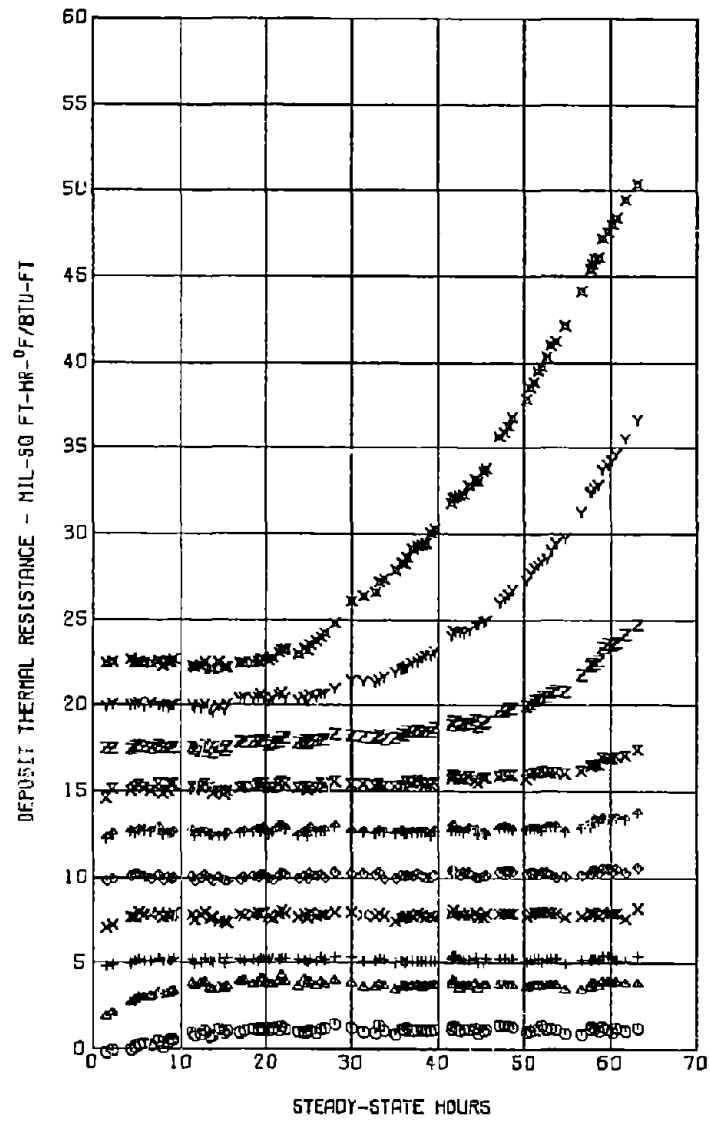


Figure 39. Calculated DTRMIL for Test 10.822

TABLE XV
SUMMARY OF MANIFOLD DATA 10.822 22 PPM

THERMOCOUPLE NUMBER	DISTANCE FROM INLET ELECTRICAL TAB. (INCHES)	CALCULATED MAX FILM TEMP °F	RATE OF CHANGE IN DTRMIL		CORRELATION COEFFICIENT	TOTAL CHANGE IN DTRMIL FOR 63.1 HRS
			RANGE (HRS)	RATE		
1	5.75	411.7	20.2-63.1	.0015	.139	.097
2	17.25	429.2	20.2-63.1	-.0021	-.184	-.129
3	28.75	447.1	1.5-63.1	.0023	.341	.142
4	40.25	455.4	4.8-63.1	.0028	.323	.175
5	51.75	484.2	1.5-63.1	.0072	.686	.450
6	63.25	503.3	53.7-63.1	.1012	.887	1.125
7	74.75	523.0	53.7-63.1	.1515	.954	2.306
8	86.25	542.9	53.7-63.1	.4428	.987	7.189
9	97.75	563.3	53.7-63.1	.7984	.997	16.514
10	109.25	584.1	44.7-63.1	.9644	.999	27.946

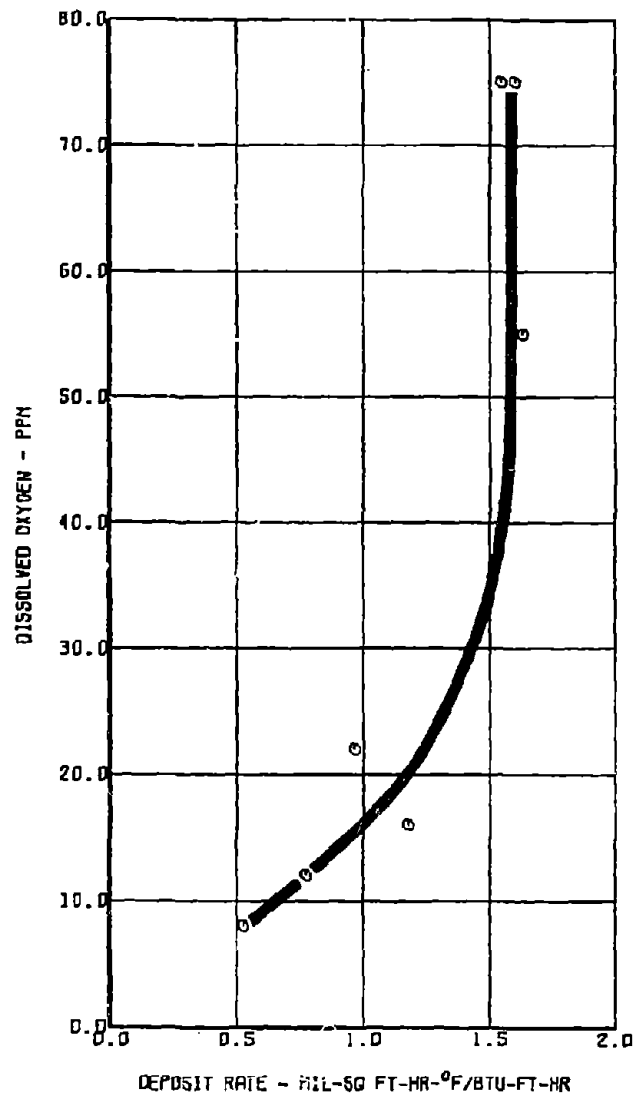


Figure 40. Effect of Oxygen in the Simulator

4. JFTOT RESULTS

The JFTOT results, plotted in Figure 41, show the temperature at which a Code 3 rating was obtained for each oxygen concentration. As was shown by the steady-state tests, the JFTOT tests indicate that oxygen removal is effective for fuel AFFB-14-70 when the concentration is reduced below 30 PPM. The agreement between the Simulator and the JFTOT indicates that the JFTOT can be used to evaluate the effect of dissolved oxygen on the thermal stability of other fuels if a means of controlling the oxygen concentration of the fuel in the JFTOT is developed.

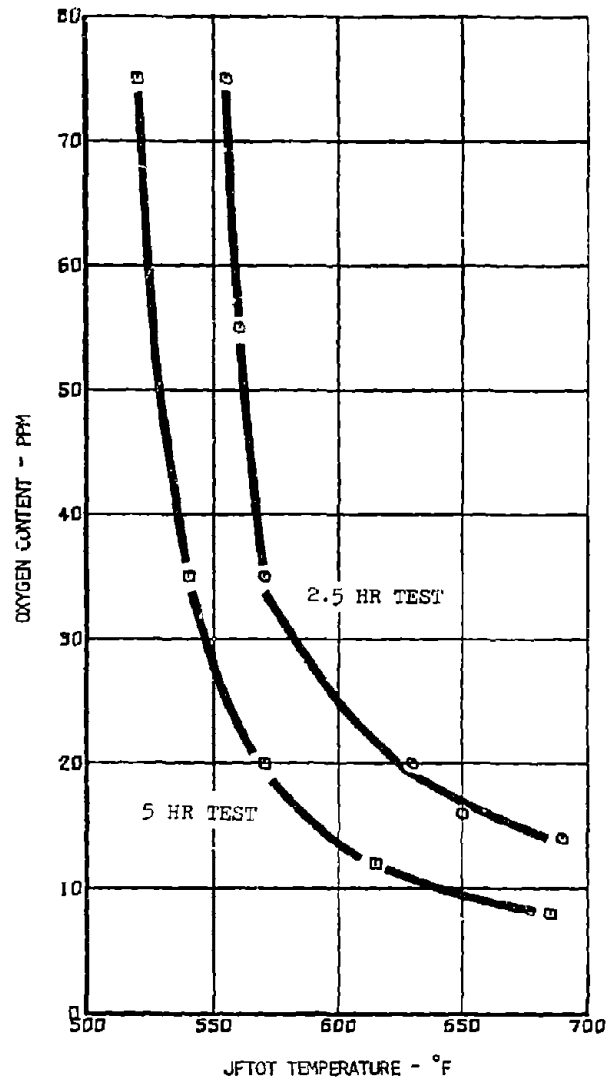


Figure 41. Effect of Oxygen on JFTOT Breakpoint

SECTION VI

EFFECTS OF SURFACE FINISH ON DEPOSIT FORMATION

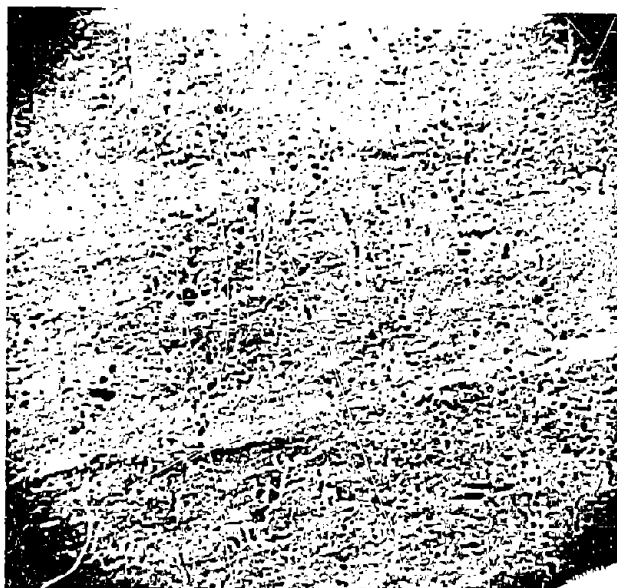
The Simulator component used to evaluate the effect of dissolved oxygen removal was the manifold. During the testing it was observed that the elapsed time from the beginning of a test until significant deposits were formed varied from test to test even when the dissolved oxygen level was held constant. However, once deposits were formed the rate of deposit formation was not affected.

It was hypothesized that the variation in test time was due to the tube surface condition. Microphotographs were made of two of the tubes where a wide variation in time was observed. These microphotographs, shown in Figure 42 at a magnification of 553 times, reveal an extreme difference in surface roughness. The calculated DTRMIL versus test time for thermocouple 10 of each of the manifolds is shown in Figure 43. It is readily evident that even though the two curves eventually become parallel there is a five hour offset between the two curves.

Further analysis and investigation indicated that the deposits on smooth tubes were multicolored whereas those on a rough tube were tan or brown. The colors were very pronounced with the brighter colors occurring at the lower levels of dissolved oxygen.



ROUGH SURFACE



SMOOTH SURFACE

Figure 42. Microphotograph Comparison of Manifold Tube Inner Surfaces, 553X Magnification

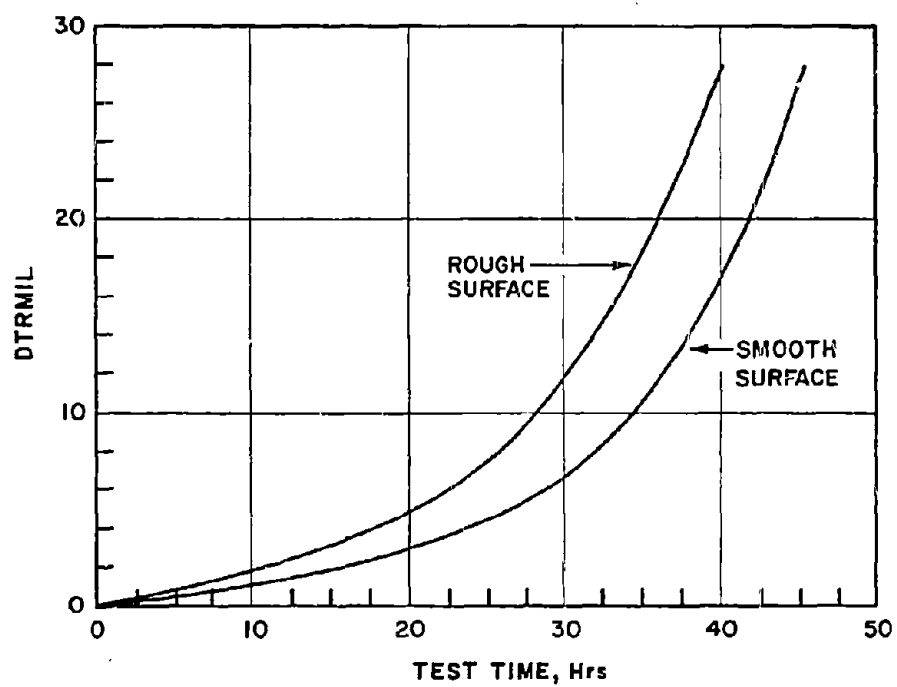


Figure 43. Effect of Manifold Tube Inner Surface

SECTION VII

SMALL-SCALE TESTS

Fuel AFFB-14-70 has been evaluated in the American Society for Testing and Materials-Coordinating Research Council (ASTM-CRC) Fuel Coker and ALCOR Jet Fuel Thermal Oxidation Tester (JFTOT). The Coker and JFTOT tests were conducted by the Air Force Aero Propulsion Laboratory except as noted.

1. ASTM-CRC FUEL COKER

The fuel was evaluated in the Coker by Ashland Oil Company prior to delivery. The fuel passed at 375/475°F (Code 2, and no increase in filter drop). A total of 28 Coker tests were conducted on the fuel by the Aero Propulsion Laboratory during the time period from 14 January 1972 to 8 September 1972. The results of these tests are tabulated in Table XVI of Appendix III. These data are plotted in Figures 44 and 45. Ratings greater than a given code number are increased by 0.5 (e.g., a 2+ is plotted as a 2.5). Based on these data, it is considered that the breakpoint of the fuel was 375/475°F based on preheater ratings and 368/468°F based on filter pressure drop.

2. JET FUEL THERMAL OXIDATION TESTER

The fuel was evaluated in the JFTOT using both the visual and ALCOR Inc. Tube Deposit Rater (TDR) methods of rating the deposits formed on the JFTOT tubes. A total of 59 tests were conducted during three time periods.

The first time period was from 14 September 1970 to 21 January 1971. All of these tests were run at a pressure of 350 PSIG. The 2.5 and 5.0 hour results are tabulated in Tables XVII and XVIII of Appendix III, respectively. Note that most of the tubes were rated twice on each of the rating devices.

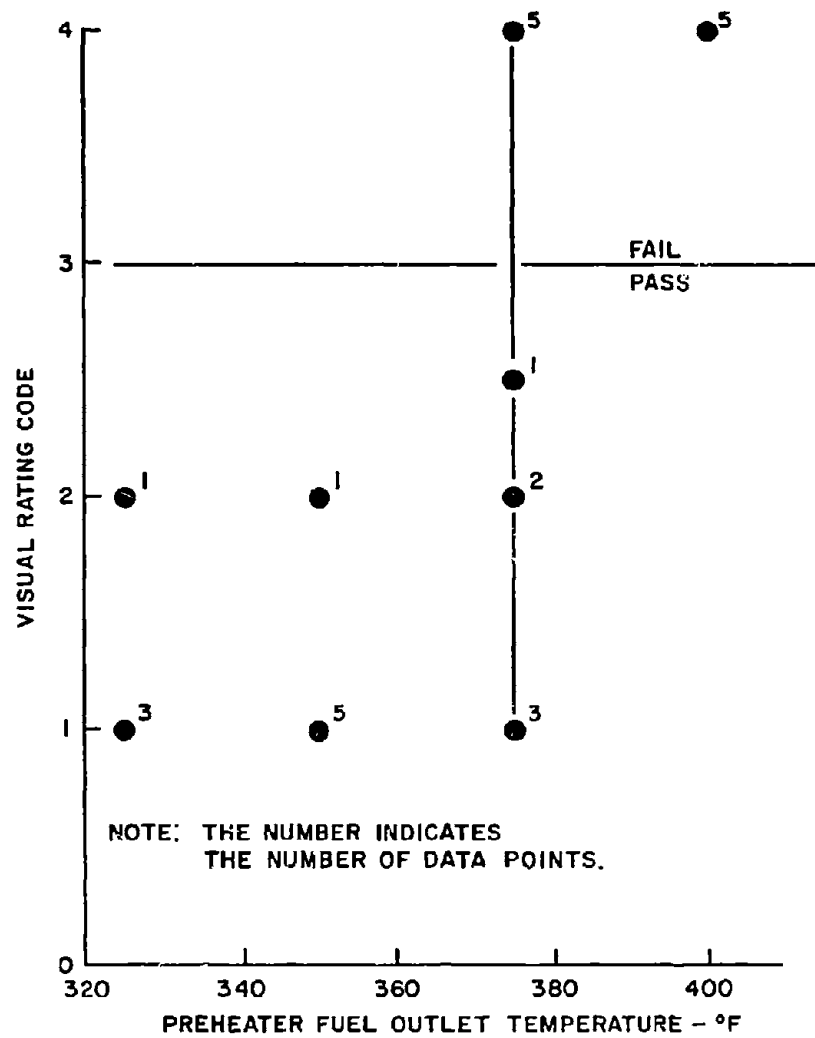


Figure 44. ASTM-CRC Fuel Coker Rating Results

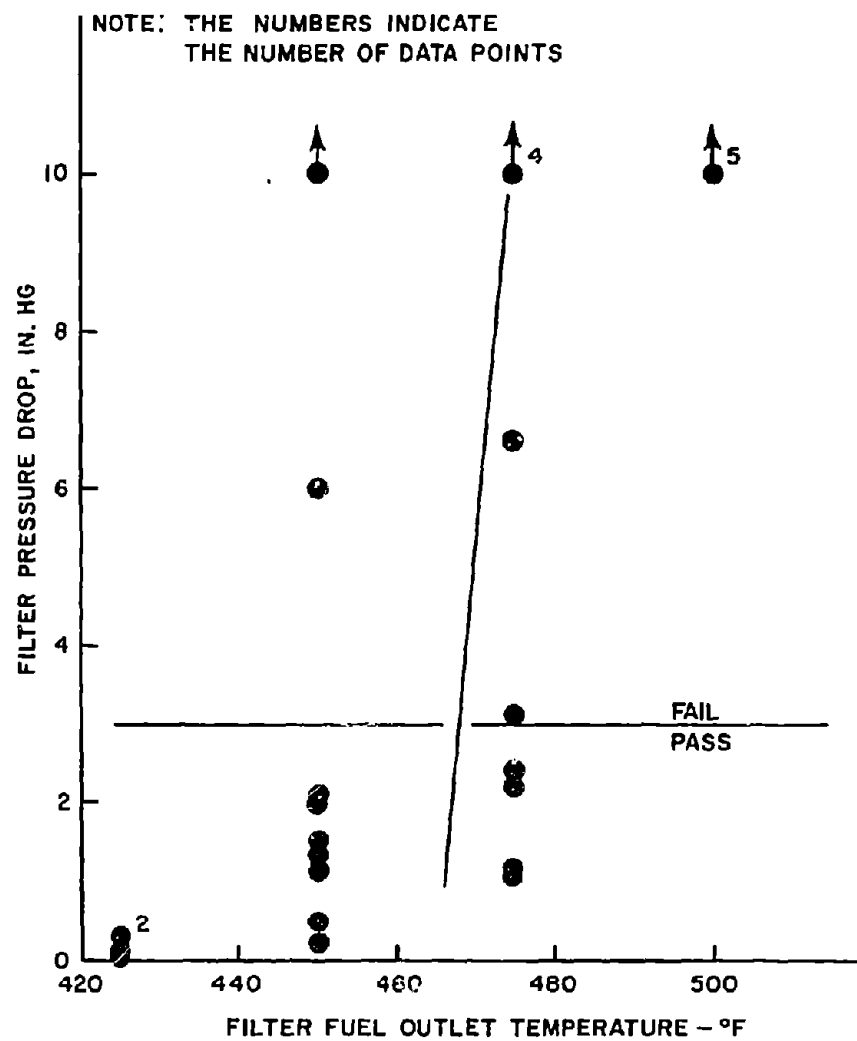


Figure 45. ASTM-CRC Fuel Coker Pressure Drop Results

The second period of testing extended from 17 September 1971 to 14 February 1972 and included 2.5 and 5.0 hour tests run at pressures of 350, 375, and 400 PSIG. These data are tabulated in Tables XIX and XX of Appendix III for the 2.5 and 5.0 hour tests, respectively.

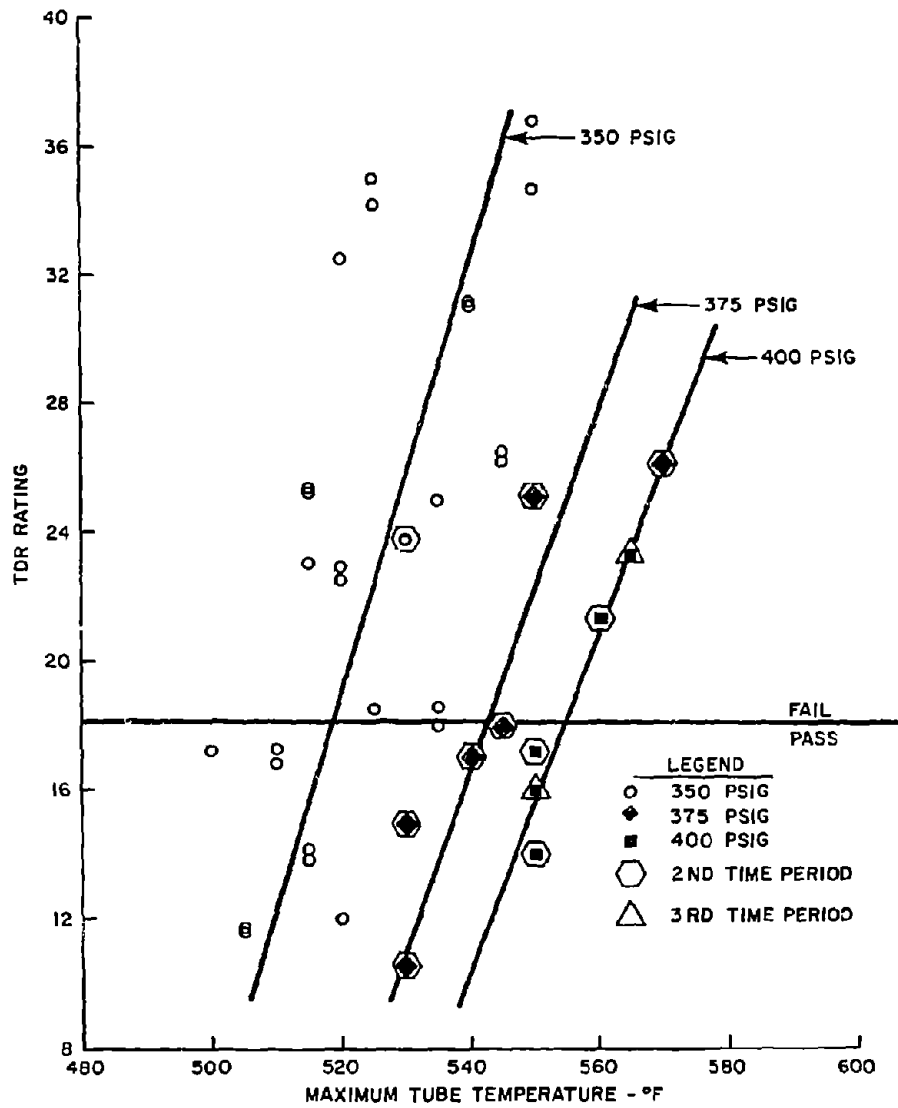
Two tests were run during the third period which extended from 12 June 1972 to 14 June 1972. Both tests were run at 400 PSIG for 2.5 hours. These data are tabulated in Table XXI of Appendix III.

The TDR ratings of the JFTOT tubes from the 2.5 hour tests are plotted in Figure 46. In analyzing the JFTOT data, it is assumed that a TDR rating of 18 or greater, or an increase in filter pressure drop of 1 in. Hg, indicates a failure of the fuel.

The JFTOT tests were run at different pressures since JP-4 tests run during the same time period indicated that vaporization was occurring in the test section at the lower pressures. The pressure was first increased from 350 to 375 PSIG and then later to 400 PSIG to prevent problems with JP-4. The standard operating pressure for all fuels is now 500 PSIG.

The data scatter resulting from the tests at 350 PSIG during the first test period, based on TDR ratings, makes it difficult to determine a breakpoint. However, a straight line has been drawn through these data that is considered to best represent the data. Straight lines have also been drawn through the data obtained at 375 and 400 PSIG. The resulting breakpoints are 519, 543, and 555 for the tests conducted at 350, 375, and 400 PSIG, respectively. Analysis of these data indicates the following:

- a. The 375 PSIG tests run at the same time as three of the 400 PSIG tests resulted in a lower breakpoint.
- b. The 350 PSIG test run at the same time as the 375 PSIG tests produced a much higher TDR rating.



c. There was no significant difference in results between the tests run at the same pressure during different time periods.

d. The 400 PSIG tests result in a higher breakpoint than that obtained from the 350 PSIG tests.

e. The 375 PSIG tests result in a higher breakpoint than that obtained from the 350 PSIG tests.

Therefore, it is concluded that time in storage did not affect the results but pressure had a significant effect on the breakpoint. Consideration of filter pressure drop does not significantly change the analysis.

The TDR ratings obtained from the 5 hour JFTOT tests are plotted in Figure 47. As can be seen in the Figure, the data obtained at 350 PSIG during September 70 are generally grouped together approximately 26°F below the data taken at 350 PSIG during November 70 and January 71. The latter data produced a breakpoint of 515°F.

The 350 PSIG data taken during the second period (17 September 71 to 3 January 72) is in agreement with the November 70 and January 71 data indicating that the 26°F apparent change between September 70 and November 70 was not due to a change in thermal stability during storage. However, the reason for the 26°F difference is not known.

The data recorded during the second time period indicate an increase in the breakpoint from 515°F at 350 PSIG to 524°F at 375 PSIG, again showing the effect of pressure on the results. Consideration of filter pressure drop does not affect the analysis.

The JFTOT results, based on visual rating of the tubes, are plotted in Figures 48 and 49 for the 2.5 and 5 hour tests, respectively. The ratings greater than a given code number were increased by 0.5.

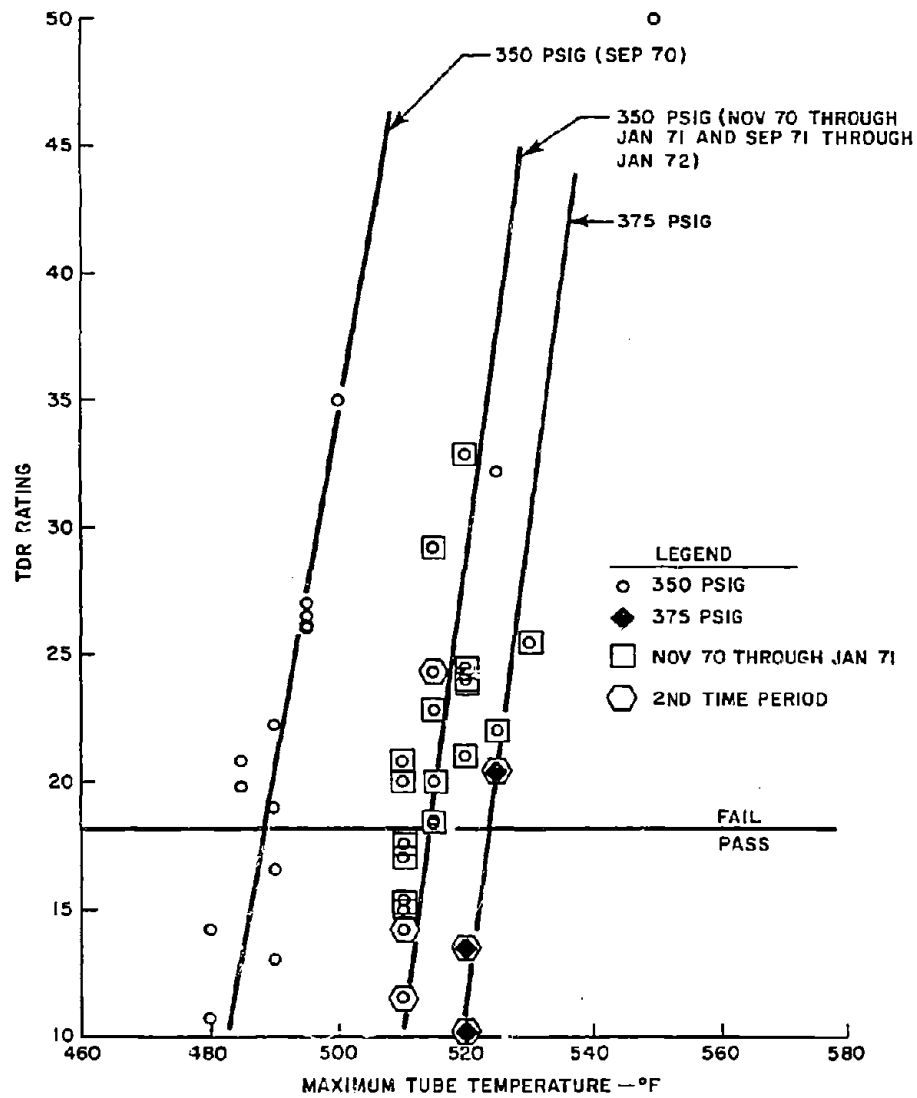


Figure 47. 5 Hour JFTOT Results Based on TDR Ratings

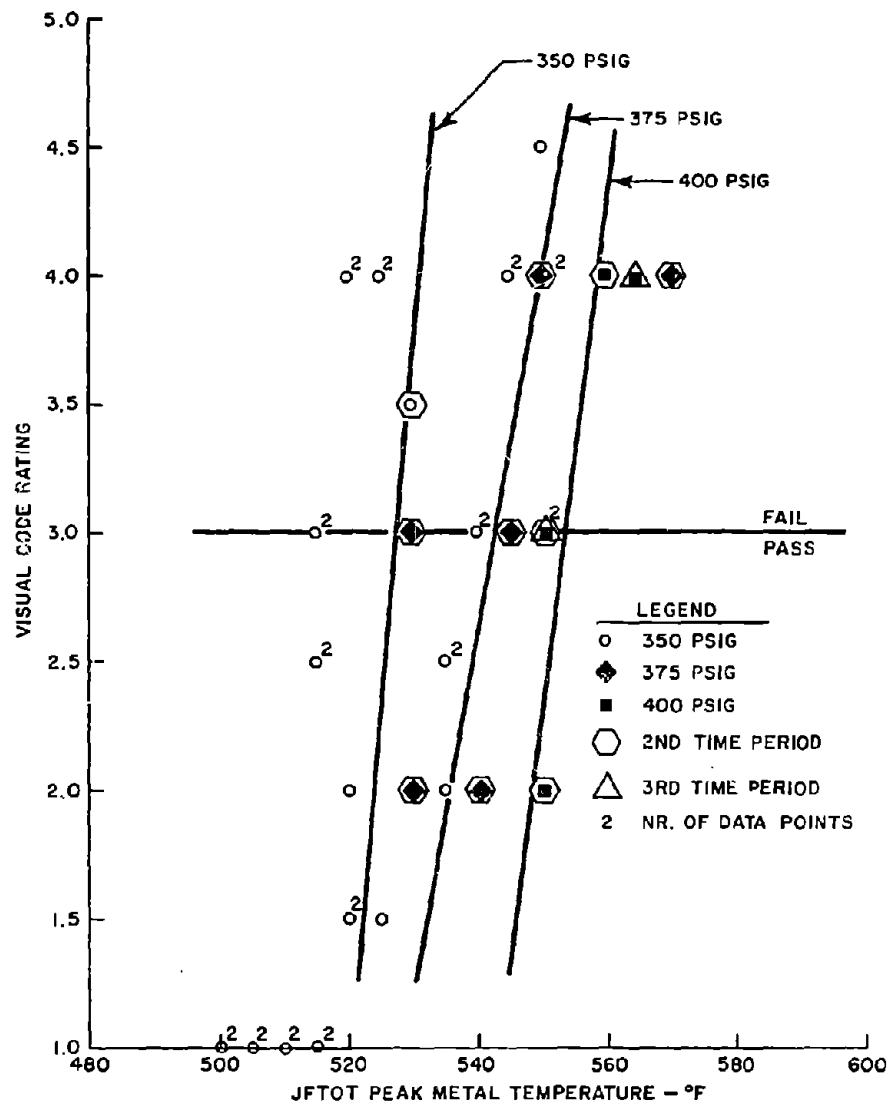


Figure 48. 2.5 Hour JFTOT Results Based on Visual Ratings

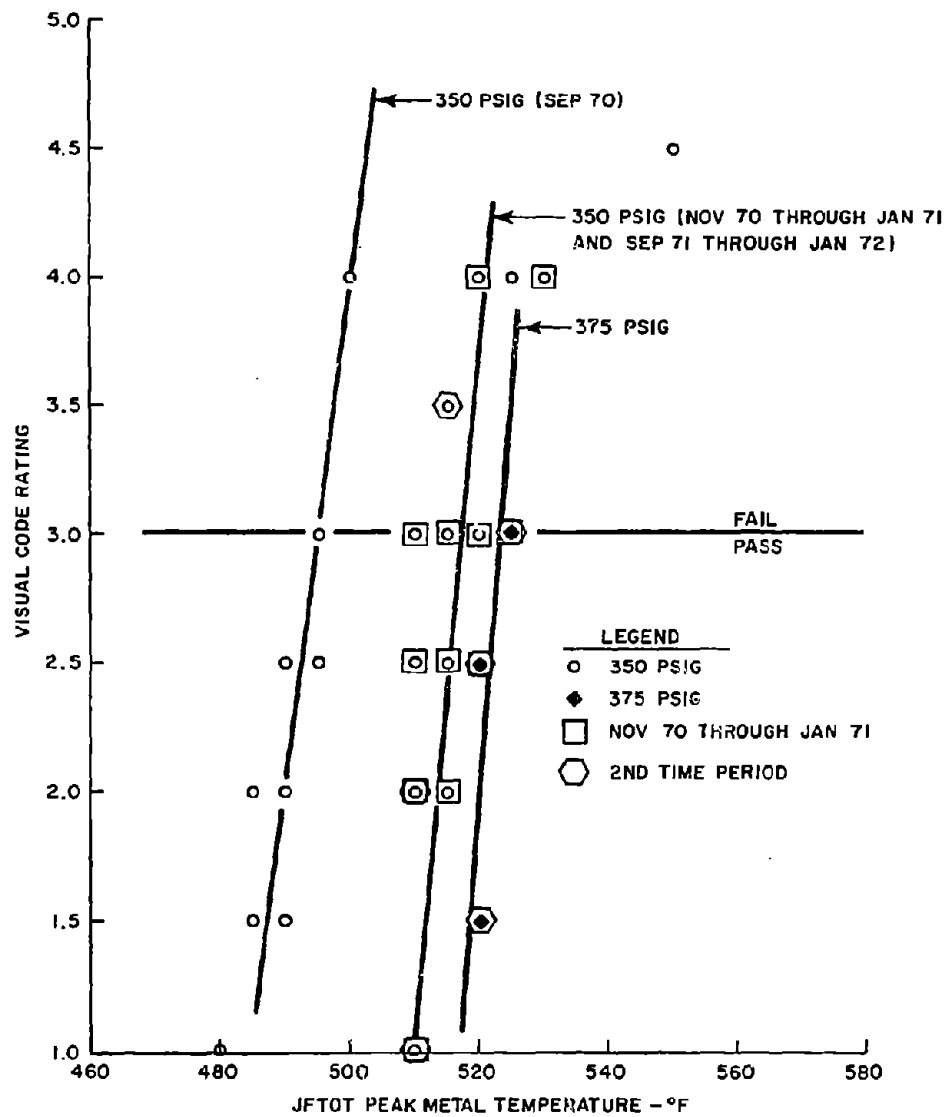


Figure 49. 5 Hour JFTOT Results Based on Visual Ratings

These data also indicate that the breakpoint temperature is a function of pressure. The results are summarized as follows:

Test Duration (Hours)	System Pressure (PSIG)		
	350	375	400
2.5	528	543	554
5	495/518	524	---

Two breakpoint temperatures (i.e., 495° and 518°F) are shown for the 5 hour tests at 350 PSIG. The reason for showing these two breakpoint temperatures is the grouping of the 350 PSIG data during the first time period into two distinct groups as previously discussed. The breakpoint temperature of 554°F obtained for the 2.5 hour tests is in good agreement with the 560°F breakpoint temperature obtained under air saturated conditions on the on-line JFTOT at 400 PSIG during the dissolved oxygen testing discussed in Section V.

In summary, the JFTOT results for fuel AFFB-14-70 appear to be significantly affected by the system pressure. The effect is more pronounced for the 2.5 hour tests. It is considered that these data do not indicate a change in thermal stability while the fuel was in storage awaiting testing.

SECTION VIII

CONCLUSIONS

1. Deposits form in the heated wing tank at a temperature between 225°F and 300°F using fuel AFFB-14-70 as the test fuel. No other problems are produced in the airframe system.

2. The use of fuel AFFB-14-70 in an engine system at the same conditions used to evaluate the fuel in the Simulator would result in problems only in the engine nozzle.

3. Results of the test manifold show that fuel AFFB-14-70 is more thermally stable than fuel AFFB-9-67 and less thermally stable than fuel AFFB-10-67.

4. Surface finish has a significant effect on the initial deposit formation in a tube, but not on the rate of deposit formation once the surface is covered with deposit.

5. Removal of dissolved oxygen to less than 30 PPM significantly improves the thermal stability of AFFB-14-70. A 66% reduction in the rate of deposit formation occurs when the oxygen concentration is reduced from 75 PPM to 8 PPM.

6. The Simulator and JFTOT data are in agreement as to the level of dissolved oxygen required to produce a significant improvement in thermal stability of AFFB-14-70. This indicates that it may be possible to use the JFTOT to conduct dissolved oxygen tests on additional fuels instead of using the Simulator.

SECTION IX
RECOMMENDATIONS

1. The effect on thermal stability of refinery processes such as desulfurization and hydrotreating should be studied.
2. The effect of dissolved oxygen on thermal stability of other fuels should be investigated.
3. The effect of surface finish on initial deposit formation should be investigated in detail.

APPENDIX I
MANIFOLD ANALYSIS

This section provides a detailed explanation of the analytical techniques utilized to perform a complete heat transfer analysis on the resistance heated manifold tubes in the Advanced Fuel System Simulator.

TUBE MATERIAL AND GEOMETRY

All manifold tubes were purchased according to MIL-T-8808A, "Tubing, steel, corrosion-resistant (18-8 stabilized), aircraft hydraulic quality." The seamless tubing was type 321 stainless steel (titanium stabilized).

The nominal dimensions for the tubes were:

Outside diameter: 5/16 in. (0.3125 in.)

Wall Thickness: 0.028 in.

Length: 10 Ft.

The permissible variations in dimensions, according to Military Standard 33533 were:

Outside diameter variation: ± 0.004 in.

Wall thickness variation: $\pm 10\%$

Therefore, according to the above standards, manifold tubes could have had the following variations:

Outside diameter: 0.3165 in. Max.

0.3085 in. Min.

Wall thickness: 0.0308 in. Max.

0.0252 in. Min.

With these permissible variations in dimensions the following was possible:

	<u>MAX.</u>	<u>MIN.</u>	<u>% DIFFERENCE</u>
Cross Sectional Area (in ²):	0.0146	0.0117	19.59
Flow Area (in ²):	0.0666	0.0606	9.12
Wall Thickness (in)	0.0308	0.0252	18.18
Inside Surface Area (in ²):	7.6642	6.9653	9.12

Geometrical data were used throughout the analysis and because of the possible percent differences in tubes, each tube was measured with a micrometer. The outside diameter was checked over its full length, and the inside diameter at each end. The outside and inside diameters of 32 tubes have been measured with the outside diameter varying from 0.3132 in. to 0.3152 in. Inside diameters varied from 0.2565 to 0.2604 in.

The outside diameter of each individual tube has not varied more than $\pm .0002$ in. throughout its length and it was therefore assumed that the inside diameter remained uniform within a tolerance of $\pm .0002$ in.

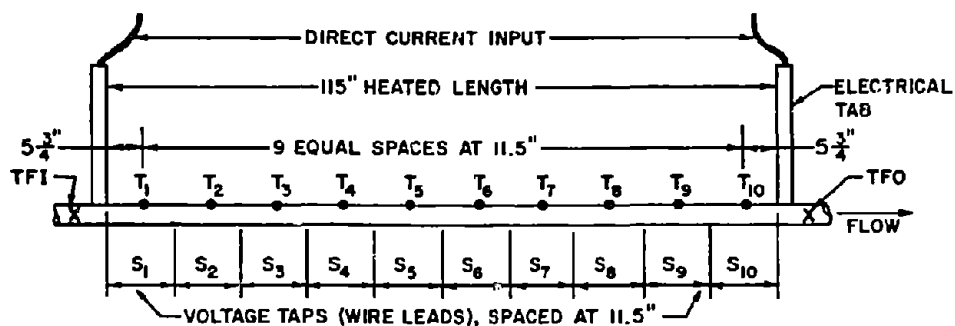


Figure 50. Manifold Instrumentation and Arrangement

Stainless steel electrical tabs were welded to the manifold tube providing a 115 in. heated length (see Figure 50). Power was supplied from four direct current welders (each rated at 10 KW), connected in parallel. Current was continually measured using a 500 amp shunt and a digital voltmeter.

Ten, type "J", stainless steel sheathed thermocouples (T_1 to T_{10}) were welded to the tube wall and located as shown in Figure 50. Fuel inlet (TFI) and fuel outlet (TFO) thermocouples were mounted in the stream to indicate the respective bulk fuel temperatures. These twelve thermocouples were connected to a single, 12 point continuous recorder.

A heat transfer analysis was performed on ten separate sections of the manifold, each 11.5 inches in length. These are indicated in Figure 50 as S_1 to S_{10} . Voltage taps were located to measure the voltage drop across each of the ten sections. The voltage tap leads were connected to a digital voltmeter through a multiple channel selector switch.

TUBE RESISTANCE AND HEAT LOSSES

Prior to each test, the new manifold tube was tested to determine the electrical resistivity (res). The tubes were electrically heated to an equilibrium temperature with no flow, and the tube resistance calculated from current and voltage measurements. With the availability of multiple voltage taps, resistance per inch of length was obtained and verified at different locations over various known lengths.

Handbooks* provide the following resistivity data for 321 stainless steel:

@ 68°F res = 28.7401×10^{-6} ohm-inches
@ 1200°F res = 45.6692×10^{-6} ohm-inches

*Allegheny-Ludlum Steel Corp., Pittsburgh, Pa.

Test results on five manifold tubes show resistivity to be:

$$\begin{aligned} @ 68^{\circ}\text{F} \quad \text{res} &= 30.4292 \times 10^{-6} \text{ ohm-inches} \\ @ 1200^{\circ}\text{F} \quad \text{res} &= 46.10155 \times 10^{-6} \text{ ohm-inches} \end{aligned}$$

By linear regression,

$$\begin{aligned} \text{res} &= 0.01384484 T_{\text{aw}} + 29.487738 \times 10^{-6} \text{ ohm-inches} \quad (1) \\ \text{where } T_{\text{aw}} &= \text{average tube wall temperature, } ^{\circ}\text{F} \end{aligned}$$

The entire manifold tube was contained within the center of an 8 in. wide by 8 in. deep steel trough that is completely filled with granular vermiculite insulation. Heat losses from the tube, as a function of outside tube wall temperature, were determined from the same power data recorded during tests to define resistivity. During steady-state tests, heat losses from the electrical tabs remain nearly constant at approximately 250 BTU per hour each. This steady, and constant, loss is accounted for in the heat balance performed on manifold section 1 and section 10. (See Figure 50).

Heat loss data (excluding tab losses) for four 2-tab manifolds are plotted in Figure 51. A non-linear regression gave:

$$\begin{aligned} q_L &= -0.28187 + 0.0044728 T_o + \frac{7.71454}{10^6} T_o^2 \quad (2) \\ \text{where } q_L &= \text{insulation loss, BTU/hr-in of length} \\ T_o &= \text{outside tube wall temperature, } ^{\circ}\text{F} \end{aligned}$$

THERMAL CONDUCTIVITY OF 321 STAINLESS STEEL

Several handbooks and texts provide the following thermal conductivity data for 321 stainless steel:

$$\begin{aligned} @ 212^{\circ}\text{F} \quad K_{\text{ss}} &= 9.3 \text{ BTU/hr-ft-}^{\circ}\text{F} \\ @ 932^{\circ}\text{F} \quad K_{\text{ss}} &= 12.8 \text{ BTU/hr-ft-}^{\circ}\text{F} \end{aligned}$$

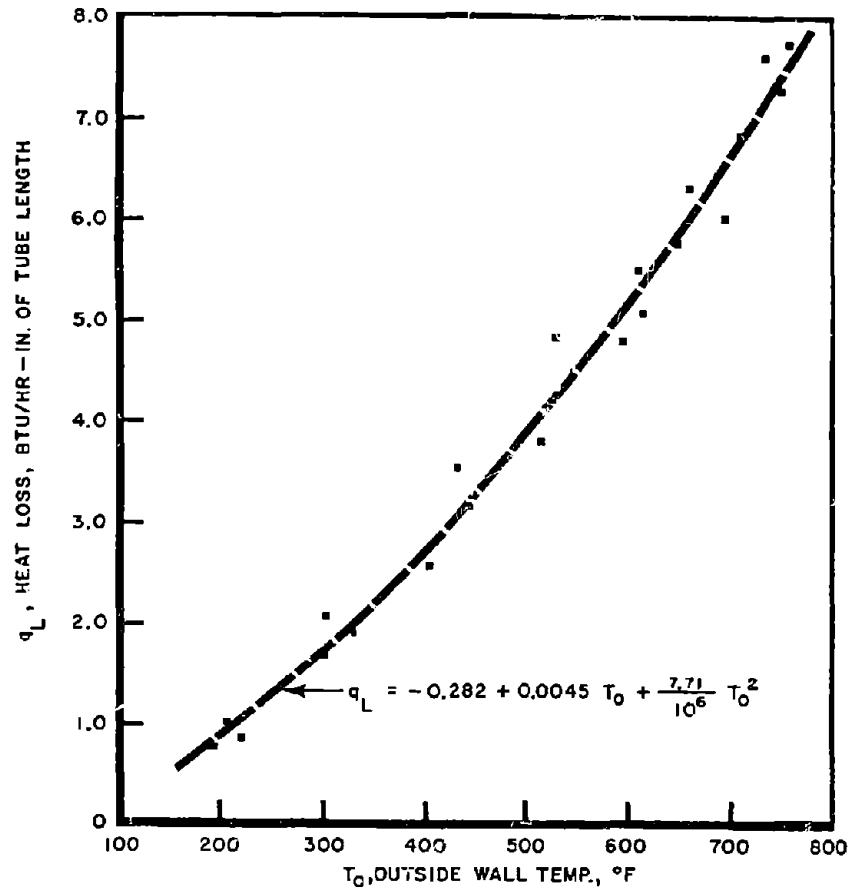


Figure 51. Manifold Insulation Heat Loss Vs. Outside Tube Wall Temperature

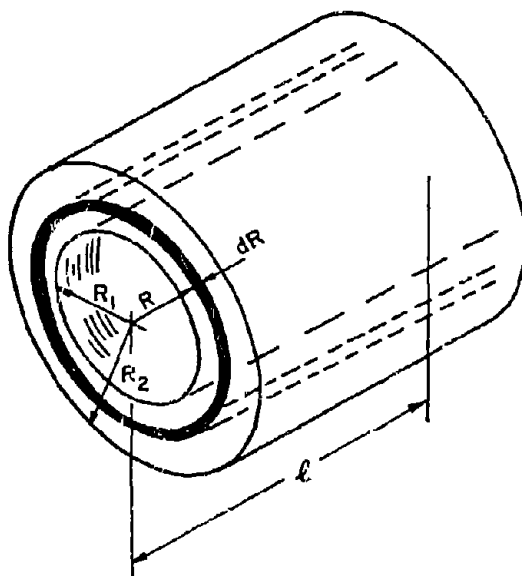
The thermal conductivity is assumed to be linear over the above temperature range, therefore.

$$K_{ss} = 8.3 + 0.0048 T_{aw} \quad (3)$$

where K_{ss} = thermal conductivity, BTU/hr-ft-°F

T_{aw} = average tube wall temperature, °F

AVERAGE TUBE WALL TEMPERATURE, T_{aw}



The energy equation for an annular element formed between an inner cylinder of radius (R) and an outer cylinder of radius ($R + dR$) is

$$-K A_R \frac{dT}{dR} \Big|_R + q 12 \pi R dR = -K A_{R+dR} \frac{dT}{dR} \Big|_{R+dR} \quad (4)$$

where.

$$A_R = 2\pi R l$$

$$A_{R+dR} = 2\pi (R+dR) l$$

q = heat generated internally per unit volume

k = thermal conductivity

T = temperature

Here it is assumed that, (a) the cylinder is sufficiently long that the temperature may be considered a function of radius only, (b) the heat sources (resistant heating by direct current) are uniformly distributed and (c) the thermal conductivity is constant.

Using the mean value theorem to relate the temperature gradient at $(R + dR)$ to the temperature gradient at (R) ,

$$\frac{d^2 T}{dR^2} + \frac{1}{R} \frac{dT}{dR} = - \frac{q}{k} \quad (5)$$

Multiplying Equation 5 by $R \, dR$ yields

$$R \, d \left(\frac{dT}{dR} \right) + dR \left(\frac{dT}{dR} \right) = - q \frac{R \, dR}{k}$$

$$d \left(R \frac{dT}{dR} \right) = - \frac{q}{k} R \, dR \quad (6)$$

Integration Yields

$$R \frac{dT}{dR} = - \frac{qR^2}{2k} + C_1$$

$$\frac{dT}{dR} = - \frac{qR}{2k} + \frac{C_1}{R} \quad (7)$$

$$dT = - \frac{qR \, dR}{2k} + C_1 \frac{dR}{R} \quad (8)$$

$$T = - \frac{qR^2}{4k} + C_1 \ln R + C_2 \quad (9)$$

Which shows a parabolic temperature distribution.

The boundary conditions are

$$\frac{dT}{dR} = 0 \text{ at } R = R_2$$

The cylinder is insulated and the heat losses are small (approx. 1.3%) compared to the total heat generated.

$$T = T_0 \text{ at } R = R_2$$

Using Equation 7 and the boundary condition

$$C_1 = \frac{qR_2^2}{2k} \quad (10)$$

Using Equation 9 and the boundary condition

$$C_2 = T + \frac{qR^2}{4k} - C_1 \ln R$$

$$C_2 = T_0 + \frac{qR_2^2}{4k} - \frac{qR_2^2}{2k} \ln R_2 \quad (11)$$

Let

$$W = \frac{q}{4k}$$

and

$$T = T_1 \text{ at } R = R_1$$

Then Equation 9 becomes

$$T_1 = -WR_1^2 + 2WR_2^2 \ln R_1 + T_0 + WR_2^2 - 2WR_2^2 \ln R_2$$

$$\Delta T_{\text{wall}} = T_0 - T_1$$

$$\Delta T_{\text{wall}} = W \left[2R_2^2 \ln \frac{R_2}{R_1} - (R_2^2 - R_1^2) \right]$$

The average tube wall temperature, T_{aw} , can be defined as

$$T_{aw} = \frac{1}{\pi (R_2^2 - R_1^2)} \int_{R_1}^{R_2} 2\pi TR dR$$

Using Equations 9, 10, and 11 and integrating gives

$$T_{aw} - T_o = W \left[\frac{2R_1^2 R_2^2}{R_2^2 - R_1^2} \ln \left(\frac{R_2}{R_1} \right) - \frac{R_2^2 + R_1^2}{2} \right]$$

Since

$$\Delta T_{wall} = W \left[2R_2^2 \ln \frac{R_2}{R_1} - (R_2^2 - R_1^2) \right]$$

Then $T_{aw} - T_o$ can be expressed as ΔT_{wall} multiplied by a constant m .

In the manifold analysis it has been assumed that $m = 0.333$. By calculation on tubes used for steady-state, m has equaled 0.311 and 0.310. Using $m = 0.333$ for calculating T_{aw} gives an error of only 0.04%. Therefore as an initial approximation

$$T_{aw} = T_o - 0.333 \Delta T_{wall} \quad (13)$$

INSIDE TUBE WALL TEMPERATURE CALCULATIONS

The equation for the temperature drop across a cylindrical wall with heat being generated uniformly in the wall by direct current and heat losses considered is:

$$\Delta T_{wall} = T_o - T_i$$

$$\Delta T_{wall} = - \frac{q R_1}{2k A_i} \left[\frac{1 - \left(\frac{R_1}{R_2} \right)^2 + 2 \ln \frac{R_1}{R_2}}{1 - \left(\frac{R_1}{R_2} \right)^2} \right] + \quad (14)$$

$$\frac{q_L}{A_i k} R_1 \ln \frac{R_1}{R_2}$$

or

$$T_o - T_i = - \frac{Q_g}{h_G} + \frac{Q_L}{h_L}$$

$$h_G = - \frac{2k}{R_1} \left[\frac{1 - \left(\frac{R_1}{R_2}\right)^2}{1 - \left(\frac{R_1}{R_2}\right)^2 + 2 \ln \frac{R_1}{R_2}} \right]$$

$$h_L = \frac{k}{R_1 \ln \frac{R_1}{R_2}}$$

- Where
- h_G = heat transfer coefficient for heat generated in the tube wall, BTU/hr-ft²-°F
 - h_L = heat transfer coefficient for heat transferred to surroundings, BTU/hr-ft²-°F
 - Q_g = heat generated by resistance heating expressed as an inside wall heat flux to the fluid
 - Q_L = heat lost to the surroundings expressed as an inside wall heat flux from the fluid
 - A_i = inside tube surface area, ft²/inch of length
 - k = thermal conductivity of tube material, BTU/hr-ft-°F
 - q = heat generated in the wall, BTU/hr
 - q_L = heat lost to insulation, BTU/hr-inch of length
 - r = tube resistance, ohm/inch of length
 - R = tube radius, ft
 - I = current, amperes

For a 0.3150 in. O.D. by 0.2575 in. I.D. tube

$$A_i = 0.005618 \text{ ft}^2/\text{in. of length}$$

$$\frac{1}{h_G} = - \frac{0.0011537}{k}$$

$$\frac{1}{h_L} = - \frac{0.0021625}{k}$$

Equation 14 reduces to

$$\Delta T_{\text{wall}} = \frac{q}{A_i k} (0.0011537) - \frac{q_L}{A_i k} (0.0021625)$$

$$\Delta T_{\text{wall}} = \frac{q}{k} (0.20536) - \frac{q_L}{k} (0.385)$$

Where

$$q = I^2 r (3.413 \text{ BTU/hr} - \text{watt})$$

then

$$\Delta T_{\text{wall}} = \frac{I^2 r}{k} (0.700883) - \frac{q_L}{k} (0.385) \quad (15)$$

From Equation 1

$$res = (0.0138 T_{aw} + 29.49) \times 10^{-6} \text{ ohm-inches}$$

and the cross sectional area of the tube is 0.02585 in^2

therefore

$$r = [0.5355 T_{aw} + 1140.534] \times 10^{-6} \quad (16)$$

Using Equation 2 for q_L , Equation 3 for k and Equation 16 for r and substituting into Equation 15 gives

$$\Delta T_{\text{wall}} = \frac{I^2 (0.5355 T_{aw} + 1140.53) (0.7009)}{(8.3 + 0.0048 T_{aw}) \times 10^{-6}} - \frac{q_L (0.385)}{8.3 + 0.0048 T_{aw}} \quad (17)$$

T_{aw} is estimated by Equation 13

$$T_{aw} = T_0 - 0.333 \Delta T_{wall}$$

A first approximation of ΔT_{wall} is obtained by substituting Equation 13 into the first term of Equation 17 giving

$$0.0016 \Delta T_{wall}^2 - \left(8.3 + 0.0048 T_0 + \frac{0.125 I^2}{10^6} \right) \Delta T_{wall} + \frac{(0.3753 T_0 I^2 + 799.38)}{10^6} = 0$$

This is a quadratic equation of the form $a\Delta T_{wall}^2 + b\Delta T_{wall} + c = 0$ and can be solved by the quadratic equation to give $\Delta T_{wall}(\text{approx})$. $\Delta T_{wall}(\text{approx})$ is then used in Equation 13 to obtain a close approximation of T_{aw} . This value of T_{aw} is substituted into the second term of Equation 17 which is a heat loss correction to ΔT_{wall} . This correction was less than 1°F which resulted in a smaller change in the original approximation of T_{aw} . It was not necessary to repeat the calculation with modified T_{aw} values. The inside tube wall temperature can now be calculated by

$$T_i = T_0 - \Delta T_{wall} \quad (18)$$

BULK FUEL TEMPERATURE CALCULATIONS

An average bulk fuel temperature, TF_i , is calculated for each 11.5 inch long section of the manifold. (See Figure 50). A linear fuel temperature increase in each section is assumed.

The total heat (BTU/hr) transferred to the fuel in each section, Q_i , is determined by

$$Q_i = Q_G - Q_L \quad i = 1, 10$$

AFAPL-TR-73-95

where Q_G = heat generated in each section

or Q_G = (voltage drop across the section) x (current) x 3.413 BTU/hr-watt

and Q_L = insulation heat loss (see Figure 51)

$$\text{or } Q_L = 0.2819 + 0.004473 T_o + \frac{7.715 T_o^2}{10^6} \times 11.5$$

T_o = measured outside wall temperature in the center of the 11.5 in. section.

Starting with section 1, an approximate fuel temperature, TF_1 is determined by

$$TF_1 (\text{approx}) = TFI + 0.5 \left(\frac{Q_1}{PPH \times C_p} \right) \quad (19)$$

where TFI = measured value of manifold fuel inlet temperature

PPH = fuel flow rate, pounds per hour

C_p = specific heat of fuel evaluated at TFI, BTU/lb-°F

$\left(\frac{Q_1}{PPH \times C_p} \right)$ is the temperature increase of the fuel over the section length. Multiplying this expression by 0.5 gives the temperature increase to the center of the section directly opposite the outside tube wall thermocouple.

TF_1 is recalculated by Equation 19 except that C_p is evaluated at $TF_1(\text{approx})$. This calculation cycle is repeated until

$$\frac{TF_1 - TF_1 (\text{approx})}{TF_1} < 0.001$$

The fuel temperature at section 2, TF_2 , is obtained by first approximating a fuel inlet temperature to the section which is

$$TFI_2 = TF_1 + 0.5 \left(\frac{Q_1}{PPH \times C_p} \right)$$

then

$$TF_2(\text{approx}) = TF_2 + 0.5 \left(\frac{Q_2}{PPH \times C_p} \right) \quad (20)$$

Here again, in Equation 20, the specific heat is first evaluated at TF_{I_2} . Then TF_2 is recalculated by Equation 20 except that the specific heat is evaluated at $TF_2(\text{approx})$. This calculation cycle is repeated until

$$\frac{TF_2 - TF_2(\text{approx})}{TF_2} < 0.001$$

The fuel temperatures in the remaining sections are obtained by the same method. In addition, a manifold fuel outlet temperature, TF_{OC} , is calculated as

$$TF_{OC} = TF_{I_0} + 0.5 \left(\frac{Q_{I_0}}{PPH \times C_p} \right)$$

This value is compared to the measured value as a check to verify the accuracy of data and calculations. The calculated and measured values of the manifold fuel outlet temperature generally compare to within 4°F.

FUEL FILM CONVECTION COEFFICIENT

Flow tests at various rates (0.68 to 4.8 gallons per minute, Reynolds number range 12,500 to 140,000) with heating, were performed on two new manifold tubes. Inside tube wall and bulk fuel temperatures were calculated as described previously for each section of the manifold.

The following relationship was assumed:

$$Nu = c Re^m Pr^n \left(\frac{\mu}{\mu_w} \right)^{.14} \quad (21)$$

where

$$Nu = \frac{h_f D}{K_f} \quad \text{Nusselt No.}$$

$$Re = \frac{\rho V D}{\mu} \quad \text{Reynolds No.}$$

$$Pr = \frac{3600 C_p \mu}{K_f} \quad \text{Prandtl No.}$$

h_f = fuel film convection coefficient, BTU/hr-ft²-°F

D = inside tube diameter, ft

K_f = thermal conductivity of fuel, BTU/hr-ft-°F

ρ = fuel density, lbm/ft³

V = fuel velocity, ft/sec

μ = fuel viscosity at bulk fuel temperature, lbm/ft-sec

μ_w = fuel viscosity at inner tube wall temperature, lbm/ft-sec

C_p = fuel specific heat at bulk fuel temperature, BTU/lbm-°F

c , m , and n are constants determined from experimental data.

The film coefficient correlation was obtained by first rearranging Equation 21 in the following form:

$$\frac{Nu}{Pr \left(\frac{\mu}{\mu_w} \right)^{.14}} = c Re^m$$

Log-log plots of $\frac{Nu}{Pr \left(\frac{\mu}{\mu_w} \right)^{.14}}$ versus Re were made for each section.

These plots revealed a minimum scatter of data at $n = 0.5$. Therefore, correlations were developed for each of the 10 sections by a least

squares fit (power curve) of $\frac{Nu}{Pr^{.5} \left(\frac{\mu}{\mu_w} \right)^{.14}}$ versus Re to determine

c and m. The empirical equations for each section were of the form

$$h_f = c \frac{K_f}{D} Re^m Pr^{.5} \left(\frac{\mu}{\mu_w} \right)^{.14}$$

with values for c and m shown below.

Section	c	m
1	0.003050	0.96
2	0.004357	0.93
3	0.004693	0.93
4	0.007100	0.90
5	0.006000	0.91
6	0.008170	0.88
7	0.008157	0.88
8	0.007530	0.90
9	0.008462	0.88
10	0.010250	0.86

A least squares fit of all data revealed for the tube:

$$h_f = 0.0058 \frac{K_f}{D} Re^{.91} Pr^{.5} \left(\frac{\mu}{\mu_w} \right)^{.14}$$

Figure 52 is a plot of all data.

DEPOSIT THERMAL RESISTANCE CALCULATIONS

The overall heat transfer coefficient for each tube section, U, referred to the inner tube surface, is by definition:

$$U = \frac{Q}{A (T_o - T_F)}$$

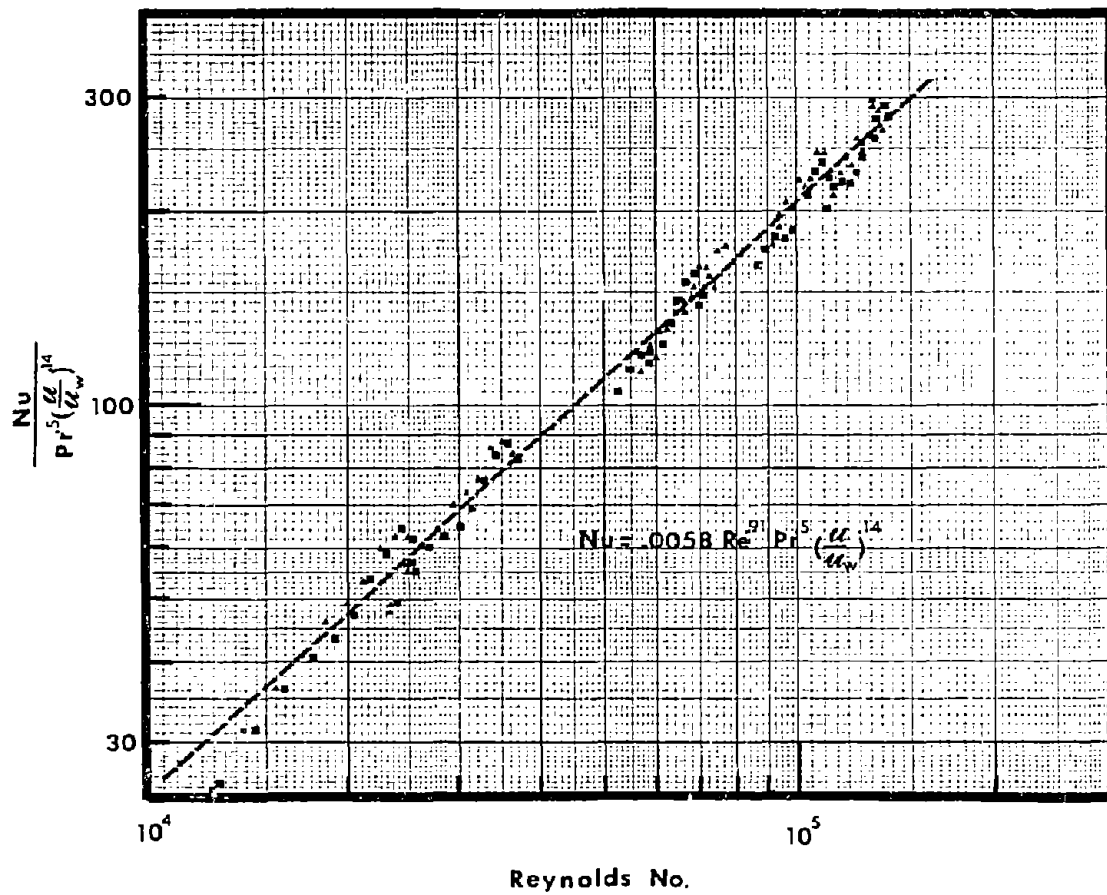


Figure 52. Curve Fit to Determine Film Convection Coefficient

or $\frac{1}{h_d}$ = overall thermal resistance to flow of heat to the fuel.

The tube wall conduction coefficient, h_G , from Equation 14 is

$$h_G = - \frac{2K}{R_1} \left(\frac{1 - \left(\frac{R_1}{R_2}\right)^2}{1 - \left(\frac{R_1}{R_2}\right)^2 + 2 \ln \left(\frac{R_1}{R_2}\right)} \right)$$

or $\frac{1}{h_G}$ = thermal resistance of tube wall

The fuel film convection coefficient, h_f , is calculated for each section as described previously by

$$h_f = c \frac{K_f}{D} Re^m Pr^{.5} \left(\frac{\mu}{\mu_w} \right)^{.14}$$

or $\frac{1}{h_f}$ = thermal resistance of the film. Therefore, for a clean tube

$$\frac{1}{U} = \frac{1}{h_G} + \frac{1}{h_f}$$

Once a deposit is formed on the inner tube surface, the thermal resistance balance becomes

$$\frac{1}{U} = \frac{1}{h_G} + \frac{1}{h_f} + \frac{1}{h_d}$$

Where $\frac{1}{h_d}$ = thermal resistance of deposit (DTR), hr-ft²-°F/BTU

$$\frac{1}{h_d} = \frac{1}{U} - \frac{1}{h_G} - \frac{1}{h_f} \quad (22)$$

At the beginning of any test series when the tube is clean $\frac{1}{h_d} = 0$. When the right hand side of Equation 22 is positive, this value represents the deposit thermal resistance.

Previous investigations (Reference 3) have indicated that the thermal conductivity of the deposit, K_d , is approximately 0.05 to 0.09 BTU/hr-ft-°F. Therefore, as a method to verify the accuracy of the

heat transfer analysis, $\frac{1}{h_d}$ values are evaluated to calculate a deposit thickness assuming $K_d = 0.05, 0.07$ and 0.09 . These calculated values of deposit thickness are compared to values measured with a micrometer by the method described in Appendix II.

The deposit thickness (x) is calculated from the following equation where all the variables are known except R_d .

$$\frac{1}{h_d} = \frac{R_1 \ln \left(\frac{R_1}{R_d} \right)}{K_d}$$

Where R_1 = inside radius of the tube, ft

R_2 = inside radius of the deposit, ft

K_d = thermal conductivity of deposit, BTU/hr-ft-°F

Rearranging gives

$$\ln \left(\frac{R_1}{R_d} \right) = \frac{K_d}{h_d R_1} \quad (23)$$

setting

$$\frac{K_d}{h_d R_1} = E$$

then

$$\frac{R_1}{R_d} = e^E$$

or

$$R_d = \frac{R_1}{e^E}$$

resulting in

$$x = R_1 - R_d$$

APPENDIX II

MICROMETER MEASUREMENT OF MANIFOLD DEPOSIT THICKNESS

The measurement of deposit thickness was obtained using a Karl Zeiss micrometer having a dial indicator movement built into the micrometer anvil so that a constant compressive load is applied to all parts measured. The smallest whole subdivision on the dial indicator is 0.0001 inch. Interpolation is necessary for readings smaller than 0.0001 inch. A 0.185-inch-diameter by 0.375-inch-long cylinder was placed on the deposit of a longitudinally bisected section of the manifold. The assembly was placed between the micrometer anvil and spindle and the thimble was rotated until the anvil dial indicator reading was zero. The micrometer sleeve reading was then the total of the cylinder diameter (0.185 inch), the deposit thickness, and the manifold tube wall thickness (0.028 inch nominal). The deposit was removed from the tube wall by a light abrasive action (rubbing with a pencil erasure). The measurement was then repeated, providing the cylinder diameter and manifold tube wall thickness. The difference in the two measurements is the deposit thickness.

AFAPL-TR-73-95

APPENDIX III

TABULATED DATA (ASTM-CRC FUEL COKER AND JFTOT)

Contained herein is the tabulated data recorded during the ASTM-CRC Fuel Coker and Jet Fuel Thermal Oxidation Tester evaluations of fuel AFFB-14-70.

TABLE XVI
ASTM-CRC FUEL COKER TEST RESULTS

Date	Preheater/Filter Temperatures (°F)	Code Rating	Filter Pressure Drop (In. of Hg)
14 Jan 72	350/450	1	>10.0
18 Jan 72	375/475	1	>10.0
19 Jan 72	400/500	4	>10.0
26 Jul 72	375/475	1	3.1
27 Jul 72	400/500	4	>10.0
28 Jul 72	400/500	4	>10.0
31 Jul 72	400/500	4	>10.0
31 Jul 72	400/500	4	>10.0
1 Aug 72	375/475	1	1.1
1 Aug 72	375/475	2+	2.2
2 Aug 72	375/475	4	>10.0
2 Aug 72	375/475	4	>10.0
3 Aug 72	350/450	1	1.5
4 Aug 72	350/450	4	2.0
7 Aug 72	350/450	1	1.1
7 Aug 72	350/450	1	0.5
8 Aug 72	350/450	4	2.1
8 Aug 72	375/475	4	2.4
21 Aug 72	325/425	2	0.3
21 Aug 72	325/425	1	0.1
22 Aug 72	325/425	1	0.0
23 Aug 72	325/425	1	0.3
28 Aug 72	350/450	1	0.2
28 Aug 72	375/475	4	6.6
8 Sep 72	375/475	4	10.0
7 Sep 72	350/450	2	6.0
7 Sep 72	350/450	2	1.3
8 Sep 72	375/475	2	1.05

TABLE XVII

2.5 HOUR JFTOT RESULTS - 25 SEP 70 TO 6 OCT 70

DATE	MAXIMUM TUBE TEMPERATURE (°F)	TDR RATING	CODE RATING	FILTER PRESSURE DROP (In. of Hg)
25 Sep 70	525	34.2	4	0.15
		35.0	4	
25 Sep 70	550	36.8	4	0.25
		34.7	4+	
25 Sep 70	500	17.2	1	0.0
		17.2	1	
25 Sep 70	515	23.0	2+	0.0
		23.0	2+	
28 Sep 70	515	25.2	3	0.1
		25.4	3	
28 Sep 70	520	32.5	4	0.0
		32.2	4	
29 Sep 70	505	11.5	1	0.0
		11.7	1	
29 Sep 70	510	17.2	1	0.0
		16.8	1	
30 Sep 70	520	12.0	1+	0.0
		12.0	1+	
1 Oct 70	515	13.8	1	0.0
		14.1	1	
1 Oct 70	520	22.5	2	0.0
		22.9		
2 Oct 70	535	25.0	2+	0.0
		-	-	
2 Oct 70	525	18.5	1+	4.3
		-	-	
5 Oct 70	535	18.5	2+	1.2
		18.0	2	
5 Oct 70	545	26.5	4	0.7
		26.2	4	
6 Oct 70	540	31.2	3	0.0
		31.0	3	

Note: All tests were run at 350 PSIG.

TABLE XVIII
5 HOUR JFTOT RESULTS - 14 SEP 1970 TO 21 JAN 1971

DATE	MAXIMUM TUBE TEMPERATURE(°F)	TDR RATING	CODE RATING	FILTER PRESSURE DROP (In. of H ₂ O)
14 Sep 70	525	32.2	4	>10.0
14 Sep 70	500	35.0	4	0.0
17 Sep 70	550	50.0+	4+	>10.0
18 Sep 70	490	22.2	2+	0.0
21 Sep 70	490	13.0	2	0.0
21 Sep 70	495	16.5	1+	0.0
		27.0	3	
		26.0		
22 Sep 70	480	14.2	1	0.0
		10.7		
22 Sep 70	485	20.8	1+	0.0
		19.8	2	
23 Sep 70	495	26.5	2+	0.0
		26.1	2+	
23 Sep 70	490	19.0	2	0.0
		19.0	2	
5 Nov 70	520	24.0	3	0.1
		24.2	3	
6 Nov 70	510	15.0	2	0
		15.3	2	
10 Nov 70	515	18.5	2	0.0
		18.4	2	
12 Nov 70	520	32.9	4	0.0
		32.9	4	
13 Nov 70	515	29.2	3	0.0
		29.2	3	
17 Nov 70	510	17.5	2	0.0
		17.0	2	
11 Jan 71	520	24.5	2+	0.0
12 Jan 71	530	25.5	4	0.0
13 Jan 71	525	22.0	3	0.0
14 Jan 71	520	21.0	3	0.0
15 Jan 71	510	20.8	1	0.0
15 Jan 71	515	20.0	2+	0.0
19 Jan 71	510	15.0	3	0.0
20 Jan 71	515	22.8	3	0.0
21 Jan 71	510	20.0	2+	0.0

Note: All tests were run at 350 PSIG.

TABLE XIX
2.5 HOUR JFTOT RESULTS - 23 NOV 71 to 14 FEB 72

DATE	MAXIMUM TUBE TEMPERATURE(OF)	TDR RATING	CODE RATING	FILTER PRESSURE DROP(In. of H ₂ O)
23 Nov 71 ⁽¹⁾	530	23.8	3+	0.0
30 Nov 71 ⁽²⁾	550	25.2	4	0.0
1 Dec 71 ⁽²⁾	530	10.5	2	0.0
2 Dec 71 ⁽²⁾	540	17.0	2	0.0
30 Dec 71 ⁽²⁾	545	18.0	3	0.0
4 Jan 72 ⁽²⁾	530	14.9	3	0.0
10 Feb 72 ⁽²⁾	570	26.2	4	0.0
10 Feb 72 ⁽³⁾	550	14.0	2	0.0
11 Feb 72 ⁽³⁾	560	21.3	4	0.0
14 Feb 72 ⁽³⁾	550	17.2	3	0.0

Notes: 1. Test run at 350 PSIG.
2. Tests run at 375 PSIG.
3. Tests run at 400 PSIG.

TABLE XX
5.0 HOUR JFTOT RESULTS - 17 SEP 71 TO 3 JAN 71

DATE	MAXIMUM TUBE TEMPERATURE(°F)	TDR RATING	CODE RATING	FILTER PRESSURE DROP(In. of Hg)
17 Sep 71	515	24.3	3+	0.0
20 Sep 71	510	14.2	2	0.0
22 Nov 71	510	11.5	1	0.0
26 Nov 71	520	13.5	2+	0.0
29 Nov 71	525	20.4	3	0.0
3 Jan 71	520	10.2	1+	0.0

Note: The first three tests were run at 350 PSIG and the remaining tests were run at 375 PSIG.

TABLE XXI
2.5 HOUR JFTOT RESULTS - 12 JUN 72 TO 14 JUN 72

DATE	MAXIMUM TUBE TEMPERATURE (°F)	TDR RATING	CODE RATING	FILTER PRESSURE DROP (In. of Hg)
12 Jun 72	565	23.3	4	0.0
14 Jun 72	550	16.0	3	1.5

Note: Both tests were run at 400 PSIG.

REFERENCES

1. H. Goodman and R. Bradley, High Temperature Hydrocarbon Fuels Research in an Advanced Aircraft Fuel System Simulator Final Report, Air Force Aero Propulsion Laboratory, Technical Report AFAPL-TR-70-13, March 1970.
2. L. Lampman and J. C. Ford, High Temperature Hydrocarbon Fuels Research in an Advanced Aircraft Fuel System Simulator on Fuel AFFB-13-69, Air Force Aero Propulsion Laboratory, Technical Report AFAPL-TR-70-70, March 1971.
3. H. Goodman, R. Bradley, and T. Sickles, High Temperature Hydrocarbon Fuels Research in an Advanced Aircraft Fuel System Simulator on Fuel AFFB-8-67, Air Force Aero Propulsion Laboratory, Technical Report AFAPL-TR-67-116, September 1967.
4. H. Goodman, R. Bradley, and T. Sickles, High Temperature Hydrocarbon Fuels Research in an Advanced Aircraft Fuel System Simulator on Fuel AFFB-9-67, Air Force Aero Propulsion Laboratory, Technical Report AFAPL-TR-68-25, February 1968.
5. H. Goodman, R. Bradley, and T. Sickles, High Temperature Hydrocarbon Fuels Research in an Advanced Aircraft Fuel System Simulator on Fuel AFFB-10-67, Air Force Aero Propulsion Laboratory, Technical Report AFAPL-TR-69-5, February 1969.
6. H. Goodman, R. Bradley, and T. Sickles, High Temperature Hydrocarbon Fuels Research in an Advanced Aircraft Fuel System Simulator on Fuel AFFB-11-68, Air Force Aero Propulsion Laboratory, Technical Report AFAPL-TR-69-88, September 1969.
7. H. Goodman and R. Bradley, High Temperature Hydrocarbon Fuels Research in an Advanced Aircraft Fuel System Simulator on Fuel AFFB-12-28, Air Force Aero Propulsion Laboratory, Tech Report AFAPL-TR-69-117, February 1970.
8. R. Bradley and H. Goodman, Advanced Aircraft Fuel System Simulator Modification and Performance Report, North American Aviation, Inc. Report No. NA-66-1380, December 1966.
9. W. Taylor, Development of High Stability Fuel, Quarterly Report, Naval Air Propulsion Test Center, Contract N00140-73-C-0547, January 1973.